USING FLOW FIELD-FLOW FRACTIONATION COUPLED TO INDUCTIVELY COUPLED PLASMA MASS SPECTROMETRY TO STUDY THE PHYSICOCHEMICAL SPECIATION OF COLLOIDAL IRON IN SEAWATER

A Thesis

by

KIMBER MARIE DE SALVO

Submitted to the Office of Graduate and Professional Studies of
Texas A&M University
in partial fulfillment of the requirements for the degree of

MASTER OF SCIENCE

Chair of Committee,	Jessica N. Fitzsimmons
Committee Members,	Peter Santschi
	Franco Marcantonio
Head of Department,	Shari A. Yvon-Lewis

August 2018

Major Subject: Oceanography

ABSTRACT

Iron is a critical micronutrient that marine phytoplankton need to perform photosynthesis that produces about half of the world's oxygen. Colloidal iron (0.003-0.2 μm) comprises a significant portion of the oceanic bioavailable dissolved iron pool (<0.2 μm). The colloidal iron phase may have different scavenging residence times and bioavailability to phytoplankton based on its physicochemical speciation, so it is imperative to understand the size distribution and composition of marine colloidal iron as a function of size. To unveil the colloidal spectrum in low salinity regimes (rivers and estuaries), past studies have coupled Flow-Field Flow Fractionation (FlFFF) and UV Visible Spectrometry (UVvis), with Inductively Coupled Plasma Mass Spectrometry (ICPMS) to quantify the size distribution of organic and metal colloids. However, this method is challenged by low detection limits at full salinity because of salt effects and low sample volumes, inhibiting the ability to determine the colloidal iron size spectrum in oceanic environments. This thesis research pioneers a new method that overcomes these hurdles by fraction collecting size-separated FlFFF aliquots and analyzing iron using an offline, low-volume pre-concentration method. This new approach couples FlFFF-UVvis-ICPMS with online Multiple Angle Laser Light Scattering (MALLS) and offline fluorescent Excitation Emission Matrices (EEMs) to calculate sphericity and determine associated fluorescent dissolved organic matter (FDOM) to help to identify the compositional characteristics across the colloidal size spectrum. We first test this method for iron blanks, reproducibility, and sampling artifacts. Results of this new method in the Damariscotta River estuary and Maine shelf waters to describe the physicochemical speciation of marine colloidal iron size continuum. Our results suggest that there are both organically-bound and inorganic iron colloids in coastal Maine waters, and the

iron distribution was not tightly correlated with organics or overall colloid abundance with compositionally distinct size fractions where: 0.25-1.5nm hydrodynamic radius is iron- and organic-rich, 1.5-3.5nm is organic, 2.5-5nm is non-spherical with low concentrations of organic iron, 5-9nm found only at Estuarine Station 2 15m is iron-poor, 9-12nm is organic and abundant, 12-15nm, found at both station's chlorophyll maximum, is iron-rich and inorganic, 15-20nm is organic-rich.

DEDICATION

I would like to dedicate this thesis to my parents, Peter and Kathleen De Salvo. They have supported me every step of the way and have been a constant source of love and encouragement. I have not met anyone else with their drive and work ethic, and I strive to emulate that in all that I do.

ACKNOWLEDGEMENTS

I would like to give an immense and special thank you to my advisor Dr. Jessica Fitzsimmons. Words do not adequately describe how her mentorship has helped me grow as a graduate student and as a trace metal geochemist. Her hard work and dedication is truly inspiring. Her support and words of encouragement buoyed me through grad school and the trickier parts of my research. I cannot thank her enough for all that she has done for me! I am so proud to be one of her first students. Additionally, I'd like to thank Dr. Mark Wells from the University of Maine for additionally mentoring me during this research project, especially for patiently coaching me through all of the hurdles thrown my way during my time in Maine. His support was also key to the success of this research.

Also, I want give a huge thank you to my committee members Dr. Peter Santschi and Dr. Franco Marcantonio for their guidance and support throughout the course of this research. A big thank you also goes to Luz Romero for her countless hours of hard work to help me troubleshoot and wrangle the ICPMS in the Williams Radiogenic Isotope Geosciences Laboratory.

I'd like to thank those at University of Maine's, Darling Marine Center (DMC) for all of their help during lab and fieldwork. Thanks to several interns who helped sample, specifically to Victoria Lydick and John Hall for being at my right hand additionally helping in the lab. A huge thank you goes to Kathleen Thornton who taught me how to use the instruments and facilities at the DMC. She spent countless hours, even after work hours, helping me troubleshoot instrument malfunctions.

Thanks also goes to my friends and colleagues and the department faculty and staff for making my time at Texas A&M University a great experience. Thanks to Dr. Chrissy Wiederwohl and Dr. Gerardo Gold Bouchot for help using MATLAB and R data analysis scripts.

I want to give a special thank you to Laramie Jensen who was my rock, support system and who ultimately kept me sane. Thanks to her for being my lab, writing, gym, and coffee shop buddy; I couldn't have done this without her. I'd also like to thank my other office mates Noura Randle and Claire McKinley who always had beautiful words of encouragement and advice.

Finally, thanks to my mother and father for their encouragement and to my boyfriend Andrew Anderson for his love and support.

CONTRIBUTORS AND FUNDING SOURCES

This work was supported and supervised by a dissertation committee consisting of my advisor Dr. Jessica Fitzsimmons, Dr. Peter Santschi of the Department of Oceanography, and Dr. Franco Marcantonio of the Department of Geology and Geophysics at Texas A&M University and by Dr. Mark Wells from the University of Maine's School of Marine Sciences.

The Matlab script used to refine the UV and MALLS output data was generated by Kathleen Thornton from the University of Maine's Darling Marine Center. She also optimized the FlFFF flows rates for seawater and helped me re-optimize the flow rates without a slot pump (described in Chapter II). Dr. Mark Wells used the Matlab script to generate all refined UV, MALLS, and Rg data. Dr. Chrissy Wiederwohl generated and ran a Matlab script to reorganize data generated from the EEMs Fluorometer to allow me to analyze it using the "eemsR" package in R studio (Chapter II). All other work conducted for the thesis was completed by the student independently.

Funding for this thesis research was provided by a National Science Foundation (NSF) grant (PIs Dr. Jessica Fitzsimmons and Dr. Mark Wells) and a NSF S-STEM scholarship (PIs Dr. Wilford Gardner and Dr. Mary Jo Richardson). In addition, graduate study was supported by various Texas A&M University scholarships: College of Geosciences Louis and Elizabeth Scherck Scholarship, College of Geosciences Diversity Scholarship, Department of Oceanography's Donald and Melba Ross Scholarship, and Graduate Student Competitive Scholarship.

NOMENCLATURE

FlFFF	Flow Field Flow Fractionation
UVvis	UV Visible Spectrometry
MALLS	Multiple Angle Laser Light Scattering
EEMs	Excitation Emission Matrices
ICPMS	Inductively Coupled Plasma Mass Spectrometry
Fe	Iron
C	Carbon
ASW	Artificial Seawater
FDOM	Fluorescent Dissolved Organic Matter
DOC	Dissolved Organic Matter
Rg	Radius of Gyration
Rh	Hydrodynamic Radius
RSD	Relative Standard Deviation
DMC	Darling Marine Center (University of Maine)
TAMU	Texas A&M University
EMCC	Eastern Maine Coastal Current
WMCC	Western Maine Coastal Current
NASW	North Atlantic Slope Water
LSW	Labrador Sea Water
SSW	Scotian Shelf Water

TABLE OF CONTENTS

LIST OF FIGURES

LIST OF TABLES

CHAPTER I

INTRODUCTION

1.1 Introduction

1.1.1 Motivation to Study Oceanic Iron

Despite iron being the fourth most abundant element in continental crust, iron is considered a trace metal in seawater because its dissolved concentrations in open ocean surface seawater are less than 0.2 nM. Low dissolved Fe concentrations result from the insolubility of Fe(III) under oxygenated conditions, efficient Fe scavenging by particles surfaces, and biological uptake by phytoplankton (Boyd and Ellwood, 2010; Sunda and Huntsman, 1995). In coastal waters, dissolved iron concentrations are typically at least an order of magnitude higher than in the open ocean due to proximity to continental margin iron sources. This allows iron to be more replete to coastal phytoplankton communities, while in contrast approximately 40% of open ocean surface waters are considered high nutrient low chlorophyll regions (HNLC) (Boyd and Ellwood, 2010; Sunda and Huntsman), where rates of primary production are limited by insufficient iron supply. Thus, iron bioavailability affects the distribution and community composition of marine phytoplankton and the magnitude of carbon that is sequestered, consequently having major implications for the carbon cycle (Boyd et al., 2007; De Baar et al., 2005; Moore et al., 2001; Sigman and Boyle, 2000). Because phytoplankton produce about half of the world's oxygen though primary production and make up the base of the oceanic food web (Sunda, 2012), it is imperative to understand biogeochemical dynamics of iron in marine waters as it directly affects the global carbon cycle and thus climate.

New iron enters the ocean through rivers, aerosol deposition, sediments (resuspension and terrestrial/coastal processes), and hydrothermal activity (Tagliabue et al., 2014). Within the water column, dissolved iron generally has a nutrient-type depth profile in the ocean (Boyd and Ellwood, 2010), with low surface concentrations because of biological uptake and higher concentrations at depth due to remineralization. Iron is arguably the most important oceanic trace metal micronutrient due to its essential role in photosynthetic and respiratory electron transport proteins, nitrogen acquisition and transformation proteins, chlorophyll synthesis enzymes, and proteins that detoxify reactive oxygen species (superoxide dismutases) (Sunda and Huntsman, 1995). However, iron does not behave strictly as a nutrient-type element. Instead certain features of the dissolved iron distribution have more scavenging-type characteristics, such as a surface-water maxima in areas of high dust inputs (Bruland et al., 1994; Johnson et al., 1997; Measures et al., 1995) and different deep water iron concentrations (>1000 m) in the Atlantic and the Pacific Oceans (Bruland and Lohan, 2006). If iron was strictly nutrient-type, we would see an increase in concentration moving from the deep Atlantic to the Pacific due to accumulated remineralization along thermohaline circulation (Bruland and Lohan, 2006). However, particulate scavenging of deep dissolved iron prevents this buildup (Johnson et al., 1997). With dissolved iron having both nutrient-type and scavenged-type tendencies, Bruland and Lohan 2006 suggest that dissolved iron has a "hybrid distribution" (Bruland and Lohan, 2006)

1.1.2 Iron Speciation

The speciation and chemical composition of iron is complex and will directly determine the bioavailability and scavenging fate of marine dissolved iron (Gledhill and Buck, 2012). Iron has two oxidation states: insoluble Fe(III) and soluble Fe(II). In ancient times when

photosynthetic life originated on earth, soluble ferrous iron Fe(II), was widely bioavailable under the reduced oxygen conditions of the ancient ocean, resulting in the evolution of iron as an essential nutrient (Shaked and Lis, 2012). However, with the prolific expansion of photosynthetic, oxygen-producing organisms, oxygen concentrations in seawater soared, resulting in the oxidation of most marine ferrous iron Fe(II) into insoluble ferric Fe(III) (Shaked and Lis, 2012). Fe(III) rapidly precipitates out of oxygenated waters as iron oxides or hydroxides and sinks as aggregates out of the water column (Shaked and Lis, 2012). Unfortunately for phytoplankton, the more scarce Fe(II) is the directly bioavailable form, due to its easy transfer across cell membranes in divalent cation transporters, while the now abundant Fe(III) is not as directly bioavailable (Morel et al., 2008).

So, if the thermodynamically-favored Fe(III) is insoluble, phytoplankton must find another mechanism to acquire sufficient iron. One mechanism that may enhance iron bioavailability (Hutchins et al., 1999) is the complexation of Fe(III) by organic ligands, which are presumably of biological origin. These ligands stabilize iron in the water column by forming chelates that limit precipitation of Fe(III) and scavenging loss. There are three general ligand classes (Bundy et al., 2016; Gledhill and Buck, 2012), with the stronger and smallest class containing siderophores, produced by bacteria to sequester iron (Hider and Kong, 2010), and the weaker and larger classes comprising humic substances (Batchelli et al., 2009; Batchelli et al., 2010; Laglera and van den Berg, 2009), exopolysaccharides (EPS) (Hassler et al., 2011a; Stolpe et al., 2010; Stolpe and Hassellöv, 2010), and other organic compounds of unknown composition. Traditionally, it has been established that >99% of dissolved iron is complexed by ligands (Gledhill and van den Berg, 1994; Rue and Bruland, 1995). However, new findings suggest that this is an overestimate, and inorganic iron colloids (such as crystalline iron

oxyhydroxides) may contribute some to the colloidal iron complexes, especially near continental or metalliferous sources rich in dissolved iron (Fitzsimmons et al., 2015a) and due to Fe's isoelectric point in natural systems (pH = 7-8), this inorganic Fe can be bound by organic matrices (Fitzsimmons et al., 2017; Toner et al., 2009; Toner et al., 2015). Therefore, the physicochemical speciation of iron needs to be measured in conjunction with carbon speciation to gain a greater understanding of iron's chemical complexation (organic or inorganic) and to understand the black box of iron bioavailability.

1.1.3 Iron Size Distribution: Colloids

In addition to chemical and redox speciation, the physical partitioning of iron into compounds of different sizes could also affect its bioavailability. Iron is typically classified into two operationally defined size fractions (Figure 1.1): particulate (>0.2 μm) and dissolved (<0.2 μm) (Wells, 2002). While this operational size distinction is useful when sampling seawater by filtration in the field, we can also separate these two size fractions more theoretically by their characteristics with respect to gravity: particles sink, while dissolved compounds are too small to sink (Wells, 2002). However, using the operational dissolved definition of <0.2 μm, the dissolved size fraction can still contain compounds significantly larger than species truly dissolved into solution, and thus the dissolved fraction can be further subdivided into two sub-fractions (Figure 1.1): colloidal and truly soluble phases. Operationally, colloids are a group of compounds with a lower size limit of 1-10 kDa (~1.5-3 nm, using globular proteins (Erickson, 2009)) and an upper limit distinguishing the transition into particles (0.2 μm) (Wells, 2002). Theoretically, colloids are defined based on having sufficient size to produce an interface separating the compound from the surrounding media, distinguishing them from truly soluble compounds on the small end, yet colloids are small enough to not sink, distinguishing them from

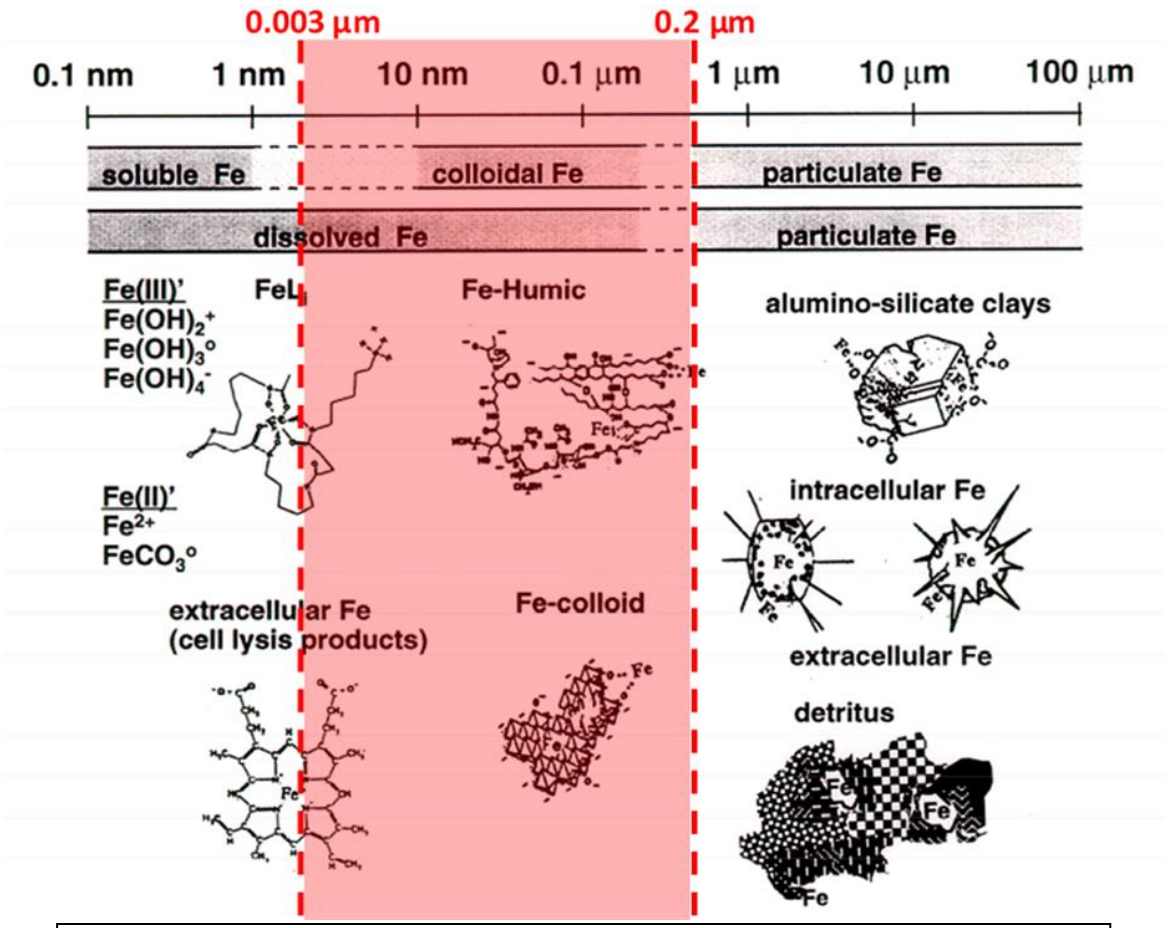

Figure 1.1: Iron's operational size fractions. Particulate Fe >0.2 µm, dissolved Fe <0.2 µm, 1 or 10kDa (0.003 µm) < colloidal Fe < 0.2 µm, soluble Fe <1 kDa (0.003 µm). Reprinted and adapted from Bruland and Rue 2001.

particles on the large end (Wells, 2002). Thus, colloids can be considered "micro particles." It has been well established that colloids account for 10-30% of dissolved organic carbon in seawater (Benner et al., 1997; Guo and Santschi, 1997). Such organic colloidal complexations include reactive ligands such as lipids, proteins, and polysaccharides, as well as biologically-resistant heteropolycondensations (humic matter) and the degradation products of these constituents.

Colloids are oftentimes compositionally heterogeneous, consisting of a mixture of dissolved organic carbon and trace elements such as iron (Wells, 2002). Studies have shown that a significant portion of dissolved iron exists in this colloidal size fraction with concentrations ranging from 0.01-1 nM in the North Atlantic (Bergquist et al., 2007; Cullen et al., 2006; Fitzsimmons et al., 2015a; Fitzsimmons et al., 2015b; Wu et al., 2001), while the North Pacific had somewhat lower colloidal Fe concentrations ranging from 0.01-0.6 nM (Nishioka et al., 2001; Wu et al., 2001). Generally, colloidal iron concentrations have a surface maximum with a minimum in the deep chlorophyll maximum (DCM), indicating it has a dust source and is either preferentially taken up by microbes and/or scavenged/aggregated at the DCM (Fitzsimmons and Boyle, 2014b; Wu et al., 2001). Furthermore, iron colloid concentrations tend to follow trends of dust deposition in the Atlantic, with the highest concentrations near the greatest dust deposition (Bergquist et al., 2007; Fitzsimmons and Boyle, 2014b). Appropriately, then, in the northeast North Pacific near Ocean Station Papa, where dust concentrations are very low, the concentrations of colloidal iron was low in the surface mixed layer (Nishioka et al., 2001). In the North Atlantic Deep Water (NADW) water mass, colloidal iron decreased from the North Atlantic to the South Atlantic due to colloidal scavenging (Bergquist et al., 2007). In the sub-tropical and tropical Atlantic Ocean, the dissolved iron size fraction was dominated by the variance in the labile colloidal iron (Bergquist et al., 2007). However, a more recent study in the North Atlantic shows that this is not always the case (Fitzsimmons et al., 2015b). Instead, Fitzsimmons et al. 2015 proposes a new model of dissolved iron size partitioning where a "steady state" of dissolved iron exchange, sorption/desorption, and aggregation/disaggregation sets the soluble/colloidal partitioning ratio near 50/50% in the deep ocean, away from active iron sources and biological processing. Thus, continental shelf environments may have increased

colloidal iron loadings due to the proximity of sources such as continental margin sediments and river inputs.

Despite all of these findings, vast areas of the global ocean have not been studied for colloidal iron partitioning. While colloidal iron has been examined in several oceanic environments, waters over continental shelves have not been well studied and very little is known about the physicochemical characteristic of colloidal iron there. This is a particular shame, since shelf systems are biological productive systems, and as such the chemical composition of bioavailable iron species is very important. It may be that because these systems are in close proximity to iron sources such as riverine and shelf sediment (rich in iron aluminosilicate clays) inputs, there may be more inorganic colloidal iron species in coastal systems. Not only would this affect iron bioavilability, but these inorganic species are prone to scavenging and loss, which would decrease the likelihood that these coastal iron colloids would be transported offshore. Therefore, a better spatial characterization of colloidal iron concentrations, especially in shelf regions, is needed to help understand its role in the fate and transport of dissolved iron throughout the ocean.

In the coastal ocean, dissolved Fe concentrations were found to range between 0.1 to >90 nM (Boyle et al., 1977; Martin and Gordon, 1988; Powell et al., 1996; Wells et al., 2000; Wu and Luther III, 1996). It has been established that metal colloids, including Fe, are very abundant in shelf and estuarine systems (Benoit et al., 1994; Guieu et al., 1998; Hassellöv et al., 1999; Martin et al., 1995; Öztürk and Bizsel, 2003; Powell et al., 1996; San et al., 1996; Stolpe et al., 2013a; Stolpe et al., 2013b; Stolpe and Hassellöv, 2007, 2010; Wells, 1998; Wells et al., 2000; Wen et al., 1999; Wen et al., 1996). It is also well known that during estuarine mixing, seawater's cations neutralize negatively charged iron colloids, causing greater than 95% of iron

colloids to flocculate out of the water column (Boyle et al., 1977; Sholkovitz, 1976; Sholkovitz et al., 1978). One study suggests that the presence and concentration of strong, siderophore-like, iron-binding ligands dictates the supply of dissolved iron from estuarine to offshore waters, since iron concentrations correlated with increasing strong ligand concentrations (Buck et al., 2007). On the other hand, the weak, humic- and exopolysaccharide-like, ligand class was not present in low salinity environments (Buck et al., 2007) suggesting that estuarine mixing and riverine input into the nearshore environment can affect iron speciation. Several studies have found that colloidal loadings in these nearshore environments are temporally variable between seasons, with smaller size colloids during spring floods and larger colloidal size fractions during the summer and spring blooms (Stolpe et al., 2013b; Stolpe and Hassellöv, 2010). Therefore, seasonal dynamics could affect the composition and scavenging fate of metal colloids. Much less is known about how the seasonal effects of phytoplankton production in shelf waters influences colloidal iron size partitioning, but it is clear that phytoplankton blooms affect colloidal organic carbon size and composition (Floge and Wells, 2007; Niven et al., 1995). Thus, it is important to understand how both organic carbon speciation and iron speciation are affected by seasonal dynamics and freshwater input into the coastal system, e.g. if they vary co-dependently or independently.

Historically, it has been thought that soluble-sized iron species were most bioavailable to phytoplankton. Such studies demonstrate that slower uptake rates occur for colloidal iron over soluble fractions and that aged colloidal iron oxyhydroxides are explicitly unavailable to diatoms (Chen and Wang, 2001; Rich and Morel, 1990). The unavailability of colloidal iron oxyhydroxides suggests that iron speciation could play a major role in determining colloidal iron's bioavailability. However, the topic of colloidal iron bioavailability remains controversial.

For example, some studies suggest that amorphous oxyhydroxides with low thermodynamic stability could provide a source of soluble iron (Wells et al., 1991; Wells et al., 1983). In addition, another study found that although bacterial growth efficiencies on soluble-sized organic matter is consistently greater than on colloidal-sized organics, the uptake rates of colloidal carbon are up to four times greater than soluble carbon (Amon and Benner, 1996). This study also suggests that the colloidal organic phase is more labile and bio-reactive while being less diagenetically altered than soluble organic matter. Another study supports this idea with carbon isotopic evidence that shows that the colloidal carbon pool is younger than the soluble carbon pool (Santschi et al., 1995). For iron colloids specifically, there has been evidence that plankton can utilize some forms of colloidal iron (Barbeau and Moffett, 2000; Chen et al., 2003; Wang and Dei, 2003). Interestingly, one study found that iron colloids bound as exopolymeric saccharides may be preferred over other soluble species of iron (Hassler et al., 2011b). Therefore, the complexity of colloidal iron bioavailability remains largely unknown since bioavailability can differ across various organisms' preferences, and among colloidal iron chemical composition, as well as size. Improved understanding of the physicochemical speciation of colloidal iron is required to improve our understanding of the biogeochemical cycling of iron and its role in the global carbon cycle.

In addition to the bioavailability rationale, colloids are further important to study because they are believed to be seeds for aggregation, especially in the organic phase (Honeyman and Santschi, 1989; Kepkay, 1994; Mopper et al., 1995). Using transmission electron microscopy, there is evidence for colloidal aggregation in surface and deep ocean waters (Grout et al., 2001; Leppard et al., 1997; Wells and Goldberg, 1993). However, the mechanism of this aggregation remains controversial. It is believed that there are two broad types of colloid aggregation

regimes: very rapid (diffusion-limited) and slower (reaction-limited) aggregation (Wells and Goldberg, 1993). Interestingly, transmission electron microscope studies have also indicated that very rapid (diffusion-limited) colloid aggregation is a critical precursor for marine snow formation, which influences the carbon pump and results in a short residence time for colloids (Heissenberger et al., 1994; Heissenberger and Herndl, 1994; Leppard et al., 1996; Wells and Goldberg, 1993). This short residence time for colloids is on the order of a few hours in coastal waters and slightly longer offshore, measured using size fractionated ^{234}Th (Baskaran et al., 1992; Moran and Buesseler, 1993; Moran and Buesseler, 1992). For truly soluble species however, residence times were longer, ranging from several days to weeks in coastal and offshore waters, respectively (Moran and Buesseler, 1992). Even though these residence times may be overestimated due to the rapid aggregation of exopolymers forming fibrils transferring to the particulate phase (Niven et al., 1995), these findings imply that colloid cycling can significantly influence the transport and scavenging fate of metals. Thus, it is not only imperative to understand the compositions of colloidal fractions because it affects their bioavailability but also because it can give further insight into their role as an aggregator of particles, both with respect to broad metal scavenging and within the carbon cycle.

1.2 Thesis Objectives

Because colloidal iron constitutes a significant portion of the dissolved iron phase in the coastal and open ocean, and the physicochemical speciation of colloidal iron could affect its bioavailability and scavenging fate, it is imperative to constrain the size and composition of colloidal Fe as well as the processes that control that speciation. Thus, I will pioneer in this thesis a new analytical method that measures the size, shape, and composition of aqueous colloids by combining several techniques and instruments in tandem:

- Asymmetrical Flow Field Flow Fractionation (FlFFF) for size separation, according to hydrodynamic radius,
- UVvis-Spectrometry for organic carbon detection,
- Multiple Angle Laser Light Scattering (MALLS) for the measurement of radius of gyration (shape) and colloidal abundance,
- Fluorescence Excitation Emission Matrix Spectroscopy (EEMs) for organic carbon characterization, and
- Inductively Coupled Plasma Mass Spectrometry (ICPMS) for iron measurement.

I will optimize this new technique and apply it to samples from the Damariscotta River estuary and offshore continental shelf waters in coastal Maine to answer the following three oceanographic questions:

(1) What is the size distribution and shape of coastal and estuarine colloidal iron?

(2) What is the chemical composition (organic or inorganic) of this colloidal iron?

(3) How do estuarine and coastal colloidal iron size distributions and compositions vary spatially (with depth and estuarine vs. offshore)?

1.3 New The FlFFF—MALLS—UVvis—ICPMS—EEMs Method

Flow Field Flow Fractionation (FlFFF) is a chromatography-like elution technique popularized in the last few decades that allows colloid particles to be separated by size due to their size-specific ability to diffuse across a perpendicular flow stream, which is applied over the cross section of a narrow, ribbon-like channel (Figure 1.2) (Baalousha et al., 2011). Unlike other popular ultrafiltration methods, FlFFF provides a continuous and high resolution spectrum of colloidal-sized particles as a function of their diffusion coefficient (directly proportional to

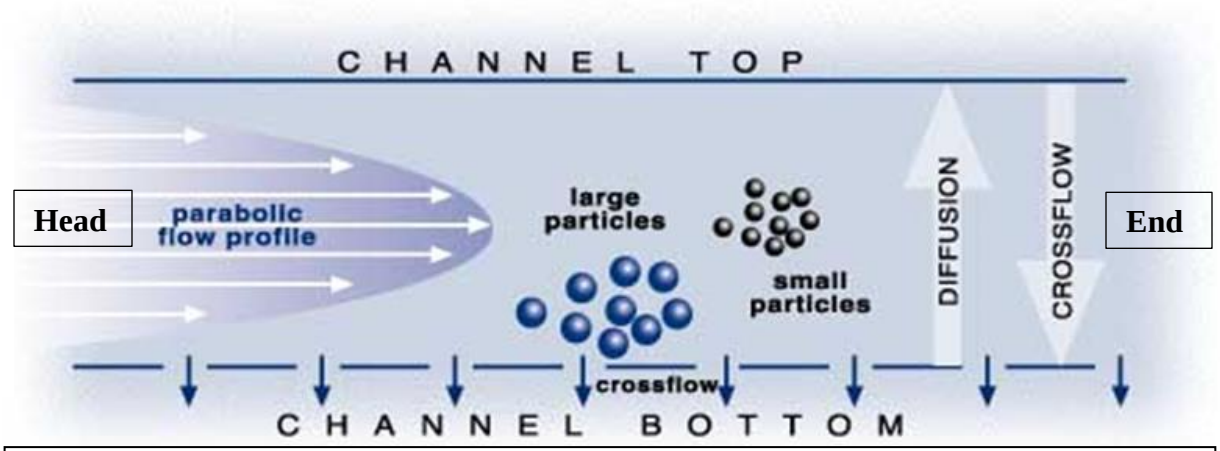

Figure 1.2: Schematic of Flows within FlFFF Channel that illustrate how the colloids are size fractionated. The wall near the channel bottom has a 10 kDa pore sized membrane. Reprinted and adapted from Nanolytics (2018).

hydrodynamic diameter), with minimal compositional perturbation. This makes FlFFF a powerful tool for studying the size spectrum of species in complex media such as natural water samples. Furthermore, when FlFFF is coupled to other detectors, it can provide a wealth of information on particulate composition as a function of size.

UV spectrometry (UVvis) is a valuable instrument when coupled to FlFFF. As an online, non-destructive detector, the size-fractionated FlFFF eluent can be transferred directly into the UVvis spectrometer, which uses light absorbance (wavelength = 254 nm) to estimate the chromophoric dissolved organic matter (CDOM) within the colloid size spectrum (Wells, 2004). Ultimately, this detector is imperative to use in this new method because it relates which fractions include organic species.

A second online detector that is critically coupled to FlFFF in this new method is a Multiple Angle Laser Light Scatterer (MALLS), which determines the radius of gyration (Baalousha et al., 2011) through a measurements of the light scattered by organic and inorganic

colloidal particles in suspension at different fixed angles (Baalousha et al., 2011). Adding the MALLS detector also compensates for the spherical assumptions of the FlFFF detector by measuring a shape factor, which relates how far a colloid deviates from spherical shape (Baalousha et al., 2011). This is especially important when considering that natural colloids are not necessarily round but may be fibrillar (e.g. exopolymers: 1-3 nm in diameter and 100-2,000 nm in length (Santschi et al., 1998)) or complex (e.g. inorganic iron nanoparticles) in shape.

Coupling FlFFF offline to Fluorescent Excitation Emission Matrix spectrofluorometer (EEMs) can provide insight into which size fractions have a particular fluorescent dissolved organic matter (FDOM) chemical composition (Coble, 1996). Maximum fluorescence at certain wavelengths would indicate whether a colloidal size fraction had more protein-like, terrestrial humic-like, or marine humic-like material (Boehme and Wells, 2006; Coble, 1996). Therefore, coupling our method to FlFFF provides essential information about organic carbon composition that UVvis alone cannot provide, all as a function of FlFFF-separated colloidal size.

This FlFFF-ICPMS coupling has been successfully executed in freshwater systems and low salinity estuarine systems (Dahlqvist et al., 2004; Hassellöv et al., 1999; Lyvén et al., 2003; Stolpe et al., 2013a; Stolpe et al., 2013b; Stolpe et al., 2010). However, when the method was applied to a higher salinity (~30 sal) estuary (Gullmarsfjord, Sweden), the study was unsuccessful in quantifying the metal concentrations in the colloidal size spectrum due to analytical hurdles and was only able to achieve relative concentrations (Stolpe and Hassellöv, 2010). Therefore, no previous study has successfully coupled FlFFF to ICPMS to quantify iron colloid concentrations in high salinity oceanic waters.

FlFFF-ICPMS have not been coupled for high salinity samples because saline waters cannot be directly injected into the ICPMS. Concentrated salt matrices degrade the performance

of the ICPMS when salts build up and occlude the cone orifice, lowering the sensitivity and diminishing the instrument's capabilities to accurately measure low metal concentrations (Hassellöv et al., 1999). If, instead, the individual FlFFF fractions are individually fraction collected, a high precision measurement of metal concentration in a small volume aliquot (~ 1.5 mL) would be required, and most metal concentration analytical methods in seawater require sample volumes of at least 10 mL. However, a recently developed ICPMS pre-concentration method to quantify trace metals in saline waters (Lee et al., 2011) enables high precision Fe measurements in only 1 mL of seawater. Thus, the innovation of this new method is to couple FlFFF offline, following fraction collection, to ICPMS, to allow for colloidal Fe analysis as a function of size in marine waters. This thesis research is the first to apply these techniques in a high salinity oceanic environment and is also the first to couple MALLS and EEMs to a FlFFF-ICPMS system in order to give complementary insight into the size, shape, and chemical composition of the colloids.

1.4 Proposed Thesis Research

My primary thesis objective was to optimize and test the new method coupling FlFFF—UVvis—MALLS—EEMs—ICPMS (Figure 1.3) for system blanks, appropriate size separation, and sampling reproducibility. Passing these tests, my secondary thesis objective was to apply the new method to seawater samples from the Damariscotta River estuary and the shelf waters offshore in coastal Maine in order to quantitatively discriminate the physicochemical speciation of the colloidal iron size continuum and evaluate how they changes in relation to various biogeochemical processes (seasonal phytoplankton dynamics, coastal processes, runoff inputs, resuspension processes, particle dynamics, and estuarine processes). This project was guided by the following steps:

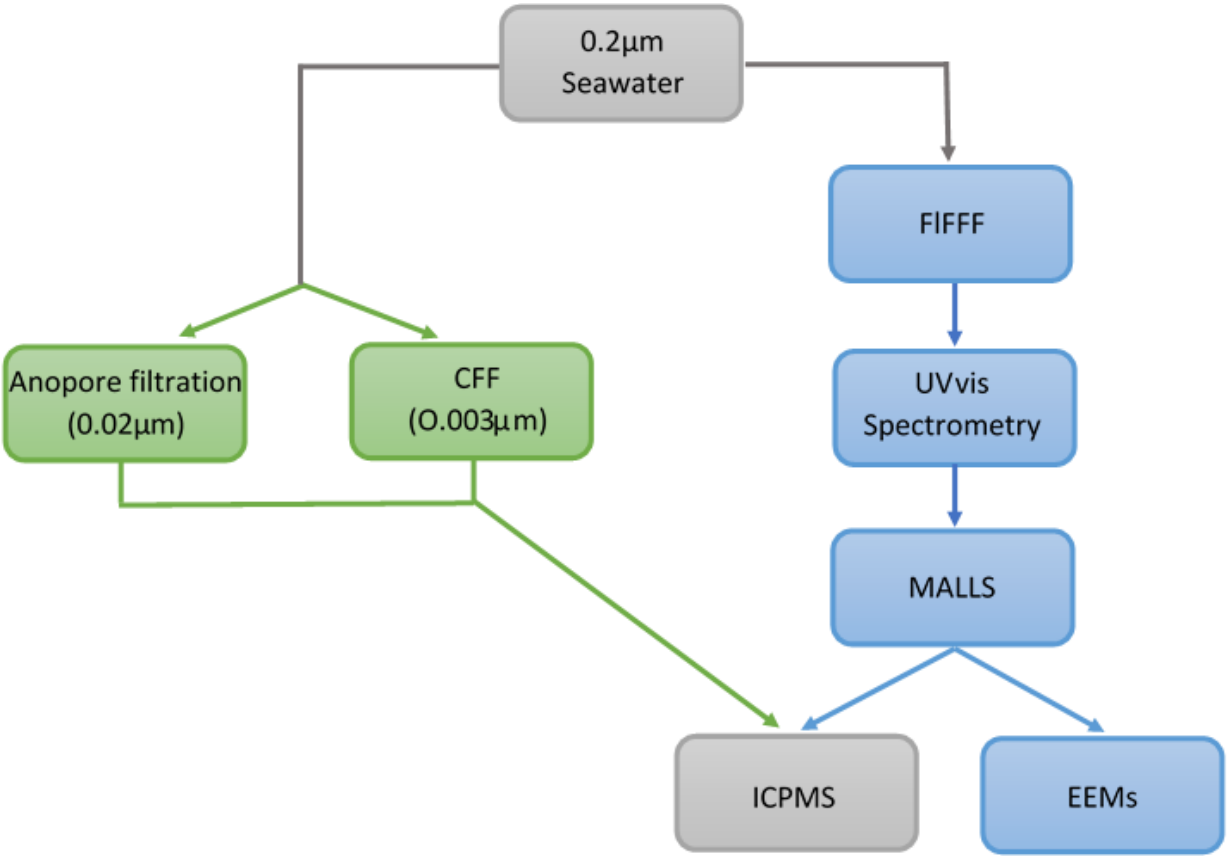

Figure 1.3: Schematic of the FlFFF—UVvis—MALLS—EEMs—ICPMS Method. This project uses this new technique along with traditional bulk fractionation techniques.

(1) Optimize FlFFF online colloid concentration, system flow rates, and processing protocols for separating the size continuum of colloidal Fe in seawater (10 kDa – 0.2 µm). Ensure FlFFF iron blanks are minimized;

(2) Optimize the offline, low-volume pre-concentration iron analysis method for coupling FlFFF to ICPMS;

(3) Determine the compositional characteristics (organic or inorganic), size (hydrodynamic diameter), and shape (sphericity) of iron colloids in coastal Maine; and

(4) Link patterns in colloidal Fe size partitioning and chemical character to biogeochemical processes by assessing spatial variability of targeted samples (offshore or estuarine, varying depths). CTD data of hydrography and chlorophyll fluorescence will guide this spatial comparison;

These four objectives are based on modifying and expanding established technologies and practices for use in new environments to answer my research questions (defined above). An immediate outcome will be a quantitative assessment of the colloidal contribution to "dissolved" iron concentrations. I first describe the results of the first two methods assessment objectives in Chapter II (Methods), and then I describe the oceanographic results of the third and fourth objectives in Chapter III (Oceanographic Application and Discussion). Finally, I conclude with a brief discussion of the future needs and applications of this new method.

.

CHAPTER II

METHODS

2.1 Synopsis

With colloidal iron (0.003 μm < cFe < 0.2 μm) comprising a significant portion of the bioavailable dissolved iron pool and with its residence time (or lability: ability to be scavenged or solubilized) being compositionally dependent, it is imperative to understand its size distribution and compositional characteristics. Thus, it is imperative to take a new approach in colloidal iron measurements that unveils the previously studied homogenized bulk phase and analyze it as a size spectrum. One promising method used previously in freshwater, but was analytically challenged in high salinity regimes, is coupling Flow-Field Flow Fractionation (FlFFF) with Inductively Coupled Plasma Mass Spectrometry (ICPMS) to quantify the size distribution of organic and metal colloids. We overcome those analytical hurdles by using an offline, low-volume pre-concentration method for iron analyses. Our new approach couples FlFFF, UV visible spectrometry (UVvis), and Multiple Angle Laser Light Scattering (MALLS) online. While FlFFF utilizes effective hydrodynamic diameter to separate colloids, MALLS uses light scattering of a number of fixed angles to calculate the molar mass and radius of gyration for each colloidal fraction, which, in turn, provides information about colloidal shape (e.g., spherical vs. fibrillar). We successfully optimized and tested the FlFFF—UVvis—MALLS—EEMs—ICPMS method to identify the compositional characteristics across the marine colloidal iron spectrum by optimizing FlFFF flow rates, optimizing FlFFF preconcentration procedures and processing protocols, and testing reproducibility. Although success in was achieved in optimizing the new method for organics characterization and iron quantification, one analytical

hurdle remains for future testing: producing a reproducible and low FlFFF system iron blank. Additionally, we tested how the freeze/thaw cycle needed to store 0.2 μm filtered seawater prior to FlFFF fractionation would affect the colloidal iron distribution, and we found negligible freezing effects for our offshore sample on the Maine continental shelf.

2.2 Introduction

Iron's biogeochemical fate in the ocean is constrained by its role as an imperative limiting micronutrient for phytoplankton and being efficiently scavenged onto the surface of particles (Boyd and Ellwood, 2010; Sunda and Huntsman, 1995). With about 40% of oceanic surface waters being limited by iron (Moore and Braucher, 2008; Moore et al., 2001) iron bioavailability affects the magnitude of carbon sequestration and oxygen production by phytoplankton primary production (Raven et al., 1999). Colloidal iron (0.003-0.2 μm), defined as non-sinking "microparticles," comprises a significant portion (up to 90% in the North Atlantic Ocean (Fitzsimmons et al., 2015b)) of the more bioavailable dissolved iron phase (Wells, 2002). Therefore, colloidal iron may play a significant role in iron bioavailability. Furthermore, the compositional characteristics of colloidal iron may not only affect its bioavailability but also its ability to scavenging and thus its residence time. As a result, it is important to understand the composition and iron concentration as a function of colloidal size.

To examine the compositional characteristics of the colloidal size spectrum, past investigations of low salinity natural waters have used the FlFFF—MALLS—UVvis—ICPMS—EEMs method coupling Asymmetrical Flow Field Flow Fractionation (FlFFF, to separate species by size), UV-Visible Spectrophotometry (UVvis, to detect carbon), and Inductively Coupled Plasma Mass Spectrometry (ICPMS, to detect iron) (Dahlqvist et al., 2004; Hassellöv et al., 1999; Lyvén et al., 2003; Stolpe et al., 2013a; Stolpe et al., 2013b; Stolpe et al., 2010; Stolpe et

al., 2005). However, due to analytical hurdles for high salinity samples, these approaches have not been applied to seawater, and thus the size distribution and composition of marine iron colloids is still unconstrained. Here, I will take the traditional method and apply it to full salinity natural water samples by fraction collecting FlFFF aliquots and analyzing by ICPMS offline, and I will couple it to a new suite of detectors to help characterize the iron colloidal composition.

2.2.1 Analytical Hurdles of Prior Methods

To date, only bulk colloidal iron concentrations have been measured in the ocean (Fitzsimmons and Boyle, 2014b; Von Der Heyden and Roychoudhury, 2015), using single pore size cutoff filters such as Anopore™ membranes (0.02 µm) or cross flow filtration systems (~1-3 nm). However, these methods homogenize the bulk colloidal phase, veiling the dynamic colloidal size spectrum and the organic or inorganic composition of the iron colloids. Thus, it is imperative to take an innovative approach in colloidal iron measurements, such as the promising technique of FlFFF. Compared to bulk colloid fractionation, FlFFF separates by size to reveal the entire colloidal iron size spectrum. In addition, carbon speciation can be evaluated by using UVvis and other detectors such as MALLS and EEMs.

FlFFF-ICPMS have not been coupled for full salinity samples because saline waters cannot be directly injected into the ICPMS. Concentrated salt matrices degrade the performance of the ICPMS when salts build up and occlude the cone orifice, lowering the sensitivity and diminishing the instrument's capabilities to accurately measure low metal concentrations (Hassellöv et al., 1999). If, instead, individual FlFFF fractions are fraction collected, a high precision measurement of metal concentration in a small volume aliquot (~ 1.5 mL) would be required, and most metal concentration analytical methods in seawater require sample volumes of at least 10 mL (Lagerström et al., 2013; Saito and Schneider, 2006; Wu, 2007). However, a

recently developed ICPMS method to pre-concentration and extract trace metals from saline waters (Lee et al., 2011) enables high precision Fe measurements in only 1 mL of seawater. Utilization of this new method allows the coupling of FlFFF, following fraction collection offline, to ICPMS. This method would be the first to apply these techniques in a full salinity oceanic environment.

Additionally, never before have iron concentrations been associated directly with both carbon absorbance and fluorescence peaks. By coupling the aforementioned UVvis and EEMs detectors with ICPMS to measure colloidal iron concentrations, we can add an important size-partitioned chemical composition piece to the iron speciation puzzle. This has been done using UVvis only in freshwater systems previously (Dahlqvist et al., 2004; Hassellöv et al., 1999; Lyvén et al., 2003; Stolpe et al., 2013a; Stolpe et al., 2013b). In a low salinity estuary (Mississippi Bight: 23.5 salinity), Stolpe et al., 2010 was the first to successfully couple FlFFF-ICPMS and associate the colloidal iron spectrum to the UVvis CDOM spectra (Figure 2.1). Their results showed two dominant colloidal populations with the smallest size fraction (0.5-4 nm) rich in both CDOM and Fe and the larger size fraction (5-20 nm) containing less CDOM and Fe (Stolpe et al., 2010). However, in a higher salinity (~30 sal) estuary (Gullmarsfjord, Sweden), one study used FlFFF-ICPMS to determine colloidal size distribution of a suite of elements, but they were unsuccessful in quantifying the metal concentrations associated with the different colloid size fractions due to the elevated salinity, and thus they only have relative concentrations (Stolpe and Hassellöv, 2010).

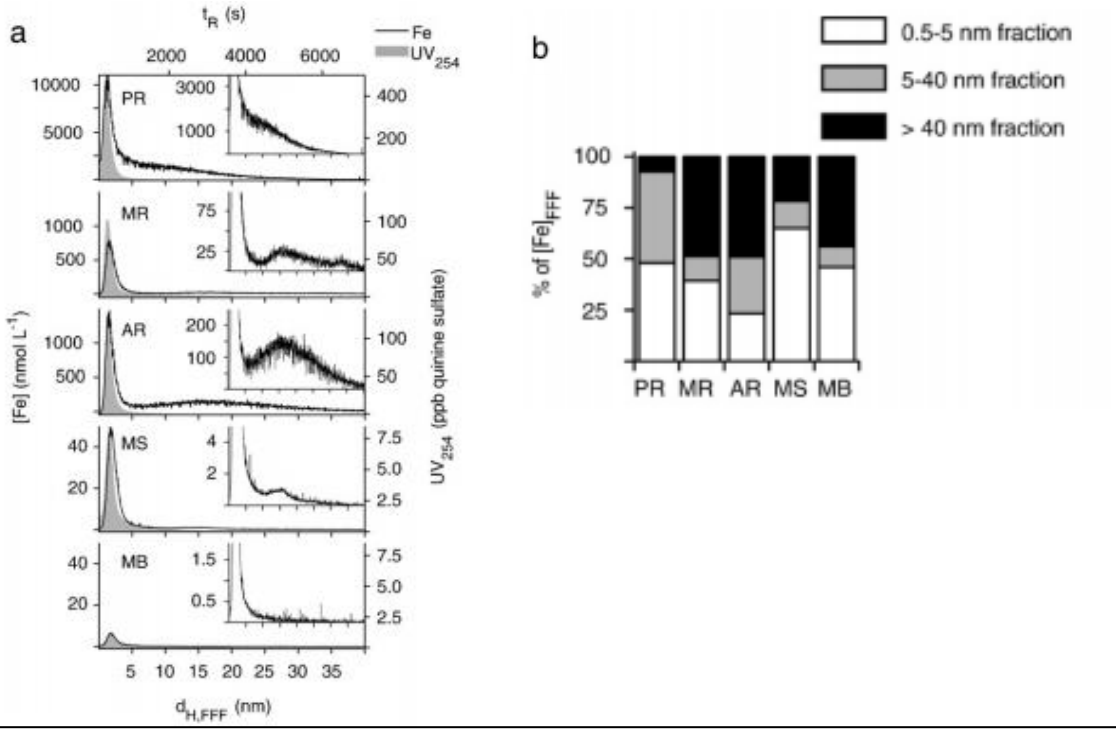

Figure 2.1: The Colloidal Spectra in the Pear River, MI River, Atchafalaya River, MI Sound, and MI Bight a. Colloidal size spectra of Fe and UV in five sampling locations (all freshwater except for estuarine water from the MI Bight (MB)). Y-axis shows concentrations in the FFF effluent, not in the actual samples. The small inserted diagrams show Fe size spectra with a smaller y-axis range. b. [Fe] between the 0.5-5 nm, 5-40 nm, and >40 nm size fractions determined by integration of the colloidal Fe size spectrum. Reprinted from Stolpe et al., 2010.

Here, we not only add the online MALLS detector, which gives complementary insight into the shape and density of the colloids as a function of colloidal size, but we also add the offline EEMs analysis, which relates the presence of fluorescent humic and protein compounds that will allow better characterization of the types of organic compounds that might bind the colloidal iron species. This is the first analysis of this kind.

2.2.2 Objectives

Because colloidal iron constitutes a significant portion of the dissolved iron phase in the coastal and open ocean, and the physicochemical speciation of colloidal iron could affect its bioavailability and scavenging fate, it is imperative to constrain the size and composition of

colloidal Fe as well as the processes that control that speciation. Thus, we pioneered a new analytical method that measures the size, shape, and composition of aqueous marine colloids by combining several techniques and instruments in tandem:

- Asymmetrical Flow Field Flow Fractionation (FlFFF) for size separation,
- UVvis-Spectrometry for organic carbon detection,
- Multiple Angle Laser Light Scattering (MALLS) for the measurement of compound radius of gyration, shape, and colloid abundance,
- Fluorescence Excitation Emission Matrix Spectroscopy (EEMS) for fluorescent carbon characterization, and
- Inductively Coupled Plasma Mass Spectrometry (ICPMS) for iron measurement.

We overcame the aforementioned analytical hurdles by taking iron analysis offline from FlFFF and implementing a low-volume ICPMS pre-concentration method (Lee et al., 2011) 1.0 mL size-separated and fraction-collected sample aliquots. In addition, we optimized this new technique and applied it to high salinity samples from the Damariscotta River estuary and offshore continental shelf waters in coastal Maine to obtain the following objectives:

(1) Optimize the offline, low-volume pre-concentration iron analysis method for coupling FlFFF to ICPMS;

(2) Optimize FlFFF online colloid concentration, system flow rates, and processing protocols for separating the size continuum of colloidal Fe in seawater (10 kDa – 0.2 μm) using an artificial seawater (ASW) carrier liquid.

(3) Ensure FlFFF iron blanks are minimized;

(4) Optimize system reproducibility to measure the size and characteristic distribution and shape of marine colloids.

2.3 Methods

2.3.1 Trace Metal Clean Techniques

This project used established trace metal clean methods during all stages of sample handling, colloid separations, and metal analysis. Low-density polyethylene bottles (60-1000 mL) and vials (2 mL) were used for sample collection and fractionated samples. Bottle cleaning procedures followed those vetted on GEOTRACES intercalibration cruses (Fitzsimmons and Boyle, 2012). All sample transfers, colloid separations, and fraction collection were completed under ISO 5 filtered air conditions at the University of Maine's Darling Marine Center (DMC) and Texas A&M University using HEPA filter modules. In addition, the FlFFF system was modified to be practically metal free by exchanging metal parts for plastic and teflon parts, and the 10 kDa nominal filter was washed with dilute acid upon installing in on the FlFFF channel.

2.3.2 Analytical Methods

Various systems for separating colloids, measuring carbon speciation, and iron concentration were coupled to evaluate the iron colloid size and composition continuum. Before putting samples through these systems, all samples were passed through a 0.2 μm filter to remove particles, and bulk colloidal ultrafiltration techniques (0.02 μm Anopore ultrafiltration and 10 kDa cross flow filtration) were applied to the same samples using methods evaluated and intercompared previously (Fitzsimmons and Boyle, 2014a). In addition, all filtration techniques including these and FlFFF were completed 2 to 5 hours after sample collection to minimize the exchange of colloidal matter to bottle walls and aggregation processes within the sample before size separation. If the samples could not be analyzed in that timeframe, then samples were frozen, based on the marine iron ligand literature (Buck et al., 2012), which indicates that freezing/thawing samples does not change the concentration and binding strength of organic

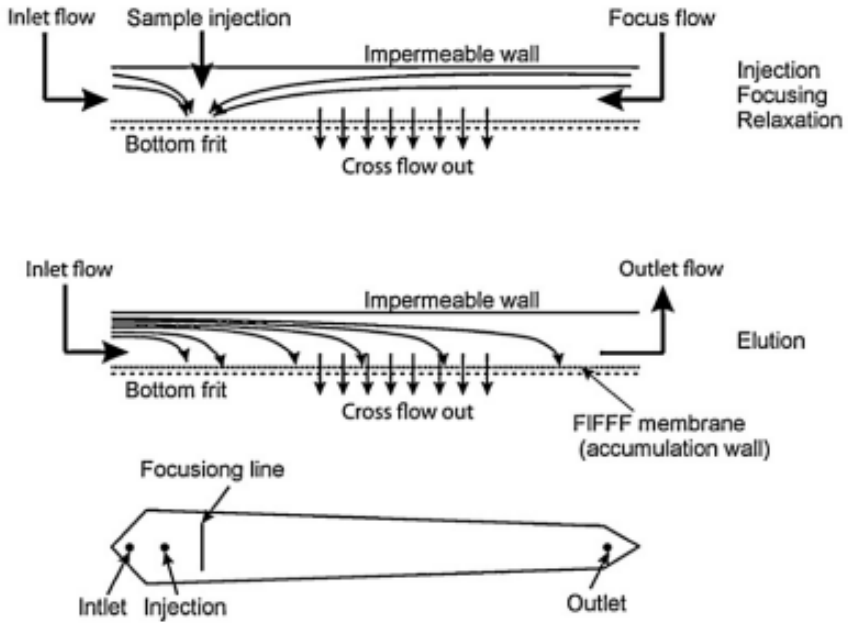

Figure 2.2: Schematic of Asymmetrical FlFFF Channel Schematic. Reprinted from Baalousha et al., 2011.

ligands. We will also test whether freezing/thawing also maintains iron physicochemical speciation using this FlFFF-UVvis-ICPMS method (see below).

2.3.2.1 Colloidal Size Separation: Flow Field Flow Fractionation (FlFFF)

FlFFF is a chromatography-like elution technique based on hydrodynamic principles, where colloid particles are separated due to their interaction with a cross-flow carrier liquid, applied over the cross section of a ribbon-like channel that is thin (~250 μm) and flat (~centimeter length) (Figure 2.2) (Baalousha et al., 2011). Here, the carrier solution was artificial seawater (ASW) that mimics the matrix of the sample solutions, such that the sample remains unaltered by the FlFFF processing. The ASW was first run through a column of Chelex resin (to remove metals) and then ultrafiltered (at 5 kDa nominal pore size, to remove any resin released during cleaning). This study is the first to use ASW as the carrier solution while coupling FlFFF to ICPMS, since previous studies worked only with lower salinity samples where

15 mmol L^{-1} NH_4NO_3 buffer (pH 7) was used as the carrier for freshwater and 55 mmol L^{-1} NH_4Cl(aq) (pH 8) was used in saltier (estuarine) water to resemble ~10% of sweater concentration to not clog the ICPMS cones (Stolpe and Hassellöv, 2007; Stolpe et al., 2005).

The bottom wall of the FlFFF channel has a permeable (10 kDa) ultrafiltration membrane where the cross flow and soluble-sized material pass through to waste so that only the colloidal sized particles are retained within the channel (Baalousha et al., 2011). Two flows govern the FlFFF size exclusion chromatography elution: the (parabolic) sample flow and the cross flow. The sample in the ASW carrier solution flows tangentially to the ultrafiltration membrane, and a parabolic flow profile is created by a function of the thin, ribbon-like channel, as the walls drag the flow on the top and the bottom of the channel, producing a faster laminar flow in the center of the channel. The cross flow through the membrane creates an opposing diffusion force, where smaller compounds with higher diffusivities can diffuse against the cross-flow better and thus remain in the center of the chamber, while larger colloids remain lower towards the wall of the parabolic flow profile (Baalousha et al., 2011). The unequal velocities in laminar flow created by the parabolic flow profile down-channel, with constant Brownian motion based on diffusion, effectively separates the colloids in a 20 mL sample by producing a gradient of different size fractions (~eighteen 1.5 mL aliquots) that elute through the channel, with the smaller colloids eluting earlier than the larger colloids (Baalousha et al., 2011). Based on the diffusion coefficients of the separately eluted colloid size fractions, the hydrodynamic diameter, e.g. the diameter of a compact sphere, can be calculated using Stokes Law (Baalousha et al., 2011).

However, there are some major challenges when implementing FlFFF that may bias the results. FlFFF is based on the diffusion coefficient which assumes every particle is spherical (Baalousha et al., 2011), while in reality they can have various shapes: spherical, elongated,

fibrillar, etc. (Stolpe and Hassellöv, 2010). Therefore, a large fibrillar colloid could elute out as a smaller size, similar to how spaghetti can escape through the holes in a colander, which could ultimately bias the size partitioning data (Baalousha et al., 2011). Other issues that could also affect the eluted size fractions are: sample loss through the ultrafilter membrane, particle membrane interactions that can clog the pores on the channel membrane, sample dilution with carrier, sample component washing (alteration), or overloading of the membrane (Baalousha et al., 2011). Thus, these factors must be taken into consideration when interpreting FlFFF data. To help mitigate these biases, we couple MALLS to FlFFF to evaluate the shapes of the colloids.

The procedure for FlFFF includes three steps: sample loading and preconcentration, relaxation or focusing, and elution or colloid separation (Lyvén et al., 1997). The AF-2000 FlFFF instrument that was employed in this project has been modified to allow large volumes (in our case 20 mL) of ultrafiltered seawater to be back-loaded into the channel, where the accumulating colloids are focused at the head of the channel (into ~70-140 μL) during the first 50 minutes of run time. This small volume allows most colloids to start down the channel at the same time, which minimizes the issue of "blurring" of the size partitioning. We had some concern that the 286x pre-concentration at the channel head would allow a change in colloidal size and shape distribution during pre-concentration, though others have found that focusing even larger volumes of up to 500 ml does not appreciably alter the size distribution of organic colloids (Floge and Wells, 2007).

Next during the relaxation stage, the sample no longer experiences a large carrier focusing force pushing it up to the head of the channel. Then, the colloids balance the forces of Brownian diffusion and crossflow velocity, resulting in the separation of colloids along the membrane. This process of separation also occurs during preconcentration but is allowed to

continue after for a short period after sample focusing but before the channel flow starts. The third phase, elution, begins when the channel flow pumps the carrier solution from the head of the channel, pushing the separated colloids through so that they elute out of the end of the channel. This channel outflow then passes through both the UVvis absorbance detector and the MALLS detectors online before being fraction collected into ~eighteen 1.5 mL aliquots. Each 1.5 mL fraction was acidified to pH 2 using Optima-grade hydrochloric acid (to 0.012 M HCl) in order to mitigate metal adsorption onto vial walls.

Prior to running each sample through the FlFFF, a daily FlFFF procedural blank was run through the system using the chelexed and ultrafiltered artificial seawater as the carrier and ultrapure water (18.2 MΩ-cm Milli-Q, MQ, Millipore) as the sample. The entire FlFFF run takes ~100 minutes with the channel outflow rate totaling 0.5 mL/min.

In addition, time was minimized between sample collection and FlFFF processing (<3 hours) to limit the potential bottle effects of storage, such as colloid sorption to bottle walls and colloidal instability (Fitzsimmons and Boyle, 2012). However, it has also been found that bottle storage for as long as 24 hours has minimal effects on colloid size distribution and that freezing does not affect the integrity of the organic colloidal size spectrum (Floge and Wells, 2007; Wells and Goldberg, 1994). Therefore, we minimized storage time and directly evaluated the effect of freezing (-20˚C) on the colloidal size distribution in fresh-frozen comparison tests on the same sample (see below).

Before each new sample run, the entire FlFFF-UVvis-MALLs system experienced a cleaning procedure of ~20 minutes each of flushing with 5% methanol (to wash out the trapped organics) and then MQ, and then dilute acid (trace metal grade 0.1M HCl) was loaded into the system and left overnight before final flushing with MQ until the pH was >6 and the MALLS

detector angles read <1.5 for the scattering intensity values. Finally, the chelexed and ultrafiltered ASW was flushed through the system to prime it for the sample.

2.4.3.2 Carbon Speciation: UV-Visible Spectrometry (UVvis)

UV-Visible spectrometry is an online, non-destructive detector to FlFFF that uses light absorbance (wavelength: 254 nm) to estimate the chromophoric dissolved organic matter (CDOM) within the colloid size spectrum (Wells, 2004). Without a carbon signature, the colloidal fraction can be assumed to be predominantly inorganic. Therefore, UVvis spectrometry aids in distinguishing whether the colloidal iron is predominantly inorganic or organically bound.

2.4.3.3 Colloidal Size and Shape: Multiple Angle Laser Light Scattering (MALLS)

MALLS is an online, non-destructive detector that measures the light scattered by particles in a suspension at different fixed angles in order to determine the absolute molar mass and the size of the particles (Baalousha et al., 2011). The size of the particles is determined by the radius of gyration, or the root mean square distance of the particle's parts from its center of gravity (Baalousha et al., 2011). Essentially, the radius of gyration represents the distribution of mass within the particles (Baalousha et al., 2011). This coupling technique compensates for the spherical assumptions of the FlFFF technique by providing information on the particle shape in parallel to particle size, allowing calculation of a shape factor that indicates how far a particle deviates from a perfect sphere (Baalousha et al., 2011). For example, if two particles have the same hydrodynamic diameter but different radii of gyration (Rg), then this indicates different mass distribution with in the particle and thus different particle shapes.

Calculating the ratio of hydrodynamic radius (Rh, from Stoke's Law and determined from FlFFF elution time) to radius of gyration (determined from MALLS) yields a shape factor (Rg/Rh), which has a value of 0.775 for spherical particles but increases as particles deviate from

the spherical shape (Kammer et al., 2005). In addition, an integration of MALLS scattering can be used as a rough estimation for colloid abundance; however, it is not an exact measure because not all particles scatter equally. For example, organic colloids that absorb more light would not scatter as efficiently as a dense, inorganic colloid. Therefore, we can measure the sphericity, size, and a rough abundance of colloids using MALLS.

We used a PostNova MALLS, with collection at angles 35°, 50°, 75°, 90°, 105°, 130°, and 145°. Each sample was run in triplicate through the FlFFF-UVvis-MALLS online system, with a single set of fraction-collected samples created for destructive analyses each time for a total of three replicate fraction sets per sample. One set was dedicated to the EEMs carbon speciation measurements (unacidified) while the other two sets were stored as duplicates for ICPMS iron analysis (acidified as above). In total, ~500 mL of 0.2 μm filtered sample was needed to properly flush and prime the 20 mL sample loop, and to complete the three triplicate runs.

2.4.3.4 Carbon Speciation: Fluorescence Excitation Emission Matrices (EEMs)

A Fluoromax-2 Spectrofluorometer (from JY-SPEX, Edison, NJ) was used to generate EEMs that characterize Fluorescent Dissolved Organic Matter (FDOM) across each colloidal size fraction generated by the FlFFF. The EEM fluorometer was set to use excitation wavelengths between 200 and 500 nm and emission wavelengths between 200 and 700 nm, with 5 nm intervals. By comparing the excitation/emission fluorescence peaks across the light spectrum, we can determine the predominant fluorescent organic phases (protein-like or humic-like) (Coble, 1996). If the peaks are protein-like, we can tease out particular fluorescent amino acids (e.g. tryptophan vs. tyrosine), giving valuable insight into the role of phytoplankton byproducts on the FDOM size spectrum (Coble, 1996). For instance, high values of tyrosine

fluorescence have been associated with elevated chlorophyll values (Mayer et al., 1999) due to a bloom of *Skeletonema costatum* diatoms (Wong and Townsend, 1999). Characterizing the protein-like organic colloids can provide a wealth of information about the dynamics of the local biological communities. Furthermore, if humic-like peaks are present within the matrix, terrestrial or marine humic signatures can be distinguished. When coupling EEMs to FlFFF, it has been found in the Damariscotta River estuary that protein-like materials occurred mainly in the smallest colloidal size fraction, while the largest size fraction consisted of predominantly humic-type materials (Boehme and Wells, 2006). Ultimately, EEMs provides insight into which portions of the colloidal iron spectrum were biotcally or abiotically associated.

EEMs of the FlFFF separated aliquots were measured on the Spectrofluorometer using a quartz low volume (3.5 mL) microcell (Hellma Industries). Prior to measurement, the FlFFF separated fractions were stored frozen until analysis (Boehme and Wells, 2006). The instrument is equipped with a 150-W Xenon arc lamp, a single excitation monochromator (1200 grooves/mm) blazed at 500 nm and a single emission monochromator (1200 grooves/mm) blazed at 700 nm, and an air-cooled, red-sensitive photomultiplier tube. Analysis was done in a quartz cell maintained at 20˚C with a temperature controlled holder, and the quartz cell was rinsed with methanol between samples to remove organics. For each set of fractionated samples, MilliQ water and artificial seawater blanks were run so that background fluorescence could be subtracted from the sample signal. Raw EEMs data were converted to user-friendly formats using a purpose-built MATLAB code, and then EEMs data were plotted using the freely available "eemR" package in R and also manually. Ultimately, the size-fractionated results were compared with the Fe concentrations (ICPMS) and colloidal shape factors (MALLS) across the

colloidal spectrum to determine the likely source and composition of organic matter binding colloidal iron in coastal waters.

2.4.3.5 Iron Concentrations: Inductively Coupled Plasma Mass Spectrometry (ICPMS)

ICPMS is an offline destructive detector that provides multi-elemental analysis of up to 45 elements in a single measurement (Baalousha et al., 2011). To conduct elemental analysis, the liquid sample is aspirated into an aerosol that is transported into the inductively coupled plasma; this plasma is produced by electromagnetic induction in ionized argon gas, in which most elements are atomized and ionized (Baalousha et al., 2011). Iron was quantified using isotope dilution using ^{57}Fe spike. We equilibrated a known amount of spike of known isotopic composition with a gravimetrically determined sample volume, and by measuring the isotopic ratio of the mixture, the concentration was determined with high accuracy and precision. Isotope dilution also helps reduce errors associated with ICPMS sensitivity fluctuations and variability in recovery (Wu and Boyle, 1997).

However, ICPMS is challenged by the small fractionated volumes that FlFFF elutes. Previous techniques to preconcentrate iron and perform isotope dilution often required too much volume (≥10 mL) per analysis (Bruland et al., 1985; McLaren et al., 1985; Obata et al., 1993). The earliest low-volume method involved $Mg(OH)_2$ co-precipitation coupled to isotope dilution (Saito and Schneider, 2006; Wu, 2007; Wu and Boyle, 1997) and only required 1.5 mL of seawater; however, the Mg-rich matrices resulted in salt buildup that could clog the ICPMS nebulizer and occlude the ICPMS cones (Lee et al., 2011). This limited ICPMS runs to only a few hours, suppressed ICPMS signal strength, and required frequent thorough cleaning of both the nebulizer and the cones and was thus non-ideal for routine measurements (Lee et al., 2011). Subsequently, a new preconcentration method by Lee et al. (2011), made measuring the low iron

concentrations in the same low volume sample colloidal fractions (~1.5 mL) possible without Mg co-precipitation. This method is a simple and highly accurate low-blank method that achieves salt-separation of a stable isotope spiked sample with a single batch extraction onto nitrilotriacetate (NTA)-type Superflow® chelating resin beads (Lee et al., 2011). Using this method, the low salts prevent clogging of the cones while retaining the high accuracy of the isotope dilution technique. This allows us to overcome the analytical hurdles that formerly challenged the study of iron colloids in high salinity environments and also unlocks our ability to measure iron colloids with FlFFF and ICPMS in seawater.

Each colloidal fraction (acidified to pH 2 for >8 weeks) underwent batch pre-concentration onto acid cleaned nitrilotriacetate (NTA Superflow®) resin and isotope-dilution ICPMS (Lee et al., 2011). For this method, 25 µL of well-calibrated (24.99 nM) Fe spike (^{57}Fe was used, although ^{54}Fe can also be used) was added to an unbuffered 1.3-1.5 mL seawater sample alongside 10 µL of ultrapure hydrogen peroxide (0.75%, SupraPur H_2O_2), followed by pre-concentration of Fe onto NTA functional groups bound to a polystyrene bead (Qiagen Inc., Valencia, CA). After at least 30 hours, the seawater-bead mixture was centrifuged, and the supernatant (seawater) was siphoned off. Then, the NTA beads were rinsed with MQ water, centrifuged, and re-siphoned three times to reduce the concentrations of salts in the sample through repetitive dilution. Finally, the beads were acidified with 150 µL of nitric acid (0.5 M, Optima grade) in order to release the sample from the beads. This 10 x concentrated solution was then analyzed by ICPMS in medium resolution using the High-Resolution Inductively Coupled Plasma Mass Spectrometer Element XR at the R. Ken Williams ’45 Radiogenic Isotope Geosciences Laboratory, Texas A&M University. To make sure that the beads in the solution did not enter the instrument, a frit filter was placed on the tip of the sample probe.

2.3.3 Fresh-frozen storage tests

Due to the extended time required for analysis of each sample by FlFFF (~14 hours for three replicates and a procedural blank), it was necessary to store samples for days between collection and analysis, especially in the event that several samples were collected in a single sampling trip. At room temperature, unacidified seawater samples undergo sorption to the walls of bottles (Fischer et al., 2007; Fitzsimmons and Boyle, 2012; Johnson et al., 2007). However, because electrochemical measurements of dissolved iron-binding ligands have found that freezing samples preserves the metal concentrations and ligand binding strength and concentration (Buck et al., 2012), and we similarly opted to freeze filtered samples at -20°C between collection and FlFFF processing to avoid bottle sorption and alteration of ligands.

However, we hypothesized that freezing and thawing might induce aggregation and/or disaggregation of the colloids, affecting the overall colloidal iron size distribution. To evaluate this, we collected samples at both the Maine continental shelf Station 1 and Damariscotta Estuary Station 2 (station map in Chapter 3) on 13 November 2017, and we analyzed them fresh and frozen. The fresh samples were in stored in two ways after immediately being 0.2 μm filtered. The offshore fresh sample was FlFFF fractionated the day of collection (11-13-17) and the estuarine fresh sample was refrigerated for <24 hours and fractionated the following day (11-14-17). The frozen samples were frozen after 0.2 μm filtration for 36 hours for the offshore sample and 60 hours for the estuarine sample.

2.4 Experimental

2.4.1 Standardizing and Calibrating: FlFFF

Both running full salinity marine samples and artificial seawater through the FlFFF system, that is composed of tiny capillary tubing prone to clogging and running without a slot

Table 2.1: Optimized FlFFF Flow Rates. Determined for an artificial seawater carrier and a marine sample.

	Preconcentration	Relaxation	Elution		
Time (min)	**0-50**	**50-51**	**51-55**	**55-75**	**75-100**
Cross Flow (mL/min)	6.5	5.3	5.3	Power decrease	0.2
Tip Flow (mL/min)	0.4	0-5.8	5.8	Power decrease	0.7
Focus Flow (mL/min)	6.6	6.6-0	0	0	0
Channel Flow (mL/min)	0.5	1.3-0.6	0.5	0.5	0.5

pump (it failed, was no longer viable, and PostNova Analytics no longer manufactures replacements) pulling out the top volume of the column, required an optimization of flow rates (Table 2.1). Each of the preconcentration, relaxation, and elution steps were then tested using a variety of qualitative and quantitative measures, as discussed below.

FlFFF preconcentration was tested qualitatively using a blue dye that was loaded into the FlFFF channel through a 2 mL sample loop and processed at "normal" sample flow rates. This allowed a visual assessment through the channel window of whether the dye was properly focused at the head of the channel during preconcentration. The blue dye did visually appear focused into a volume <140 μL, confirming that the pumps were appropriately pre-concentrating the sample.

Standardization of the colloidal separation during the relaxation and elution steps were completed by processing molecular weight standards through the 2 mL sample loop using the flow rates given in Table 2.1 on 11-19-17. Three different molecular weight polystyrene sulfonate standards (PSS) (14.9, 29.1, 63.9 kDa) and one bovine serum albumin (BSA) protein standard (double elution peak: 9.25 & 131.9 kDa) were processed through the FlFFF, and the elution time at their maximum peak height was recorded (Figure 2.3a). We compared these

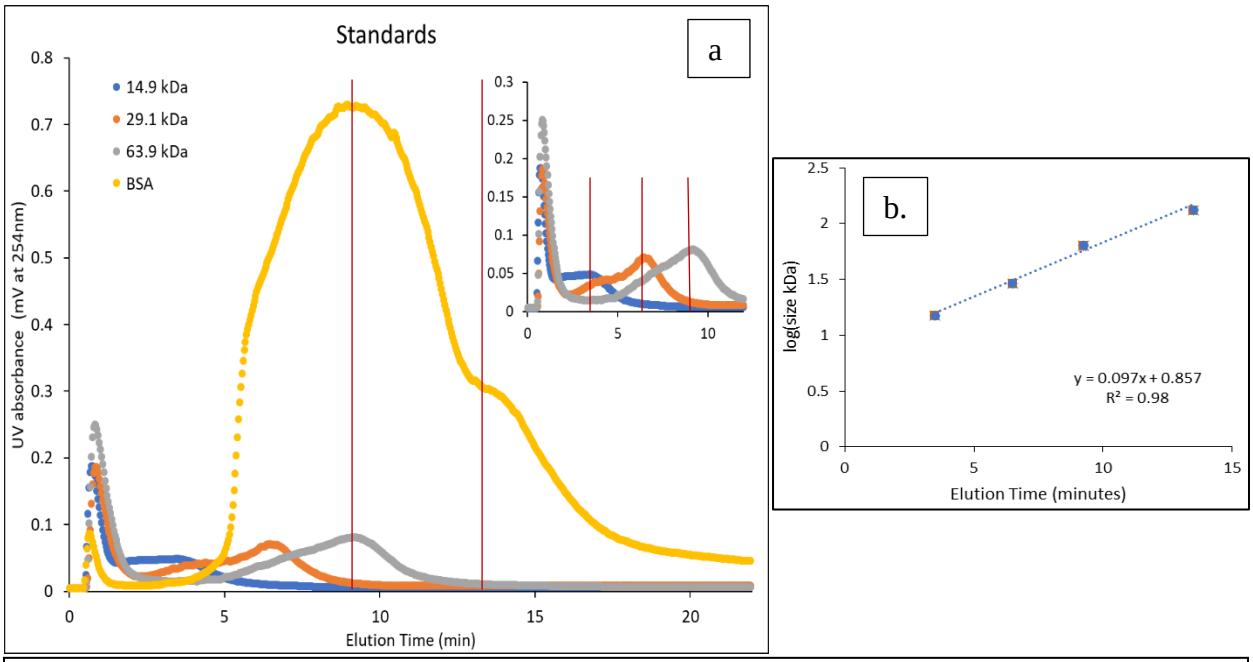

Figure 2.3: Standard Calibration. a. PSS and BSA elution times. The smaller figure shows elution time from 1-12 minutes without BSA. There is a void peak for all standards rom 0-1.5 minutes. Red line indicates the apex of standard peak b. Equation generated from the log (size kDa) of the standards (PSS and BSA) y=0.097x+0.857.

elution times with the log of their molecular weights to generate the linear relationship in Figure 2.3b (y = 0.097x + 0.857, R^2=0.98). This standardization procedure was completed two previous times using only the PSS standards (7-6-17 and 10-29-17) and the linear relationship was the identical for these three standards (y = 0.110x + 0.777, R^2= 1.0).

To convert the weights generated from this equation, we compared it to a set of equations based on the assumed specific volume (inverse density) of a protein (Erickson, 2009).

$$V(nm^3) = \frac{(1.05\ cm^3/g) \times (10^{21}\ nm^3/cm^3)}{6.023 \times 10^{23}\ Da/g} \quad \text{(Eq. 1)}$$

Using the specific volume of PSS (v= 1.05cm^3/g) instead of a protein (v= 0.73cm^3/g), we modified Equation 1 (Erickson, 2009) and used it to generate a new equation that calculates the minimum molecular diameter from M (the molecular weight of PSS standard).

Standard (MW kDa)	Elution (min)	Erickson d_{min}(nm)	Giddings d_H(nm)
14.9	3.5	3.56	2.68
29.1	6.5	4.45	4.98
63.9	9.25	5.78	7.08

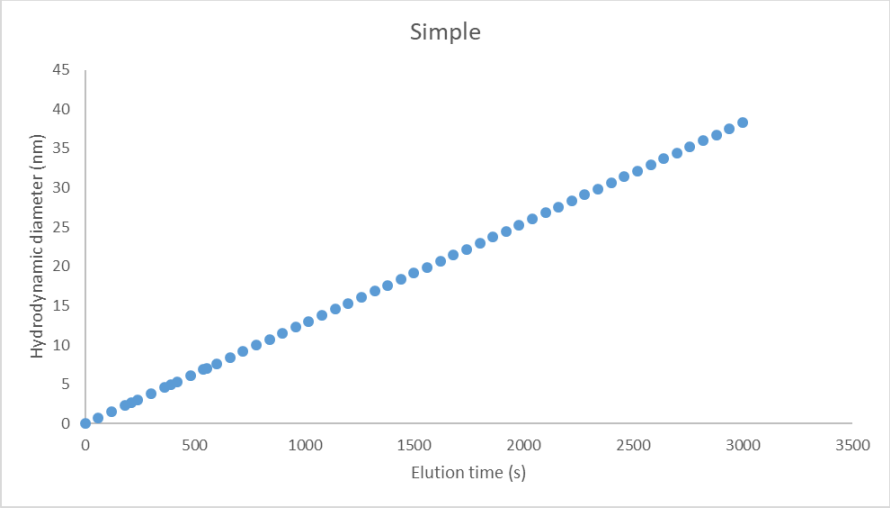

Table 2.2: Molecular Weight Standard Elution Times. Shows the minimum diameter (Erickson et al., 2009) and the hydrodynamic diameter (Giddings et al., 1976) of the colloid that would elute at the elution time and molecular weight of the PSS standards. Figure 2.4: Hydrodynamic radius with elution time using equation 2.

$$Minimum\ Molecular\ diameter\ (nm) = 0.0723M^{\frac{1}{3}} \qquad \text{(Eq. 2)}$$

By combining Equations 1 and 2, we were able to convert elution time into molecular weight and then into minimum molecular diameter (and radius). The results for the four standards are tabulated in Table 2.2. However, the Erickson equation is based on several assumptions (including that the colloids are spherical and of equal density) and does not account for the hydrodynamic radius, or the effective radius of a colloid moving through a liquid, which is how FlFFF instruments' elution time is determined. Ideally, the hydrodynamic radius should be slightly larger than the minimum diameter of the colloid because it also includes the waters of hydration or the shell of water, one to two molecules thick, that surrounds the colloid (Erickson, 2009).

Thus, to calculate the hydrodynamic radius, we modified the "simplified" relation from (Giddings et al., 1976) that equates elution time (t_r) to the square of the column width (w = 250 µm in our FlFFF system) and the inverse of the solute's diffusion coefficient (D, in m^2/s):

$$t_r \sim w^2/2D \qquad \text{(Eq. 3)}$$

The diffusion coefficient can be converted to hydrodynamic radius using the Stokes-Einstein relationship of Brownian motion:

$$R_h = \frac{k_b T}{6\pi\eta D} \qquad \text{(Eq. 4)}$$

where R_h is the hydrodynamic radius (m), k_b is the Boltzmann constant (1.38064852 x $10^{-23} m^2$ kg $s^{-2}K^{-1}$, T is temperature (294.15 K), and η is solvent viscosity (1.08x10^{-3} kg/m•s). The calculated hydrodynamic diameters for the four standards using Equations 3-4 are also tabulated in Table 2.2. We note that the "simplified" Giddings Eq. 3 was used instead of the more complex Giddings equation (see Giddings et al. 1976), which accounted for the changing flow rates, because the results of the complex equation were unrealistic overestimates of the size of our standards (Table 2.2). Thus, Equations 3-4 were chosen to associate hydrodynamic diameter to elution time and molecular weight (Figure 2.4). Because the dyes and standards were not trace metal clean, the system was rigorously cleaning for >12 hours before any samples were processed through the FlFFF.

One of two types of blanks were run prior to each sample, each using ASW as a carrier: 20 mL sample of MQ water or a 20 mL sample of ASW. Prior to these tests, it was not clear which blank would be a better approximate of the procedure blank, so both were run at the beginning of the sample runs to assess which would be a cleaner and more accurate blank. The

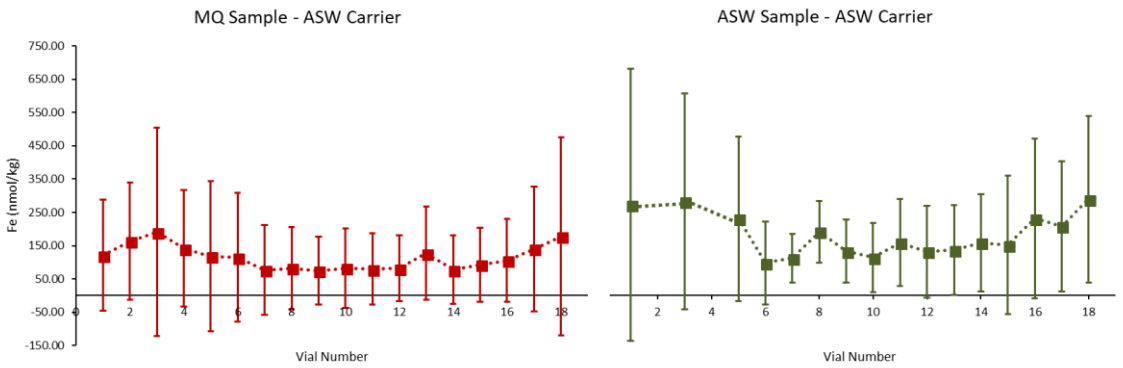

Figure 2.5: FlFFF System Blanks: averaged fractions. Comparison of ASW carrier solution with MQ sample and ASW sample showing each averaged fraction (increasing vial number coincides with increasing colloidal size). MQ is relatively cleaner with an overall average of 103 ± 150 nmol/kg with RSD 147% and n= 11 runs and ASW is relatively dirtier with overall average of 181 ± 194 nmol/kg with RSD 107% and n= 5 runs.

cumulative results of these blanks showed that running the MQ as a sample was relatively (but not significantly) cleaner, with an average of 103 ± 150 nmol/kg and a relative standard deviation (RSD = standard deviation/mean in percent) of 147% (n = 11 runs), than running ASW as a sample, with an average of 181 ± 194 nmol/kg and an RSD of 107% (n = 5 runs) (Figure 2.5). On each day, samples were run in triplicate with two sets of FlFFF samples saved for iron analysis to assess the reproducibility between each FlFFF run and the last set of samples was saved for EEMs analysis.

2.4.2 Standardizing and Calibrating: MALLS

During the rigorous cleaning between each sample when MQ is flushed through the system after dilute acid, the different MALLS angled lasers are monitored to see that the scattering intensity of colloidal material is below 1.5. Once the reading of colloids through the system are minimized, the FlFFF sample run can then be checked for the zeroed UVvis reading described in Methods 2.4.3.

The MALLS data was processed and quality controlled using a MATLAB script developed by Kathleen Thornton at the DMC. This script goes beyond PostNova's software standard raw MALLS data analysis by additionally analyzing (smoothing erratic signals) individual angles and selecting the best angles (angles that had a "smooth" enough or certain output) to include in shape analysis (Rg). When the scattering intensity had too much uncertainty for an individual angle to show a reasonable value (signal is too erratic, not smooth output), the script excluded the data for smoothed scattering intensity per individual angle and for Rg calculation. Rg calculation was calculated using the Zimm first-order fitting method (Kammer et al., 2005). We chose to present the 50° MALLS data because it was one of the "smoother" angles that was representative of the majority of the angle's outputs.

2.4.3 Standardizing and Calibrating: UVvis

Daily, after cleaning the FlFFF system overnight and loading the sample onto the 20 mL sample loop, the FlFFF flows are set to their preconcentration step levels (Table 2.1), and the UVvis system is calibrated. The UVvis baseline was allowed to stabilize at this flow rate, and then it was zeroed and monitored to ensure it read zero for at least a couple of minutes. Once the UVvis detector is zeroed and stabilized, the run is then started with the preconcentration focusing step where the sample is loaded into the FlFFF column.

When analyzing the UVvis data, some had an increasing baseline absorbance values over the course of the run. This occurs when sticky carbon colloidal material gets trapped within the detector and builds up over the course of the day (why we clean with methanol at the end of a FlFFF run day: to wash out the organics).

To account for this in our evaluations and zero our baseline, the slope (linear regression) would be subtracted from the raw UVvis values so that the adjusted data product would have an overall baseline slope of ~0 (Equation 5)

(Eq. 5)

$$U_f = U_i - (mx + b)$$

where U_f is the zeroed UVvis value, U_i is the initial or raw UVvis value, m is the slope of the linear regression, x is the elution time (minutes) and b is the y-intercept.

2.4.4 Standardizing and Calibrating: EEMs

Coble (1996) found that fluorescent dissolved organic matter (FDOM) compounds have fluorescence patterns at characteristic excitation and emission wavelengths that allows distinction between protein-like and humic-like FDOM, as well as specific characterization of tyrosine vs. tryptophan proteins and marine vs. terrestrial humic compounds. These characteristic "Coble wavelengths" are tabulated in Table 2.3. We also chose to include a second set of lower-wavelength excitation emission wavelengths because (Mayer et al., 1999) discovered that these lower excitation wavelengths (220-230 nm) were particularly beneficial for FDOM characterization in two central coastal Maine estuaries (Kennebec and Damariscotta), which overlap with our sampling region.

Table 2.3: EMMs Low and High Wavelengths. Low-wavelength (Mayer et al., 1999) and High-wavelength (Coble 1996) wavelengths used for measuring EEMS.

Peak		**Coble**		**Mayer**	
		Ex_{max}(nm)	Em_{max}(nm)	Ex_{max}(nm)	Em_{max}(nm)
B	Tyrosine-like, protein-like	275	310	220-225, 275-280	305
T	Tryptophan-like, protein-like	275	340	215-220, 275-280	340
A	Humic-like	260	380-460	240	440
M	Marine humic-like	312	380-420	310	420
C	Humic-like	350	420-480		

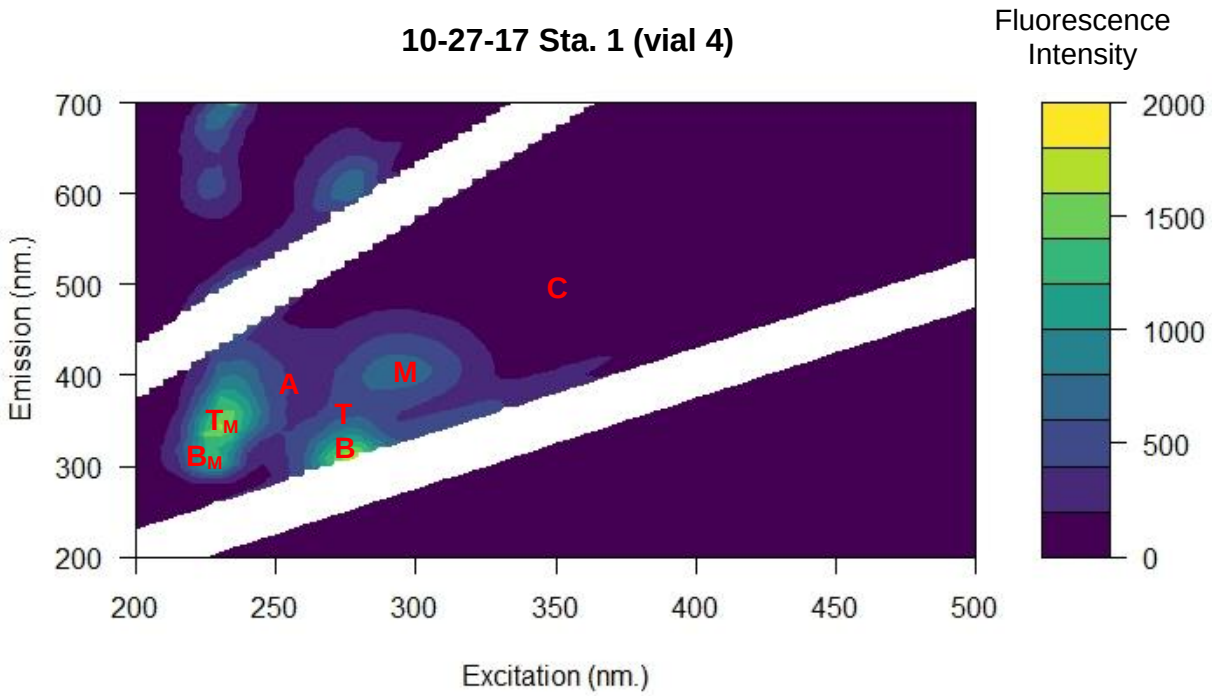

Figure 2.6: EEMs. Excitation emission matrices for Offshore Station 1, vial #4. Red letters indicate various coble peaks, and letters with subscript M indicate low excitation emission delineated by Mayer. B is tyrosine protein-like, T is tryptophan protein-like, A is terrestrial humic-like, M is marine humic-like, and C is humic-like.

For initially EEMs processing and plotting, the "eemR" package in R was used (Figure 2.6). For these plots, the Rayleigh scattering and Raman scattering were removed, and then the EEMs from all 18 fractions of a single sample could be compared, and the fluorescence at the Coble wavelengths could be automatically tabulated. However, the eemR package does not consider Mayer peaks nor monitor for slight adjustments in peak location, and so we manually collected the maximum fluorescence at both Coble and Mayer wavelength ranges for each sample.

2.4.5 Standardizing and Calibrating: ICPMS

The low-volume Lee et al. (2011) extraction and preconcentration method for iron analysis was optimized for a different ICPMS instrument than the Thermo Element XR high

resolution ICPMS that we have at TAMU, and thus a series of internal checks were required to establish this method at TAMU. First, a rigorous ^{57}Fe spike calibration was accomplished by analyzing gravimetrically-constrained, high-concentration mixtures of spike and a known iron standard.

The original TAMU spike was a secondary ^{57}Fe spike made in August 2016 by Fitzsimmons from the primary dissolved Fe spike at Rutgers dissolved in April 2015. The Rutgers secondary ^{57}Fe spike was calibrated over the course of six separate runs, using (Berglund and Wieser, 2011) for the true ratios (^{56}Fe /^{57}Fe: 43.299) and natural abundances (^{56}Fe: 91.8 & ^{57}Fe: 2.1 %). This Rutgers spike calibration resulted in iron concentration of the TAMU spike of 24.99 nmol/kg and 93% pure ^{57}Fe.

To re-calibrate the spike and calculate isotope dilution at TAMU, we used Equation 5 below, where c_x is the elemental concentration in the sample (nM), c_y is the elemental concentration in the spike (nM), m_x is the weight of sample in the blend (mL), m_y is the weight of spike in the blend (mL), R_y is the certified isotope ratio measured in the blend, R_x is the natural isotope ratio of ^{56}Fe /^{57}Fe, K is the mass bias correction coefficient (in % bias per atomic mass unit), f_x is the abundance of spike isotope in the sample, and f_y is the abundance of spike isotope in the spike (Equation 6):

$$c_x = c_y \cdot \frac{m_y}{m_x} \cdot \frac{\left(R_y - KR_b\right)}{\left(KR_b - R_x\right)} \cdot \frac{f_y}{f_x} \qquad \text{(Eq. 6)}$$

The resulting spike concentration was 24.99 nmol/kg and 93% ^{57}Fe purity.

Then, seawater samples from Station ALOHA that had been analyzed previously in the lab using other established techniques (Lagerstrom et al. 2012, using a different, mixed isotope spike) were re-analyzed by this new method in order to practice trace-metal-clean sample

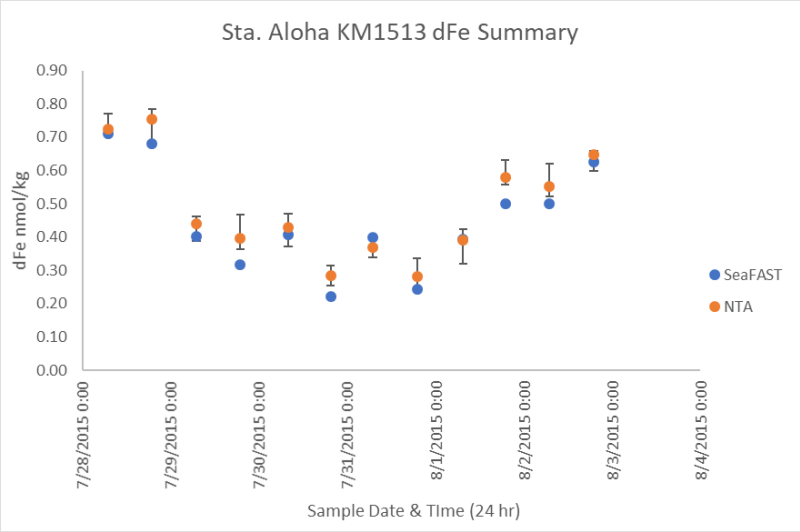

Figure 2.7: Fe NTA and SeaFast Intercalibration Results. Comparison of dissolved samples (0.4µm filtered) from Station Aloha (KM1513) measured through isotope dilution using the SeaFAST method and the Lee et al., 2011 NTA method. The NTA method had an average standard deviation of 0.03 from the SeaFAST method.

handling and to test the accuracy of the new ^{57}Fe spike. During this trial process, the Lee et al (2011) method was modified to add 175µL of 0.5M HNO_3 eluant instead of 150 µL to account for the faster sample take-up time on TAMU's ICPMS. In addition, the ^{57}Fe spike concentration was monitored and doubled or tripled in volume if expected iron concentrations exceeded the proper range of $^{56/57}$Fe in the spike-sample mixture (based on error propagation calculations through the isotope dilution equation. Indium was also added to the 0.5M nitric acid eluant and instrument blanks in order to track the in change in sensitivity over the course an ICPMS run.

The Station ALOHA samples were measured using the modified Lee et al. (2011) method in triplicate on each of four analytical sessions and are compared to the results of the established analytical method metal clean sampling (Figure 2.7). This comparison verifies the accuracy of the new spike calibration and the ability for the modified Lee et al. (2010) method at TAMU to produce accurate iron concentrations. The procedure Fe blank of 0.020 ± 0.021 nmol/kg (RSD of

143%) improved to 0.019 ± 0.014 nmol/kg (RSD77%) over the course of the four analytical sessions, suggesting that practicing trace metal clean procedures improved data quality over time.

During each analytical session, there were several reagents run with the samples for quality control of the data over the 16 analytical sessions that generated data for this project: an elemental iron standard for mass bias calculation, internal laboratory seawater from the Southern Ocean ("LTER") for external reproducibility estimates, >10 procedure blanks, and 0.5 M Nitric acid blanks for instrument background subtraction. Based on the elemental Fe standard, there was an average mass bias of 0.7 ± 5.57% per amu from the natural isotopic ratio over all of the analytical sessions, and mass biases were applied to the isotope dilution calculations on a per analytical session basis. The procedure Fe blanks during the analytical sessions averaged 0.310 ± 0.096 nmol/kg (RSD 31%) and were also subtracted on a per-analytical session basis. The detection limit (calculated as three times the mean of the standard deviations of the procedure blanks for each analytical session) averaged 0.26 nmol/kg. Comprehensive analyses of the LTER internal lab standard reference material averaged 0.67 ± 0.08 nmol/kg (n=32, RSD 12%).

2.5 Assessment

We were able to successfully associate all results from the suite of detectors (FlFFF—MALLS—UVvis—EEMs—ICPMS) as a function of hydrodynamic diameter, which was the goal of this method development (Figure 2.8). We also highlight in this figure how halfway through the FlFFF colloidal size spectrum, at 20 nm hydrodynamic diameter, is the literature bulk pore size cutoff between small and large colloids using 0.02 µm Anopore ultrafiltration (Fitzsimmons and Boyle, 2014a). The oceanographic details of how different samples' colloidal iron distributions compared is the subject of Chapter III.

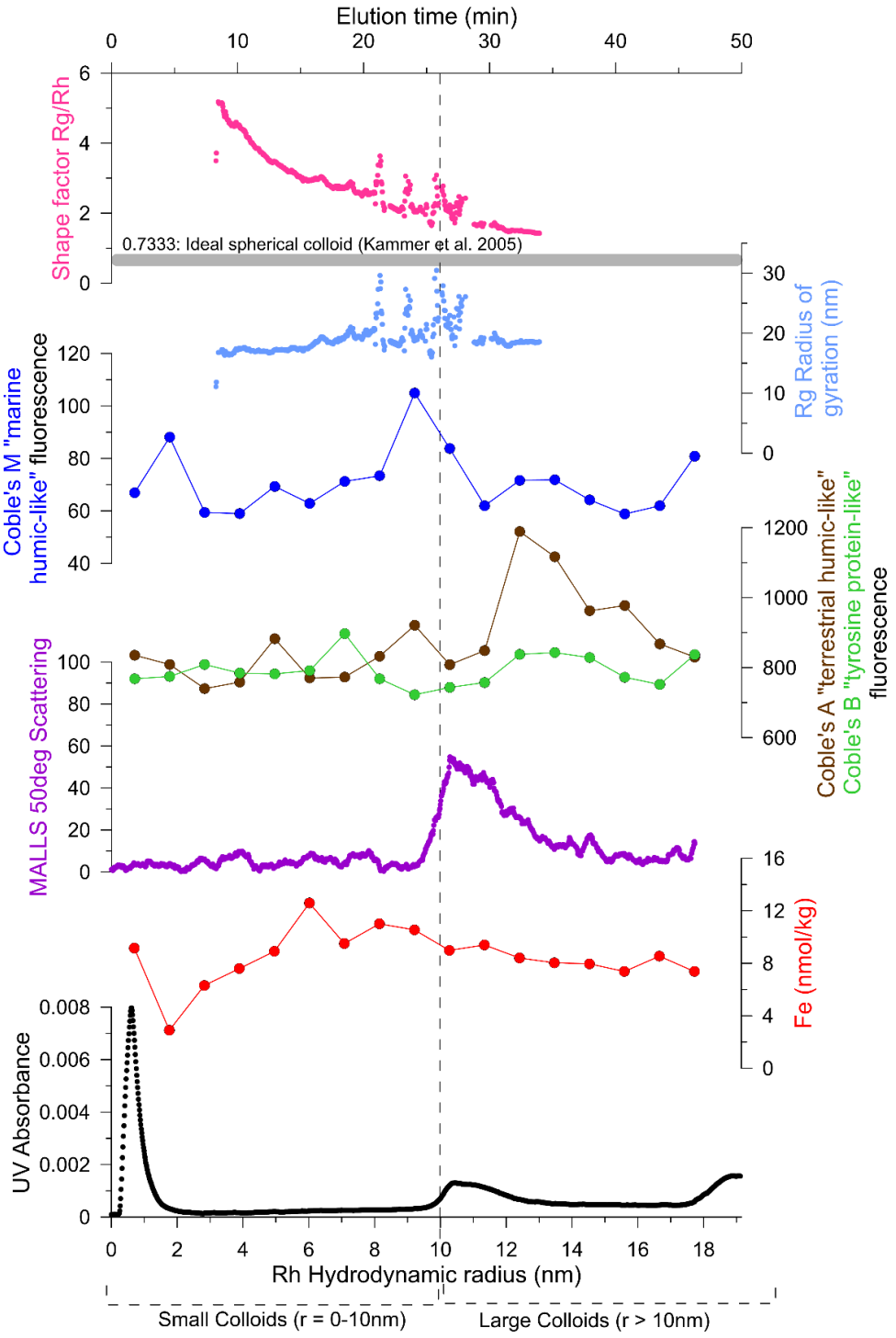

Figure 2.8: FlFFF—MALLS—UVvis—ICPMS—EEMs Results. Data from Estuarine Sta. 2, 15m depth sample. Combined results from all detectors and associating it to a hydrodynamic radius and elution time. The vertical dashed line indicates the cutoff between large and small colloids. The thick gray line shows the ideal spherical colloid at 0.7333 shape factor with anything greater being less spherical.

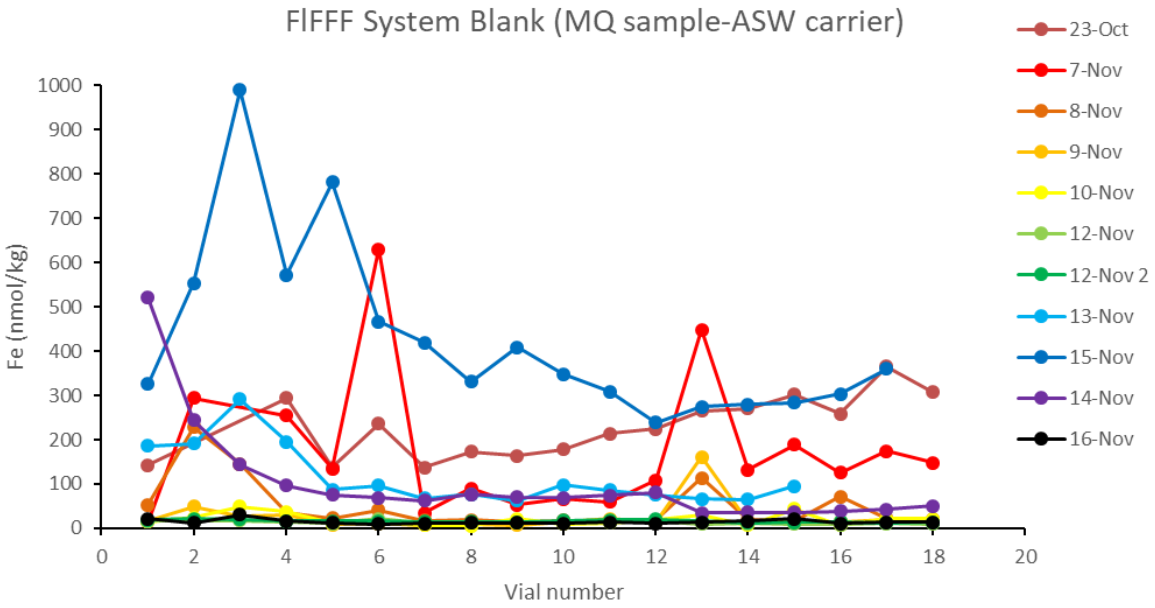

Figure 2.9: Daily FlFFF system blanks. These were analyzed for iron concentration. The smallest vial number corresponds to the smallest colloidal fraction. Blue dye was run on 10-19-17 and standards were run on 29-Oct and 19-Nov.

2.5.1 Iron Blank Assessment

We had planned to subtract out the background FlFFF iron concentrations using the MQ procedural blanks. However, these blanks proved to have very high and variable iron concentrations, averaging 102.99 ± 150.96 nmol/kg (RSD 147%), that were not a clear function of sampling date (i.e. the system was "cleaned out" slowly over time) nor proximity to the blue dye or molecular weight standard analyses (that might have contaminated the FlFFF) (Figure 2.9).

Thus, we investigated a daily, non-systematic iron blank source to the FlFFF. Candidate iron contamination sources included ASW, MQ, internal 4F parts, and iron colloid extraction and preconcentration procedures. Our first thought was that the ASW was contaminated, but triplicate iron concentration analyses of the five ASW batches used across these analytical

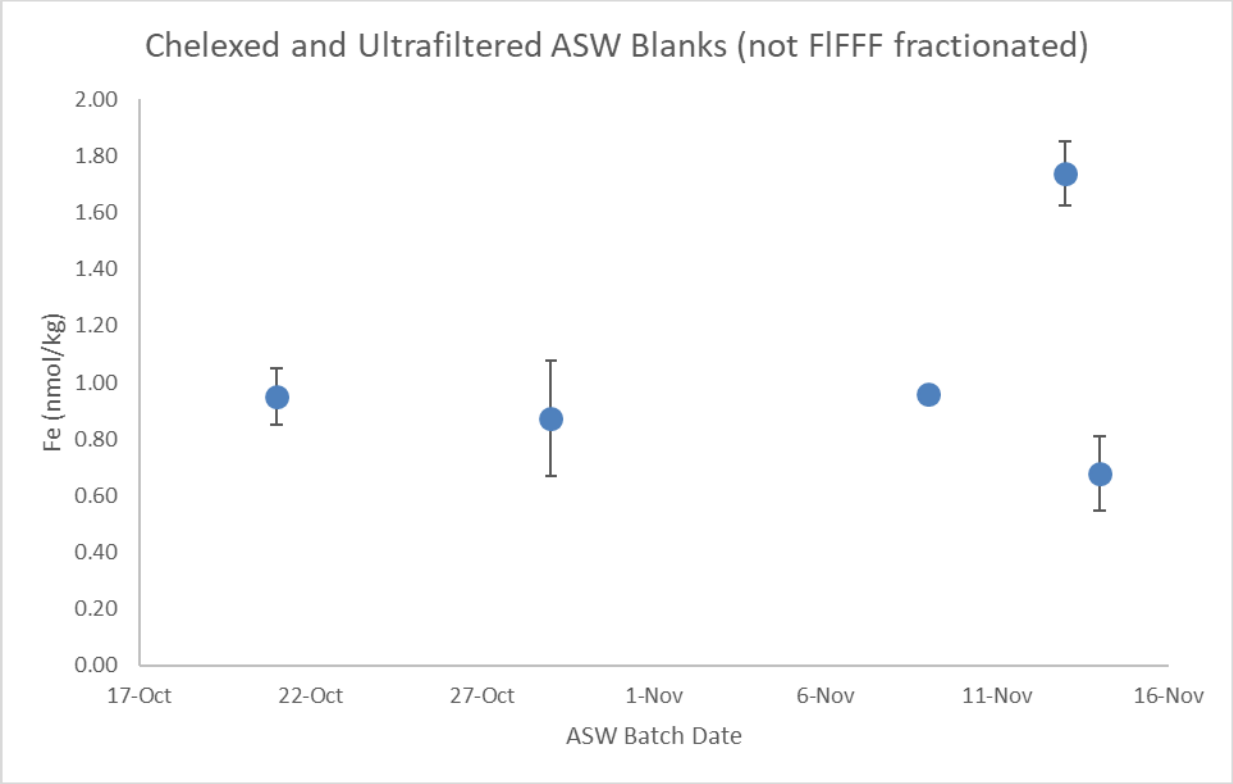

Figure 2.10: Chelexed and Ultrafiltered ASW Blanks. Each batch generated overtime was analyzed for Fe.

sessions revealed a 0.68-1.74 nmol/kg range of iron concentrations, averaging 1.04 ± 0.41 nmol/kg (Figure 2.10). This was not enough to explain the >100 nmol/kg iron blank. The lab's MQ system was also analyzed for iron and found to have a concentration of 0.32 nmol/kg, which also could not explain the high iron blank.

We had repeatedly switched out internal FlFFF parts for all-plastic replacements, and we had tracked down an internal iron contamination source as recently as July 2017, so we were fairly confident that the internal FlFFF parts were not our contamination source. However, two clues helped us track down our anticipated contamination culprit. Throughout the course of a day's run, the procedural blank (MQ sample with ASW carrier) 8 out of 9 blanks had higher iron concentrations than the subsequent duplicated sample runs (Figure 2.11). Additionally, for 6 out

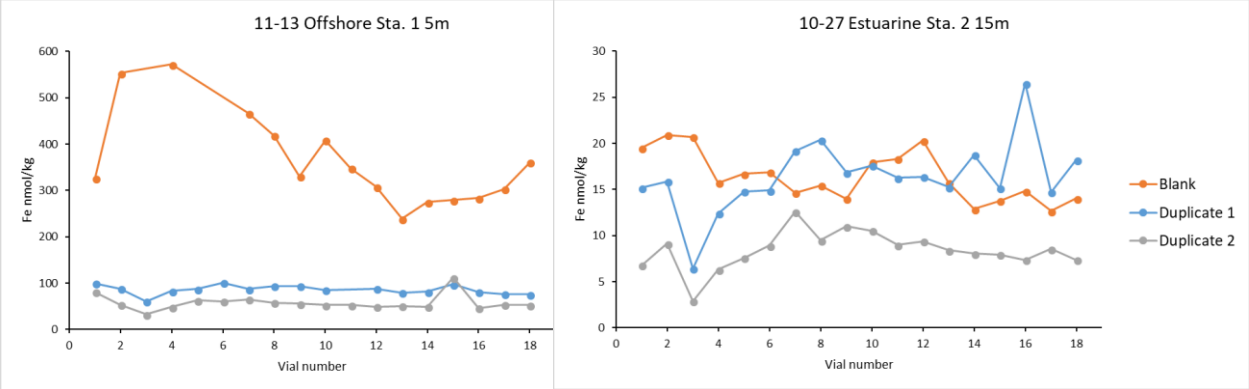

Figure 2.11: FlFFF Samples Duplicates. These got cleaner over the course of a FlFFF run day with the second duplicate being the cleanest. However, the distributions show a similar iron distribution shape overall.

of the 9 samples analyzed, the sample iron concentrations were lower in the duplicate sample analyzed second (Figure 2.11). These clues suggest that the methanol and/or acid used to clean the FlFFF system each night was actually contaminating the system for iron. To assess this, we plan to analyze the iron concentration of the cleaning acid in the future. We could also perform a test where a FlFFF system blank would be measured after varying periods (days) of cleaning. However, we feel it is important to continue to clean the system to ensure that all colloids are removed from the membrane between sample runs. Future work must constrain the source of the high iron FlFFF blank and eliminate it so that backgrounds can reliably be subtracted from sample FlFFF runs.

Finally, to confirm that the iron contamination was coming from the FlFFF system itself and was not due to sample handling and processing during extraction and preconcentration, one FlFFF replicate was separated into two halves by pipetting ~700 mL of each 1.5 mL sample into a new, clean vial. Thus, for each sample, one set of 1.5 mL fractions was analyzed as is, and the replicate set of 1.5 mL fractions was split and analyzed as two unique subsamples in order to

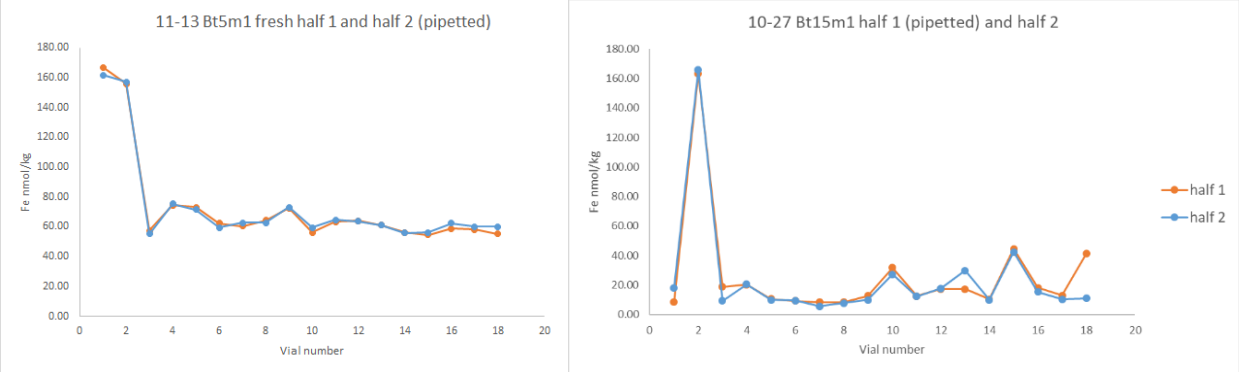

Figure 2.12: Fe NTA Duplicates. Samples were halved (~750 µL) showing the precision of Fe NTA method.

monitor reproducibility. The results show that every sample (9 out of 9) had almost identical Fe values for the halved set of fractions (Figure 2.12), confirming that the Fe blank contamination must be attributed to some FlFFF-specific contamination. We still hypothesize that the overnight cleaning is the largest source of contamination to the FlFFF system, though this needs future testing.

To summarize, our FlFFF system procedural blank proved to be an unreliable FlFFF system background subtraction, since when the FlFFF system blank was subtracted from the sample, it resulted in negative values that were more negative for the second replicate sample. Thus, background FlFFF iron blanks were not subtracted from sample runs, and most samples maintained reproducible overall shape of iron distribution with colloidal size, but would vary in background Fe concentration (Figure 2.11). For interpretation, the lowest concentration sample replicate (usually the second one) was selected.

2.5.2 Fresh-frozen sample storage comparison

To assess how freezing and thawing would affect a sample's colloidal iron size distribution, a "fresh/frozen" storage test was performed, as descried in the Methods 2.3.3

Section. For the Station 1 offshore continental shelf sample from 5 m depth, the frozen sample produced a very similar iron size distribution to the fresh samples, with iron concentrations between the first and second duplicate of the fresh sample (Figure 2.13). Given the general pattern of background iron concentrations decreasing over the course of a FlFFF run day with the last duplicate being the cleanest, it is reasonable to have the same shape of the iron size distribution, with the values of the frozen test in range of the fresh duplicates. Additionally, the shape factor, radius of gyration, MALLS scattering, and the UVvis absorbance for this sample are nearly identical between the fresh and frozen replicates (Figure 2.13). This provided assurance that storing samples frozen did not affect the size distribution of colloidal iron or carbon compounds in seawater samples.

However, the estuarine sample from Station 2 at 5 m depth did not have as similar iron concentrations or iron size distribution between fresh and frozen replicates (Figure 2.14). In particular, the frozen sample did not have the large increase in small Fe colloids that the fresh sample had. This may be due to an anomalously low FlFFF procedural blank concentration on the date of the frozen sample run, which averaged 14.6 nmol/kg across the size spectrum, as opposed to the fresh sample FlFFF procedural blank, which averaged 101.2 nmol/kg. As a result of this, we are not confident in attributing the differences in the iron concentrations and colloidal size distribution to a freeze/thaw changes during sample storage.

However, we do note that for this estuarine sample, some of the other measurements also did not match well between the fresh and frozen replicates (Figure 2.14), in particular the MALLS chromatograms. The MALLS scattering has a peak in the same region from 10-14 nm radius for both fresh and frozen treatments; however, the frozen data seems to have a greater abundance of colloids within that higher peak, while the fresh sample was more evenly distributed across the size spectrum and had a higher background. The UVvis distributions are similar with peak locations matching in location from 10-12 nm radius and 18-19 nm radius.

Because the chromatograms were so similar for all of the detectors in the fresh/frozen samples of offshore Station 1 and for a good portion of estuarine Station 2, we determined that freezing and thawing produce negligible speciation effects. However, we plan to repeat this test in future field trips to Maine in order to verify these results, especially by eliminating the 24 hour refrigeration that was applied to the Estuarine Station 2 “fresh” sample in this earlier fresh/frozen test.

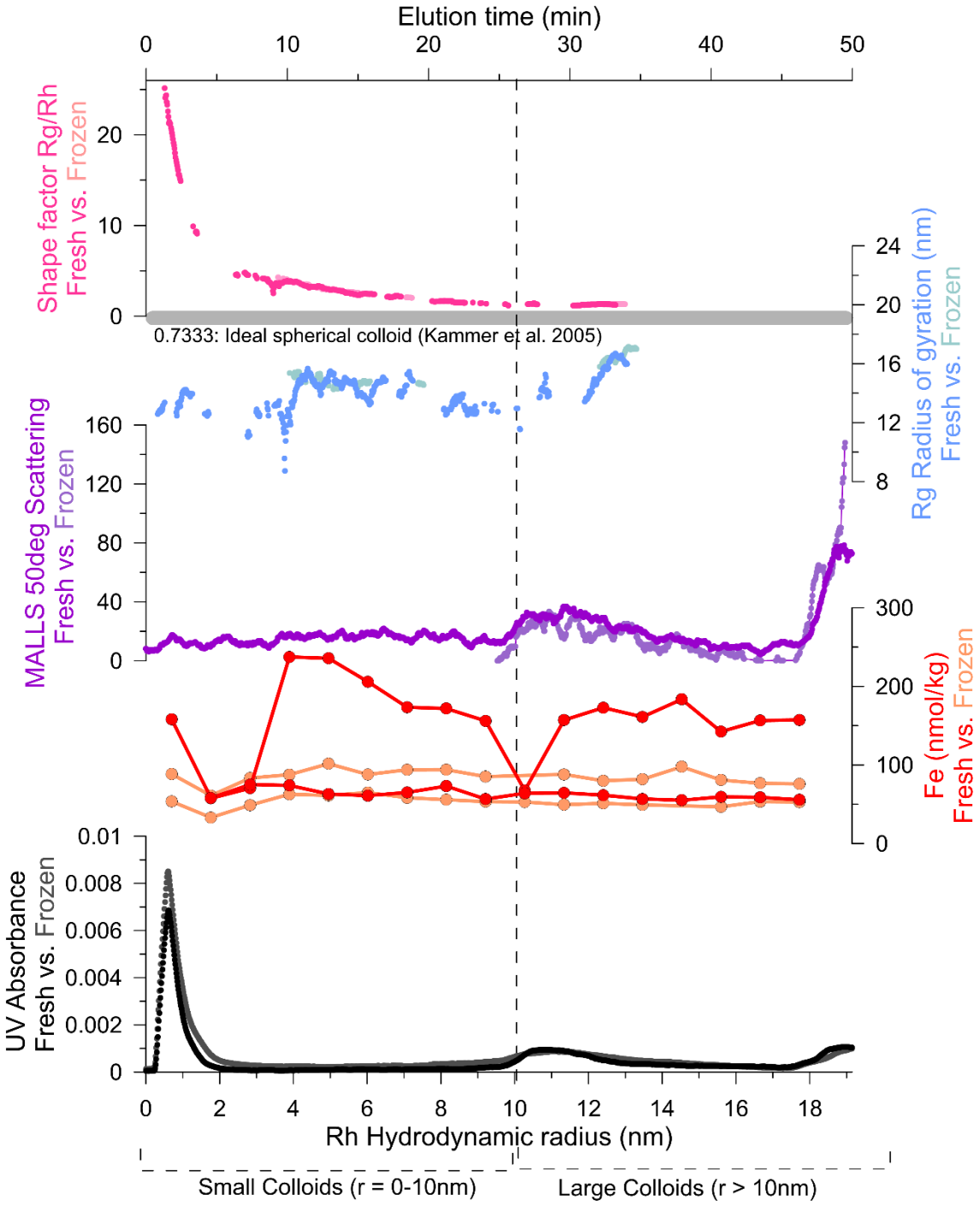

Figure 2.13: Offshore Fresh/Frozen Test. Collected at 5m depth, the "frozen" data in the lighter colors and the "fresh" in the darker colors. Combined results from all detectors and associating it to a hydrodynamic radius and elution time. The vertical dashed line indicates the cutoff between large and small colloids. The thick gray line shows the ideal spherical colloid at 0.7333 shape factor with anything greater being less spherical.

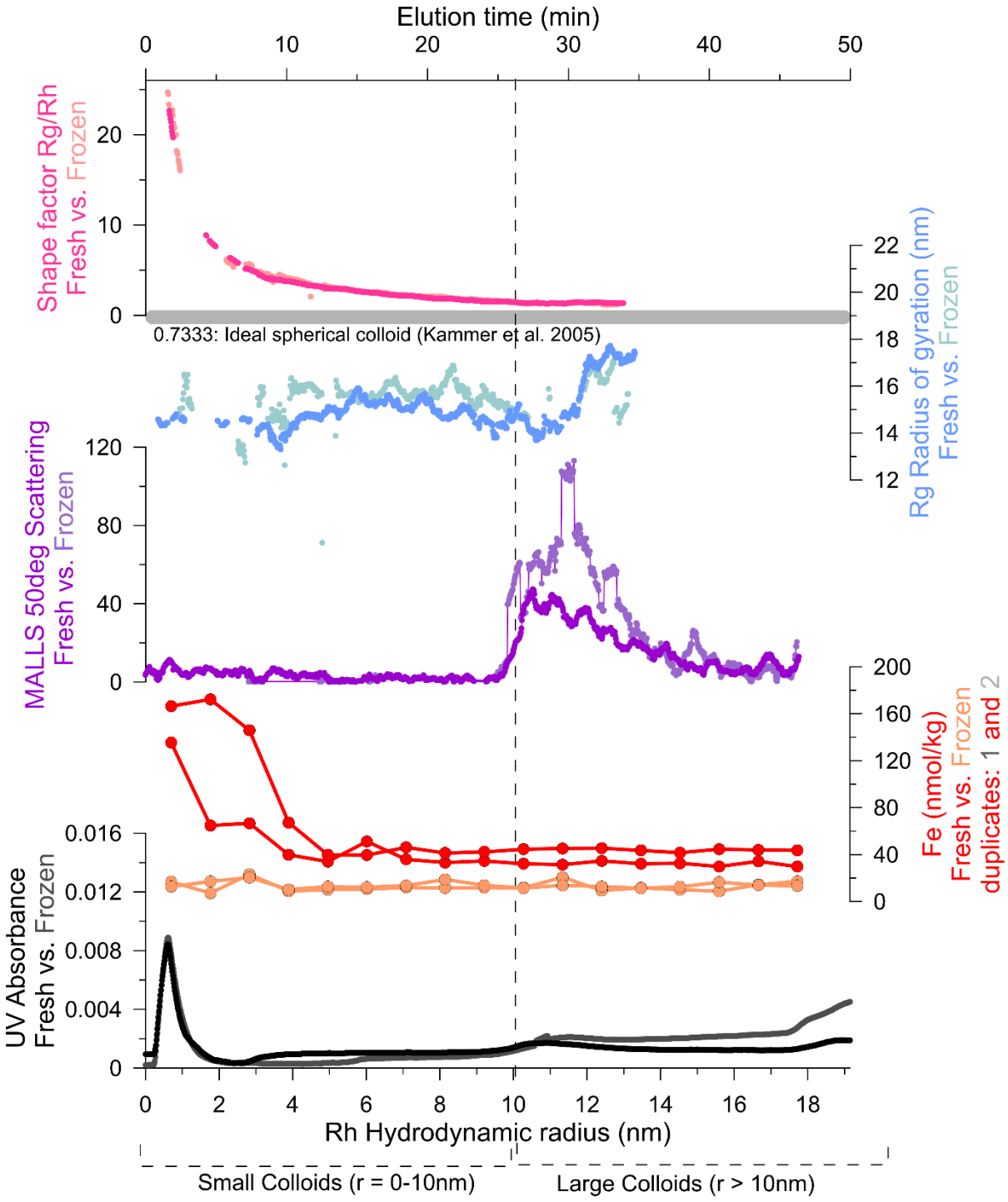

Figure 2.14: Estuarine Fresh/Frozen Test. Collected at 5m depth, the "frozen" data is displayed in the lighter colors and the "fresh" in the darker colors. Combined results from all detectors and associating it to a hydrodynamic radius and elution time. The vertical dashed line indicates the cutoff between large and small colloids. The thick gray line shows the ideal spherical colloid at 0.7333 shape factor with anything greater being less spherical.

2.6 Conclusion

The objective of this chapter was to optimize and test an innovative method coupling FlFFF—UVvis—MALLS—EEMs—ICPMS to generate the colloidal iron and carbon size distribution, carbon speciation, and colloidal shape as a function of colloidal size in full salinity, natural marine samples. While past studies have coupled FlFFF-ICPMS in low salinity waters, we innovated a fraction collection step of 18 x 1.5 mL size fractions for offline ICPMS iron analysis following iron extraction from its salt matrix and preconcentration in order to avoid occluding the ICPMS cone orifices with salts. Several instrument optimizations were completed. We successfully optimized the flow rates to account for high salinity samples and an ASW carrier solution. In addition, we optimized the FlFFF online colloid concentration procedures and processing protocols for separating and quantifying the size continuum of colloidal Fe in seawater using both molecular weight standards in the FlFFF system and iron standard reference materials in the ICPMS analysis. Furthermore, we tested the reproducibility of FlFFF using replicate analyses that confirmed the overall colloidal iron size distribution profile, though it did reveal an iron contamination that we believe we have traced to the overnight methanol and acid cleaning steps. Finally, we tested whether the freeze/thaw cycle needed to store samples before FlFFF analysis would affect the iron and carbon colloidal concentrations and size distributions, and for our offshore sample on the Maine continental shelf, freezing was found to have no effects. Thus, one major hurdle remains for future testing: producing a low and reproducible FlFFF system iron blank. However, overall we reached our goal of developing a FlFFF—UVvis—MALLS—EEMs—ICPMS method that is viable for full salinity, low iron concentration samples.

CHAPTER III

APPLICATION OF FLFFF-UVVIS-MALLS-EEMS-ICPMS TO COASTAL MAINE WATERS: THE MARINE COLLOIDAL IRON SIZE CONTINUUM

3.1 Synopsis

Iron is an essential nutrient required by phytoplankton for basic metabolic functions such as photosynthesis. Because the chemical composition and characteristics of colloidal iron control the fate of iron bioavailability and scavenging, it is important to analyze the iron colloidal distribution for is physicochemical speciation. Using a new method, FlFFF—UVvis—MALLS—EEMS—ICPMS, here we quantitatively and compositionally describe the colloidal iron size distribution at marine salinities for the first time. In aqueous samples collected from coastal Maine's Damariscotta River estuary and offshore continental shelf waters, we investigate (1) how the colloidal Fe size distribution changes spatially and with depth and (2) the physicochemical speciation of colloidal Fe, i.e., mainly organic or inorganic. Our results suggest that Fe colloids are not distributed uniformly across the colloidal size spectrum and instead have discrete sizes. We also found that there were both organic and inorganic Fe colloids at both stations and that the Fe size distribution was not tightly correlated with the organic size distribution or overall colloid abundance. We suggest that the 3-4 broad colloidal size classes found in prior freshwater/estuary literature need to be expanded to fit coastal Maine's more complex colloidal iron size distribution: class I (0.25-1.5 nm hydrodynamic radius) is ubiquitously iron and organic-rich, class II (1.5-3.5 nm) is organic rich, class III (3.5-5 nm) is non-spherical with low concentrations of organic iron, class IV (5-9 nm) found only at Estuarine Station 2 15 m is iron-poor, class V (9-12 nm) is organic and comparatively abundant, class VI

(12-15 nm) found at both station's chlorophyll maximum is iron-rich and inorganic, and class VII (15-20 nm) is organic-rich.

3.2 Introduction

Iron is a micronutrient required by phytoplankton to perform photosynthesis. However, about 40% of primary production in the ocean is limited by iron (Boyd and Ellwood, 2010; Sunda and Huntsman, 1995). Therefore, bioavailable iron not only affects the distribution of phytoplankton, but it in turn affects up through the higher trophic levels of the oceanic food web and influences overall carbon cycling in our oceans and on our planet. Dissolved iron (<0.2μm), which consists of soluble iron (<0.003 μm ~ 10 kDa) and colloidal iron (0. 003μm-0.2μm), is considered more bioavailable than particulate iron (>0.2 μm) (Wells, 2002). Because colloidal iron has been shown to make up a significant portion, up to 90%, of dissolved iron in the North Atlantic (Fitzsimmons et al., 2015b), colloidal iron must play a role in iron bioavailability. Colloids are labile and can have short residence times of a few hours in coastal waters and slightly longer offshore (Baskaran et al., 1992; Moran and Buesseler, 1993; Moran and Buesseler, 1992; Santschi et al., 1995). They can aggregate and be scavenged onto particles (which are considered the least bioavailable phase), or they could experience microbial degradation and become solubilized (considered the most bioavailable phase) (Chen and Wang, 2001; Honeyman and Santschi, 1989; Kepkay, 1994; Mopper et al., 1995; Rich and Morel, 1990). In addition, the composition of colloidal iron may also influence its bioavailability. For instance, aged inorganic iron is not as bioavailable as organic iron colloids, such as exopolymeric saccharides (Amon and Benner, 1996; Barbeau and Moffett, 2000; Chen et al., 2003; Chen and Wang, 2001; Hassler et al., 2011b; Rich and Morel, 1990; Wang and Dei, 2003), and humics are highly resistant to further microbial degradation compared to the lability of proteins (Azam et al.,

1983; Swaby and Ladd, 1962). Because the size and composition of colloids could largely affect the bioavailability and scavenging fate, it is imperative to study colloids as a size spectrum from the smallest to the largest colloids.

Traditional techniques examine colloids as a bulk fraction, homogenizing the colloidal phase and veiling the dynamic colloidal iron distribution and compositional characteristics. Newer techniques have examined the iron colloidal distribution using Flow Field Flow Fractionation to separate colloids based on size and then quantify them for iron using Inductively Coupled Plasma Mass Spectrometry in low salinity natural waters (Hassellöv et al., 1999; Lyvén et al., 2003; Stolpe et al., 2013a; Stolpe et al., 2013b; Stolpe et al., 2010; Stolpe et al., 2005). However, these previous studies were unable to quantify iron in high salinity environments due to the high salinity matrices decreasing the sensitivity of ICPMS measurements (Stolpe and Hassellöv, 2010). Using the new FlFFF—UVvis—MALLS—EEMS—ICPMS method described in Chapter II, here we successfully size fractionate the colloidal iron spectrum in high salinity waters and analyze each size fraction for organics, fluorescent dissolved organic matter (terrestrial humic-like, marine humic-like, and proteins-like) and shape (sphericity) for the first time.

3.2.1 Prior Findings and Hypotheses

Various studies have used FlFFF-ICPMS in low salinity environments (Dahlqvist et al., 2004; Hassellöv et al., 1999; Lyvén et al., 2003; Stolpe et al., 2013a; Stolpe et al., 2013b; Stolpe et al., 2010; Stolpe et al., 2005), but only one has used this technique in high salinity environment (a Swedish fjord); however, they were unsuccessful in quantifying the concentrations of iron (Stolpe and Hassellöv, 2010) (Table 3.2). Looking at a salinity gradient ranging from 0-23.5, Stolpe et al., 2010 examined three different rivers ranging from 0.1-0.3 in

salinity (Atchafalaya River, Mississippi River, and Pearl River) and the outflow of the Pearl River into the Gulf of Mexico at two stations moving away from the estuary (Mississippi Sound: salinity 8.7, and Mississippi Bight: salinity 23.5) (Stolpe et al., 2010). This study found 3-4 colloid populations in these regions: (1) hydrodynamic diameter (Dh) = 0.5-4 nm are DOM rich iron binding representing terrestrial fluvic acid, (2) Dh = 3-8 nm are protein-like colloidal matter in estuarine water representing in situ biological production, (3) Dh = 5-40 nm are Fe-rich colloids representing inorganic Fe(III) oxyhydroxides, (4) Dh > 40 nm are protein-like colloids binding iron (Stolpe et al., 2010). Furthermore, this study found discrepancy between different rivers with the lowest salinity river, the Pearl River, having the highest colloidal concentrations (Stolpe et al., 2010). In addition, they discovered a decrease in colloid concentration seaward towards the Gulf of Mexico (Stolpe et al., 2010). The pattern in these findings suggests higher salinity environments have lower concentrations of colloids suggesting that marine colloids may have low colloidal concentrations. Moreover, in this estuarine environment, more iron-rich colloids seem to occupy the larger size fractions within the colloidal size spectrum.

In a high salinity fjord (salinity 31-34), the Gullmarsfjord on the Swedish west coast, they also found three to four classes of colloids (Stolpe and Hassellöv, 2010). However, because this study also coupled atomic force microscopy (AFM: an imaging technique) to the method, they additionally examined the surface topography of the colloids (Stolpe and Hassellöv, 2010). The smaller colloids (Dh = 0.5-3 nm) were terrigenous, spherical iron-rich dissolved organic matter that occurred ubiquitously in the sampling sites and mostly likely derived from the river runoff. (Stolpe and Hassellöv, 2010). Medium sized iron-poor colloids (Dh = 3-7 nm) were globular of slightly elongated in shape (Stolpe and Hassellöv, 2010). The larger iron-rich colloids (Dh = 7-40 nm) were more fibrillar in shape and formed by *in situ* biological production (Stolpe and

Hassellöv, 2010). Therefore, the different size fractions within the colloidal spectrum reflect their source of origin: smaller lithogenic colloids and larger biogenic colloids. This is a conflicting pattern compared to Stolpe et al, 2010 with the larger colloids being iron oxyhydroxide rich instead of biogenic; however, both had a small size fraction abundant with iron-rich organic colloids. The difference can be attributed to a different environmental salinity in the two systems and/or due to a difference in primary productivity. However, due to complications with the high salt samples decreasing the sensitivity of the ICPMS, Stolpe and Hassellov, 2010 were unable to quantify the concentrations of the metals. To better understand colloidal iron's role in estuaries and offshore environments, our study is the first to addresses this gap in the literature and quantitatively measure the concentrations of the iron colloid distribution in high salinity environments.

Overall these past studies coupling FlFFF to ICPMS found ~3 size classes (I: Rh=0.25-1.5 nm, II: 1.5-4 nm, IV: 2-40 nm) in the riverine and estuarine colloidal size spectrum where 0.25-1.5 nm colloids are spherical and organic-rich, 1.5-4 nm colloids are globular and organic/iron rich, and 2-20 nm colloids are iron-rich that and either organic or inorganic (Stolpe et al., 2013a; Stolpe et al., 2013b; Stolpe et al., 2010; Stolpe and Hassellöv, 2010). However, no previous study has measuredt the marine iron size distribution. When considering environment, we were curious to determine whether the patterns found in riverine and estuarine environments would persist in the ocean: would we see a dynamic colloidal iron distribution as a function of size, or would it be static (Figure 3.1)?

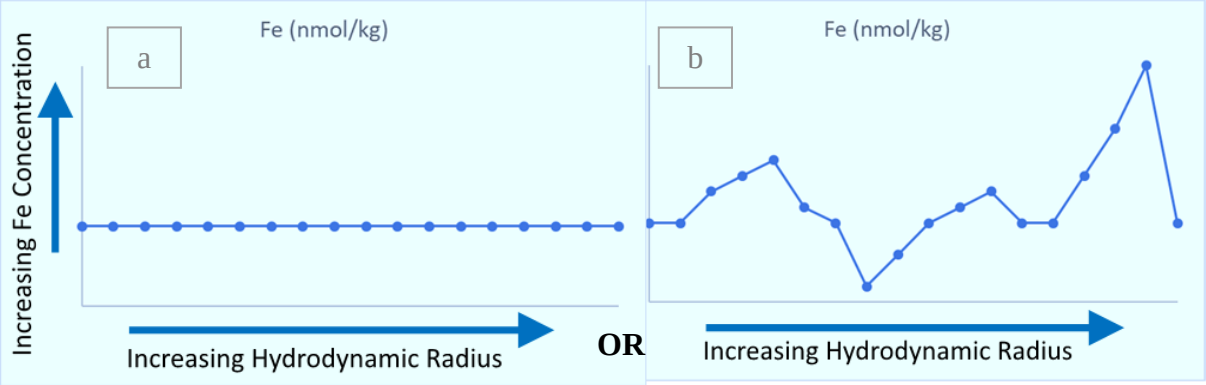

Figure 3.1: Schematic of possible Marine Colloidal Iron Distributions. This depicts if the marine colloidal iron distribution is (a) static with unchanging iron concentrations or (b) dynamic with varying iron concentrations with size.

Based on the previous findings in rivers and estuaries, we hypothesized that:

(1) The colloidal distribution is dynamic in iron concentration and compositional characteristics as a function of size;

(2) Where there is more direct runoff influence (Estuarine Station 1), there are higher concentrations of iron and carbon absorbance;

(3) There would be inorganic iron colloids in the mid- to large- size fractions;

(4) With increasing hydrodynamic radius, there is a decrease in sphericity due to presence of biogenic fibrillar colloids;

(5) At the offshore station, there is a larger amount of marine humic-like fluorescent dissolved organic matter.

3.2.2 Justification for Sampling Location and Hydrography

Seawater sample collection in the continental shelf region of the central Gulf of Maine took place near the University of Maine's Darling Marine Center (DMC), located along the

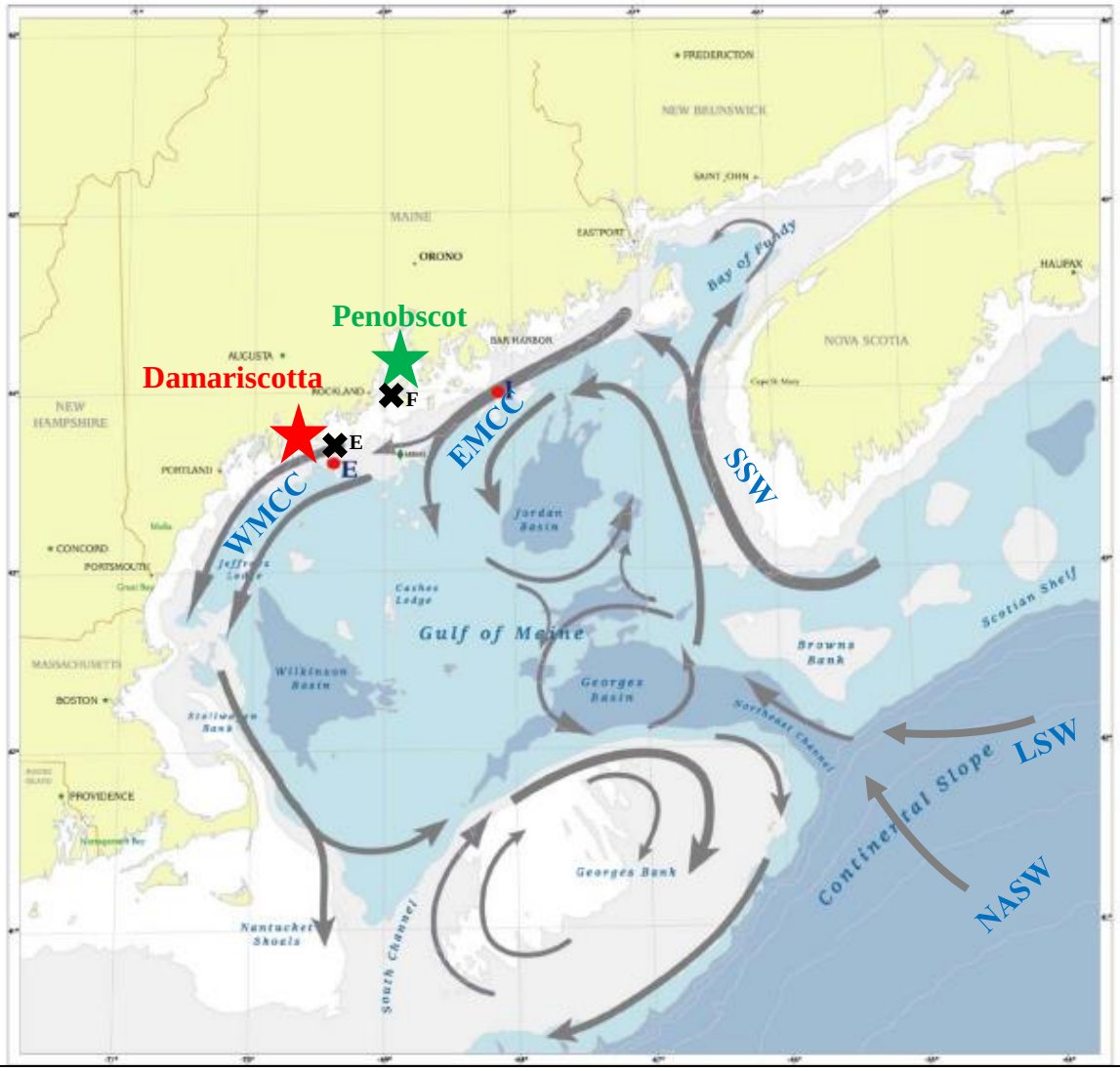

Figure 3.2: Map of Gulf of Maine's Surface Currents. Schematic of surface currents (<50m) in the Gulf of Maine: North Atlantic Slope Water (NASW) and Labrador Sea Water (LSW) come in through Northeast Channel, Scotian Shelf Water (SSW), EMCC (Eastern Maine Coastal Current (EMCC), Western Maine Coastal Current (WMCC). Red star indicates sampling region, green star indicates Penobscot outflow, black x's indicate NOAA buoys E01 and F01. Red dots indicate buoys used in Pettigrew et al., 2005. Reprinted and adapted fom Pettigrew et al., 2005.

banks of the Damariscotta River estuary (Figure 3.2). This coastal ecosystem is considered to be subject to substantial climate change (Pershing et al., 2001) and has both strong terrestrial and oceanic inputs of dissolved and particulate carbon (Balch et al., 2012). The diversity of inputs was one major reason that we chose this area for study of the colloidal iron physicochemical speciation.

The Damariscotta River estuary itself is a narrow, submerged river valley that receives little freshwater input and is classified as a partially mixed estuary (Mayer et al., 1996; McAlice, 1993). In the Damariscotta River estuary, salinity ranges from 25 to 34, with a range of 29-34 near its mouth (Lee and McAlice, 1979; Sanders, 1987). The Maine continental margin offshore from the Damariscotta River estuary (Figure 3.2) is fed by the Western Maine Coastal Current (WMCC), a buoyant current that has terrestrial inputs from the Penobscot River into Penobscot Bay, which is about 40 km east of the Damariscotta (Balch et al., 2012). The Penobscot is Maine's largest watershed, with a distinct peak in river flow rate during spring's snowmelt and a trough during the late summer and early fall (Hodgkins and Dudley, 2005). Interestingly, snowmelt is the largest contributor to the seasonal watershed variation, as liquid precipitation is relatively evenly distributed over the seasons (Balch et al., 2012). Furthermore, 90% of organic carbon transported from the watershed is in the form of dissolved organic carbon (DOC), and this transport varies seasonally with the lowest concentrations occurring during the winter and spring, despite high discharge, and the highest concentrations during intermittent high flow periods in the fall (Balch et al., 2012; Cronan et al., 1999) perhaps due to high litter inputs and shallow hydrologic flow paths within the Penobscot drainage basin (Cronan, 2012).

On the other hand, this region of Maine's continental shelf also experiences significant marine influences from the North Atlantic Slope Water (NASW) and the Labrador Sea Water (LSW) currents coming from West Greenland as well as Scotian Shelf Water (SSW) derived from the shelf of Nova Scotia, which then loops through the Bay of Fundy to become the Eastern Maine Coastal Current (EMCC) (Balch et al., 2012; Geyer et al., 2004; Pettigrew et al., 2005) (Figure 3.1). The EMCC carries significant macronutrients; as a result, Maine's continental shelf supports high levels of primary production (Balch et al., 2012; Ji et al., 2007). Numerical

modeling studies based on springtime climatology indicate an offshore deflection of this EMCC, but it reattaches to the coast after being deflected 50m offshore at the Penobscot River plume (Lynch et al., 1997). Additionally, it has been suggested that since the volume of freshwater transport in the WMCC exceeds the Penobscot River input by 30%, a significant contribution of the coastal freshwater transport must be sourced from the EMCC and that the prevalence of the EMCC signature varies with the Penobscot outflow (Geyer et al., 2004). Because this region within the Gulf of Maine is highly influenced by both terrestrial freshwater and marine sources, it is a great place to examine iron physicochemical speciation and monitor its effects on biogeochemistry and primary production, especially in the face of ongoing climate change in the region.

Two sampling locations were chosen for this study: one within the mouth of the Damariscotta River estuary and the other offshore in the Gulf of Maine beyond the 100 m isobath. These stations were chosen for several reasons, which are outlined here. (1) The sampling of saline (S>30) waters at both stations is conveniently within close proximity to the DMC (1-2 hour transit by small boat for the estuary station and by ship for the offshore station), which allows for filtration at the DMC within 3 hours of sampling to avoid colloid aggregation, adsorption, or desorption to and from bottle walls; (2) this region experiences high seasonal variability in phytoplankton production (spring and fall blooms) (Thomas et al., 2003), phytoplankton community composition (Balch et al., 2012), and oceanographic influence from near- and far-shore forcing (Ji et al., 2007), which we hypothesized might influence iron physicochemical speciation in a way that we could measure over time; and (3) this region's primary productivity (e.g. phytoplankton) supports the large local fisheries (e.g. lobster and oyster) (Carnegie and Barber, 2001; Palma et al., 1999; Revelante and Gilmartin, 1987; Sanders,

1987), and thus factors influencing this productivity (such as iron bioavailability) are important to understand.

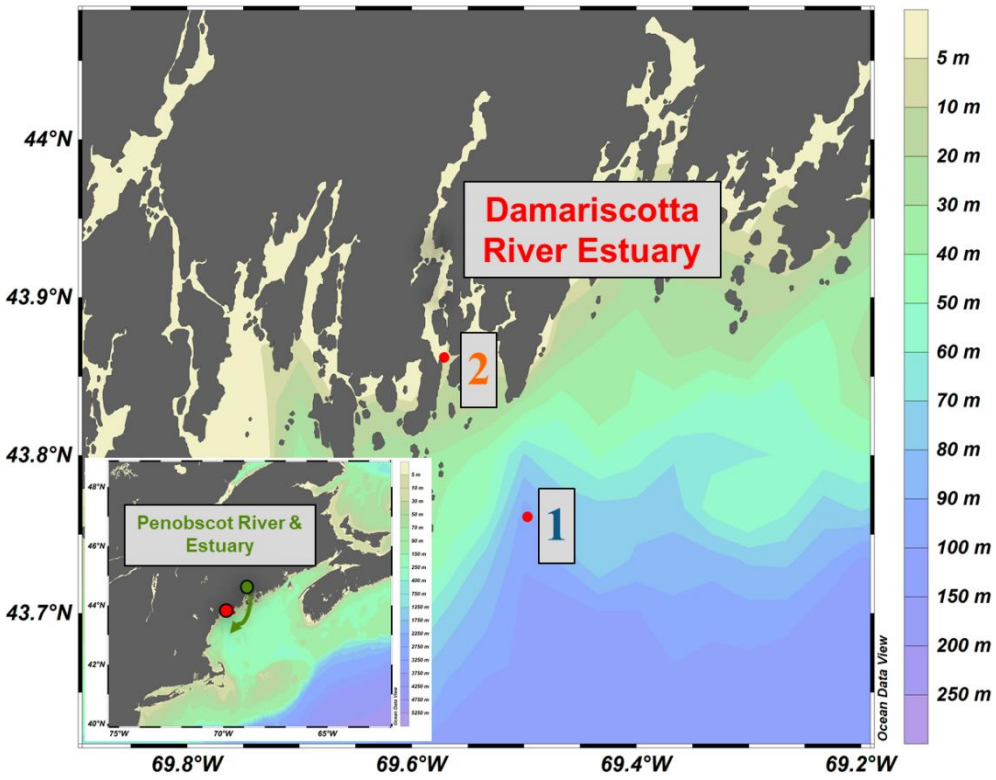

Figure 3.3: Map of Sampling Stations. Offshore 1 and Estuarine 2. Zoomed out map of region shows the Gulf of Maine and the surface currents (WMCC: green arrow) bringing influence from Maine's largest watershed: The Penobscot River and estuary (green dot).

3.3 Methods

3.3.1 Sampling Methods

Sampling occurred during the spring bloom of June 2017 and after the fall bloom for two weeks in late October 2017. During the Fall, when there was less primary production and runoff compared to the spring season, there were two mini-cruises that left from the DMC dock on the R/V *Ira C.*, a 13 m research vessel operated by the University of Maine. The cruise went

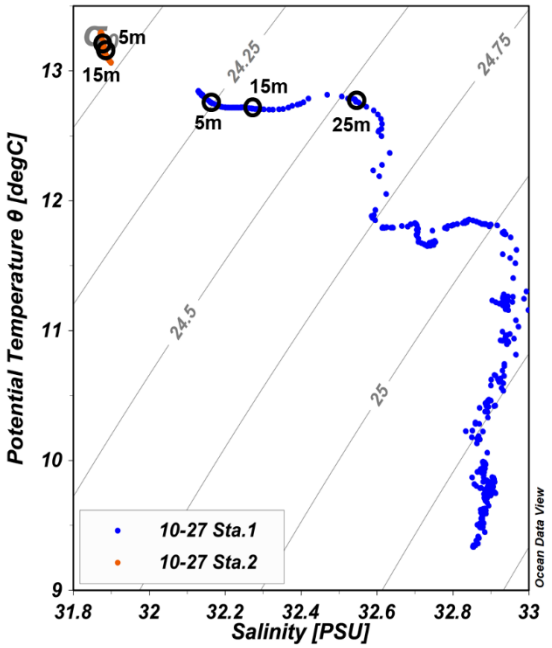

Figure 3.4: Temperature Salinity Plot. Potential temperature (degree C) and salinity (PSU) for the Offshore Sta. 1in blue and the Estuarine station in orange. Black circles indicate the sampling depths associated with the potential temperature and salinity at each station. Grey lines indicate density contours.

offshore to the 110 m isobath (sta. 1: N 43˚44.989', W 69˚30.230'), where samples were collected at three different depths: 5, 15, and 25 m (Figure 3.3). Surface measurements at the 5 m depth were chosen to be deep enough so that sampling was uncontaminated by the hull of the boat (1.83 m draft). Samples were collected in a MERCOS, teflon-lined sampling rig, which collects >1 L of seawater (Freimann et al., 1983). The bottles were then transferred to a cooler to maintain cold temperatures prior to filtration back to the DMC within three hours. *In situ* measurements were obtained using a Seabird SBE 25+ Sealogger CTD that measured temperature, conductivity, pressure, oxygen, chl a fluorescence, turbidity, beam transmission, and PAR irradiance. All samples were passed through a 0.2 µm filter to remove particles within ~3 hours of sampling to minimize exchange of colloidal matter onto bottle walls (Fitzsimmons

and Boyle, 2012). If samples could not be immediately FlFFF fractionated and then acidified, they were frozen for future analysis (see Chapter II for details).

3.3.2 Analytical Methods

The FlFFF—UVvis—MALLS—EEMS—ICPMS method was used to measure the marine iron colloidal size distribution. The details of this method were delineated in Chapter II.

3.4 Results

3.4.1 Coastal Maine's Hydrography

The thermohaline structure was different at Offshore Station 1 and Estuarine Station 2, as expected during our station planning. In November, the surface waters (<50 m) of Offshore Station 1 were saltier ($32.1 < S < 32.4$) and cooler ($12.5 < \theta < 12.8$) than the Estuarine Station 2, which were fresher ($31.8 < S < 31.9$) and warmer ($13 < \theta < 13.5$), indicating that the two regions were sourced by different waters (Figure 3.4). We hypothesized that Estuarine Station 2 was influenced from the Damariscotta river outflow, while Offshore Station 1 received water inputs from the Damariscotta, and from the WMCC, which carries species from the both the Penobscot watershed and marine EMCC waters.

To test the importance of the marine EMCC influence, we compared the *in situ* temperature and salinity from our offshore Station 1 to data from two NOAA buoys located at the mouth of the Penobscot Bay (Buoy F01: Latitude: 44.055, Longitude: -68.998) and west of it at the Central Maine Shelf (Buoy E01: Latitude: 43.716, Longitude: -69.355), 13km east of our Offshore Station 1 (National Buoy Data Center, 2017) (Figure 3.2). Our Offshore Station 1 temperature and salinity data are comparable to that of nearby Buoy E01 (Figure 3.5). We also related the temperatures and salinities at buoys E01 and F01 to see if the Penobscot outflow is

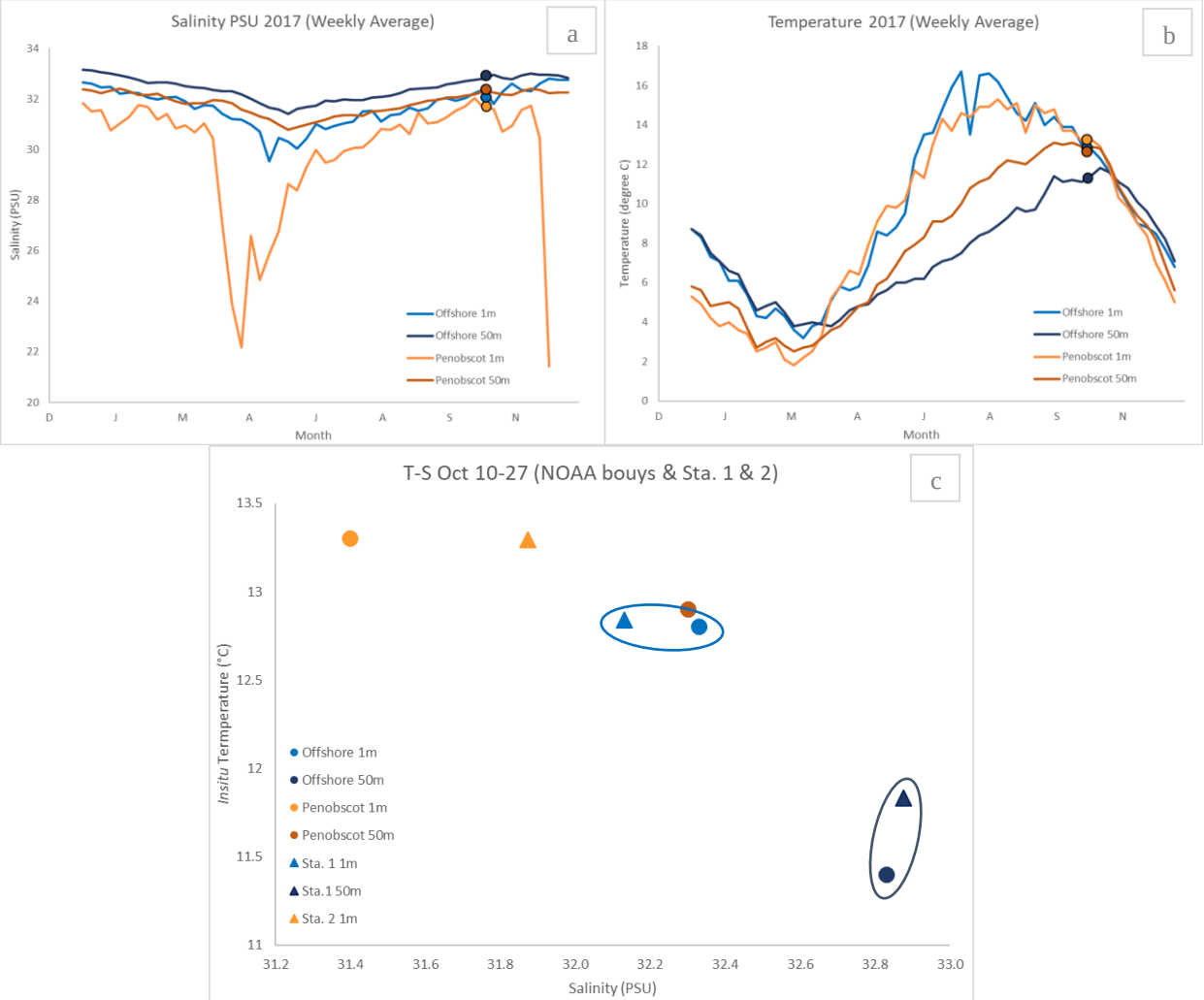

Figure 3.5: Western Gulf of Maine Coastal Current NOAA Buoy Data. Annual weekly averaged (a) Salinity (PSU) and Temperature (degree C) data from buoys 44032 (Offshore Central Maine Shelf Buoy E01) and 44033 (Penobscot Buoy F01) at 1m and 50m depths. The Offshore buoy is 13km from this study's Offshore Sta. 1 and is 47km away from the Penobscot buoy. The Penobscot buoy is located at the mouth of Penobscot Bay. (c) *Insitu* temperature and salinity filled-in circles indicate data from NOAA buoys and triangles indicate data from this study's Offshore Sta. 1 and Estuarine Sta.2. Open circles include Sta. 1 and buoy T-S signatures from the same depths.

affecting our sample region. Looking at the 2017 annual trend at the limits of the surface water current of 1 m and 50 m, both salinity and *in situ* temperature follow similar trends, with E01's

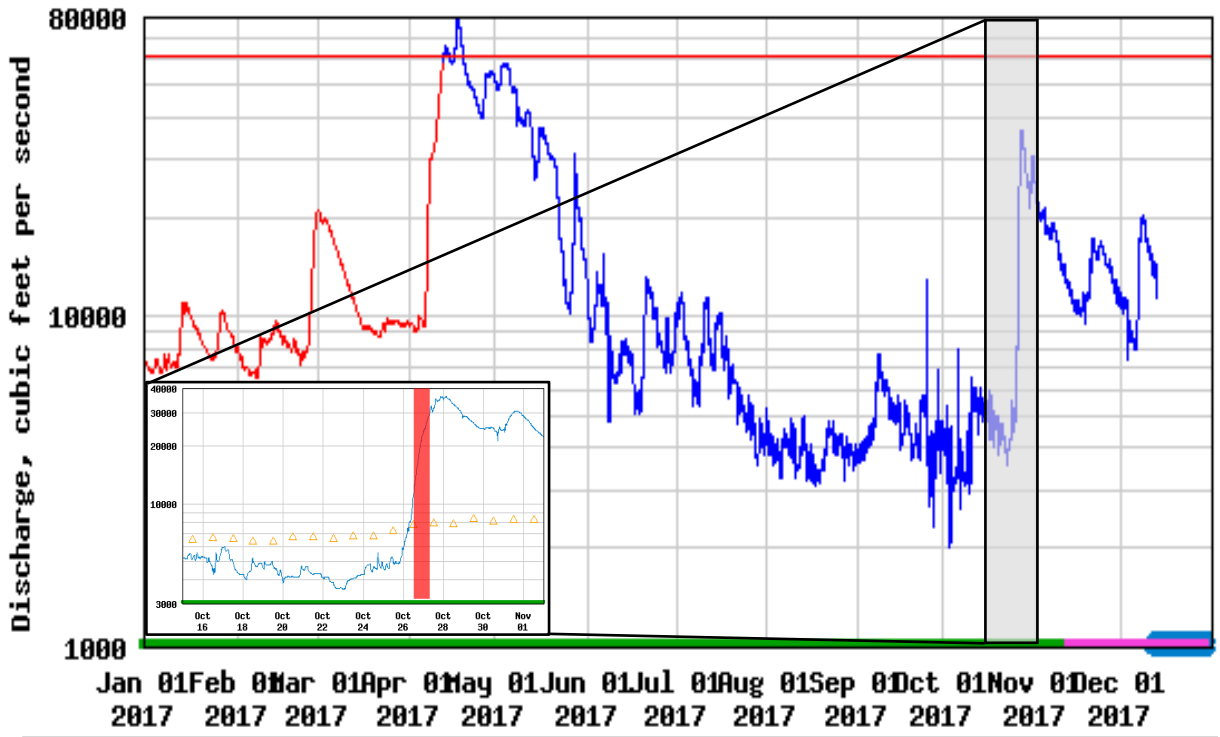

Figure 3.6: Penobscot River Discharge. Discharge of the Penobscot River at West Enfield, Maine (134 km from the mouth of Penobscot Bay and 188 km from Offshore Sta. 1). The secondary graph shows the zoomed in data for the shaded region showing a low outflow from the River prior to our sampling date 10-27-17 where the red box indicates the sampling date. Reprinted and adapted from USGS (2017)

temperature and salinity having dampened signatures compared to F01 that is positioned closer to the mouth of the Penobscot outflow. This suggests that the Penobscot river outflow is at least somewhat affecting the water mass signature of our Offshore Station 1 sampling region. Prior to our sampling date of October 27th, the Penobscot River discharge was relatively low at the USGS West Enfield, Maine station, 188 km away from our Offshore Station 1 site, suggesting that it may have been experiencing a comparatively lower Penobscot River plume signature in

the WMCC compared to May or even the days following 10-27 (Figure 3.6). While there are peaks in the Penobscot discharge simultaneous with our sampling dates, we note that it would take some time for Penobscot waters to travel southward the >188 km to our sampling site at Station 1, and thus we interpret our October data as representing a "low flow," more marine-(EMCC-) influenced sampling period. While the Estuarine Station 2 was well mixed in its 20 m water column depth range (Figure 3.7), the Offshore Station 1 had a pycnocline starting at ~20 m depth (Figure 3.7). Offshore Station 1 also had a subsurface chlorophyll maximum (up to 3.5 fluorescence mg/m^3) at 10-15m depth, while the Estuarine Station 2 had a chlorophyll maximum (1.5 fluorescence mg/m^3) at shallower 5 m depth. Offshore Station 1 had a particle maximum (18.5 % beam transmission) at 5 m, while the Estuarine Station 2 had increasing particles with depth that dropped light transmission from 17.5 to 17.0%. While Estuarine Station 2 has more particles in the water column, they were likely more lithogenic in nature, since Offshore Station 1 had more chlorophyll in the surface waters (0-20 m).

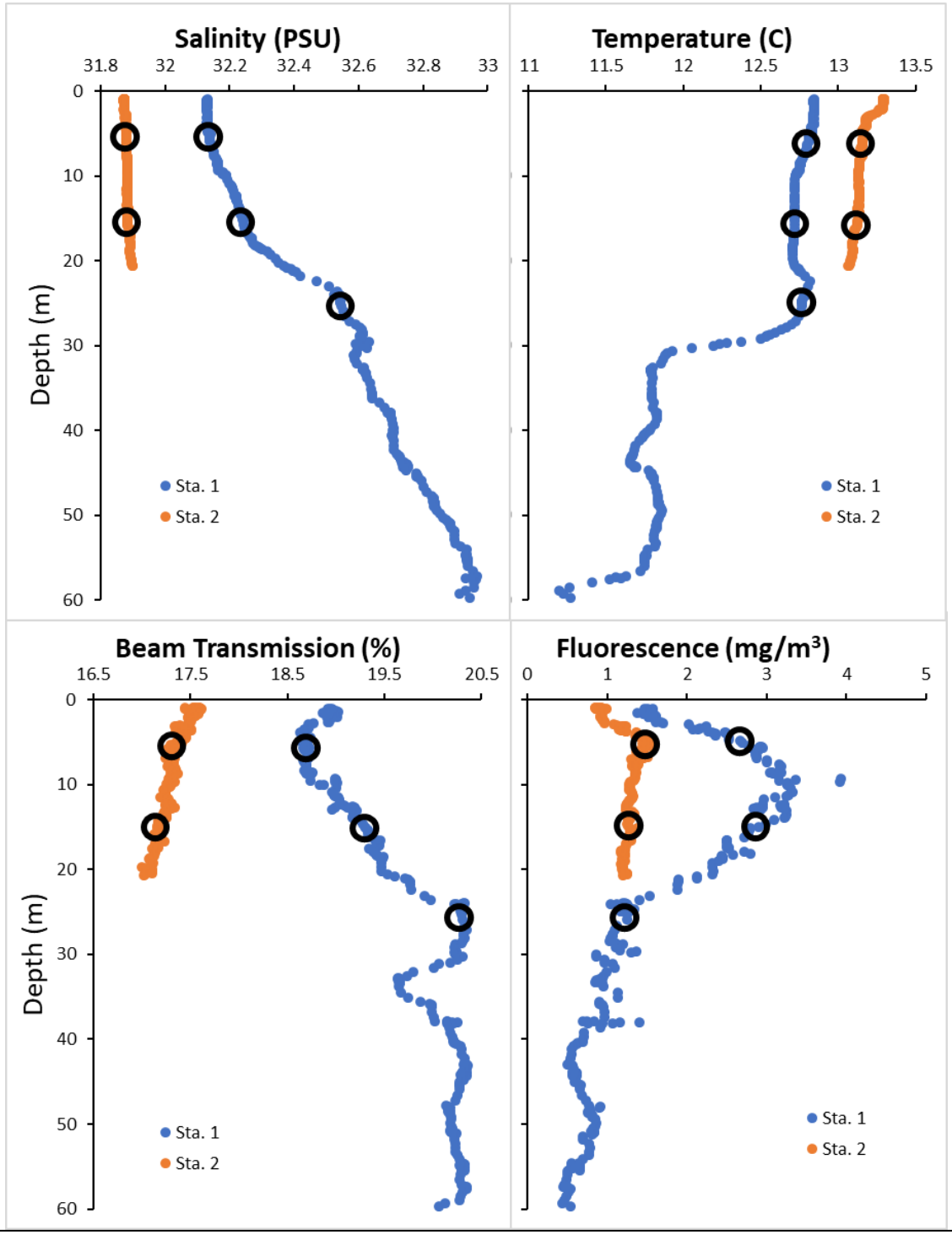

Figure 3.7: Sta. 1 and 2 Hydrography. *Insitu* temperature, salinity, percent beam transmission, and fluorescence in the upper surface layer (<60m). Offshore Sta. 1 (blue) and Estuarine Sta. 2 (orange) have black circles indicating the sampled depths for the Fe colloidal distribution (5m, 15m, & 25m).

3.4.2 FlFFF—UVvis—MALLS—EEMs—ICPMS

Here, we show the results of colloidal iron size distribution, shape, and chemical composition data from the FlFFF-UVvis-MALLS-EEMs-ICPMS analyses. An example of a complete dataset for a single sample (in this case Estuarine Station 2, 15 m depth) plotted as a function of hydrodynamic radius (Rh) is shown in Figure 3.8. We note that for the remainder of the datasets, we do not include the fluorescence Coble's peaks of tryptophan-protein like, tyrosine protein-like, or terrestrial humic-like because, with presumably much higher concentration (~µM) than colloidal Fe (~nM), the signals did not correlate in a meaningful way with the iron size distribution and thus, detracted from our iron speciation story.

3.4.3 Colloidal Fe Distribution at Offshore Station 1

At Offshore Station 1, the 5 m depth sample was located above the chlorophyll maximum at a mid-salinity of 32.1 that connoted both a terrestrial and EMCC marine influence (Figure 3.7). The FlFFF-UVvis-MALLS-EEMs-ICPMS results show the smallest colloids (Rh = 0-2 nm) were very abundant (scattering intensity = 85), organic rich (UVvis absorbance at λ=254 nm = 0.05), and Fe-rich (129 nmol/kg) (Figure 3.9). In the medium sized fraction (Rh = 10-12 nm), there was an abundance (scattering intensity = 80) of iron rich (Fe = 184 nmol/kg) colloids that correlated with a small but distinguishable carbon peak (UVvis absorbance = 0.005). Based on the concomitant peak in Coble's "M" peak that connotes marine humic-like fluorescent dissolved organic matter (FDOM) at the same size (EEMs M fluorescence = 400), these iron species may be bound to marine humic species. Finally, in the largest size fraction (Rh = 17-19 nm), there were abundant (scattering intensity = 95) organic colloids (UVvis = 0.005). No shape factor data were generated for this sample.

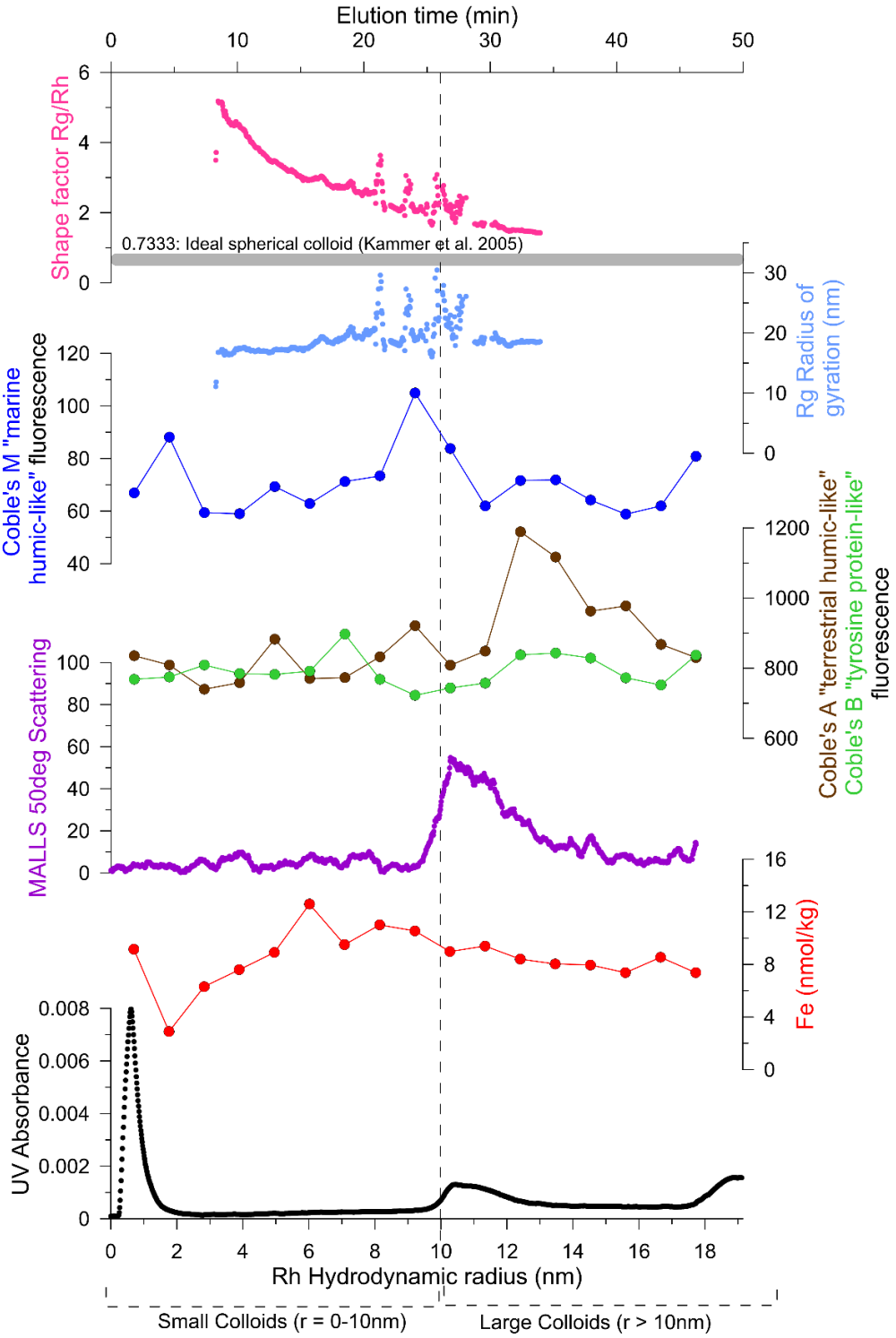

Figure 3.8: Estuarine Sta. 2 15m depth Fe Colloidal Spectra. Combined results from all detectors and associating it to a hydrodynamic radius and elution time. The vertical dashed line indicates the cutoff between large and small colloids. The thick gray line shows the ideal spherical colloid at 0.7333 shape factor with anything greater being less spherical.

At Offshore Station 1, the 15 m depth sample located near the subsurface chlorophyll maximum at a slightly higher salinity of 32.2, connoting more marine influence than the 5 m depth sample (Figure 3.7). The FlFFF results (Figure 3.9) showed that the smallest size fraction (0-2 nm) had a lower abundance of colloids (scattering intensity = 0-10), varying in sphericity (Rg/Rh = 5-37), that were organic rich (UVvis absorbance = 0.015). In the medium size fraction (Rh = 10-12 nm), there was a large abundance (scattering intensity = 125) of organic (UVvis absorbance = 0.003) colloids that were near-spherical in shape (Rg/Rh ~ 0.733) that were not associated with iron. We did not generate shape data for colloids >12 nm Rh; however, there was a general pattern of increasing sphericity with increasing Rh. In a larger size fraction (Rh = 14-15 nm), there was a great abundance (scattering = 230) of iron colloids (Fe = 45 nmol/kg) that are most likely inorganic in nature (UVvis absorbance = 0).

At Offshore Station 1, the 25 m sample was located below the chlorophyll max at the highest salinity of 32.6, representing our sample with the greatest marine influence (Figure 3.7). The FlFFF data (Figure 3.9) showed that the smallest sized colloids (Rh = 0-2 nm) were organic- (UVvis absorbance = 0.0095) and iron-rich (Fe = 50 nmol/kg) but must have been too small to generate a strong abundance signal (scattering intensity = 0-5) and did not seem to be associated

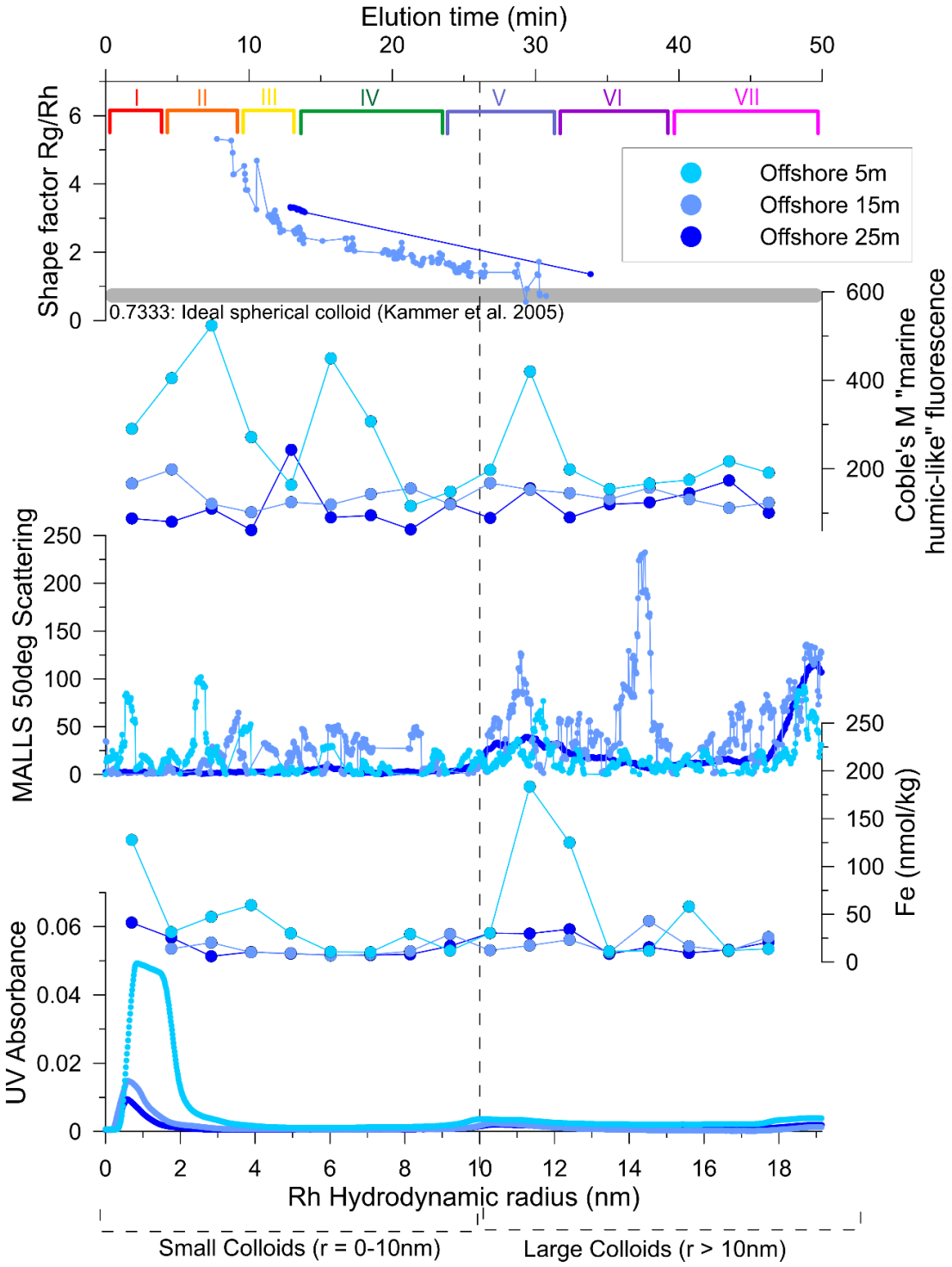

Figure 3.9: Offshore Sta. 1 Colloidal Fe Spectra. Combined results from all detectors and associating it to a hydrodynamic radius and elution time for depths 5, 15, and 25m. The vertical dashed line indicates the cutoff between large and small colloids and the colored brackets delineate size classes. The thick gray line shows the ideal spherical colloid at 0.7333 shape factor with anything greater being less spherical.

with marine humic-like FDOM. Although there was an increasing trend in sphericity with increasing hydrodynamic radius, there was not shape factor data generated for colloids with Rh 0-4 or 13-19 nm due to instrumental issues. In the medium size fraction (Rh = 10-12 nm), there was an abundance of organic- (UVvis absorbance = 0.003) and iron-rich (Fe = 30-35 nmol/kg) colloids of non-spherical (Rg/Rh = 1.5-2.5) colloids possibly associated with marine humic-like FDOM (EEMs M fluorescence = 160 λ). In the largest size fraction (Rh = 17-19 nm), there was a minor abundance (scattering intensity = 25) of organic (UVvis absorbance λ=254 = 0.003) iron (Fe = 20 nmol/kg) colloids that were not associated with an increased signal of marine humic-like FDOM.

3.4.4 Colloidal Fe Distribution at Estuarine Station 2

At Estuarine Station 2, the sample from 5 m depth was situated at the chlorophyll maximum and the lowest salinity of our study, 31.85 (Figure 3.7). The FlFFF results (Figure 3.10) showed that the smallest size fraction (Rh = 0-2 nm) had organic- (UV absorbance = 0.05) and iron-rich (Fe = 50 nmol/kg) colloids that generated a very low abundance scattering signal (scattering intensity = 0-5), likely due to their very small size, and did not seem to be associated with marine humic-like FDOM. In the medium size fraction (Rh = 9-11 nm), there were abundant (scattering intensity = 30) organic colloids (UV absorbance = 0.002). There was no iron immediately coincident with these organic colloids, but in a slightly larger size fraction (Rh = 11-14 nm), there were slightly abundant (scattering intensity = 5-10) iron-rich (Fe = 40-45 nmol/kg) inorganic colloids (UV absorbance ~0) colloids. In the largest size fraction (Rh = 17-19 nm), there was an abundance (scattering intensity = 20) of organic- (UV absorbance = 0.002) and iron-rich (Fe = 38 nmol/kg) colloids. No shape factor data was generated for this sample.

Finally, at Estuarine Station 2, the sample from 15 m depth still had elevated chlorophyll fluorescence (1.3 mg/m^3) and a similar salinity to the 5 m sample, given the relatively well-mixed water column at this site (Figure 3.7). The FlFFF data (Figure 3.10) showed that the smallest size fraction (Rh = 0-2 nm) had organic-rich (UV absorbance = 0.01) colloids with some iron (Fe = 8 nmol/kg Fe) that generated a very low abundance signal (scattering intensity = 0-5) and did not seem to be associated with marine humic-like FDOM. Although there was a general trend of increasing sphericity with increasing hydrodynamic radius, even the largest colloids never reached ideal spherical shape. This sample was unique in that the iron colloids were dispersed across a range of sizes at lower abundance, instead of having unique sizes with higher abundance (Figure 3.10). Within the medium size fraction (Rh = 10-12 nm), there was an abundance (scattering intensity = 60) of organic (UV absorbance = 0.002) colloids with some iron (Fe = 10 nmol/kg Fe) that had sharp removal from spherical shape at distinct points. In the largest size fraction (Rh = 18-19 nm), there was little iron (Fe = 8 nmol/kg) in the organic colloids (UV absorbance = 0.002) that may have been associated with marine humic-like FDOM (fluorescence emission λ=80).

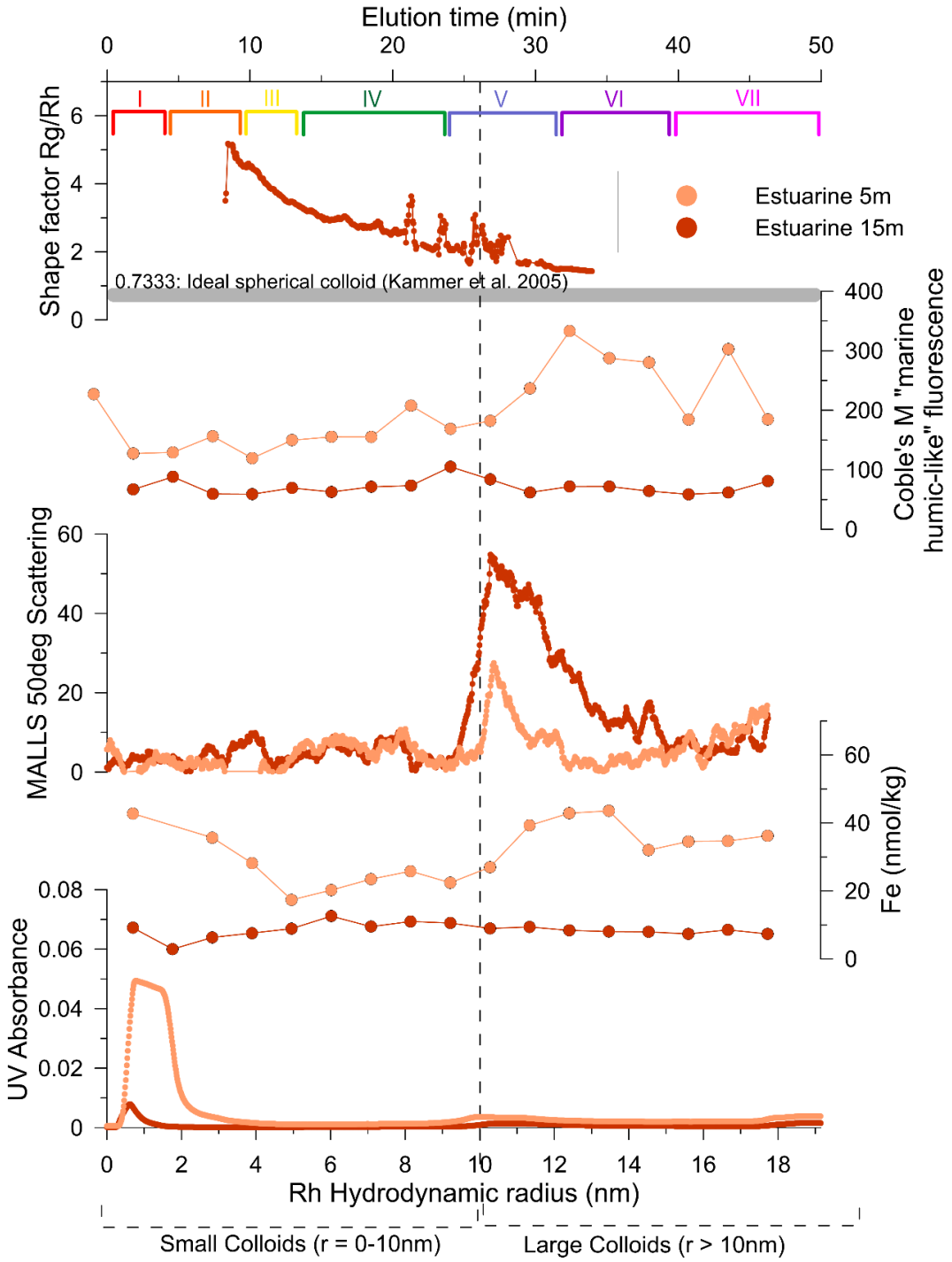

Figure 3.10: Estuarine Sta. 2 Colloidal Fe Spectra. Combined results from all detectors and associating it to a hydrodynamic radius and elution time for depths 5 and 15m. The vertical dashed line indicates the cutoff between large and small colloids and the colored brackets delineate class sizes. The thick gray line shows the ideal spherical colloid at 0.7333 shape factor with anything greater being less spherical.

Table 3.1: Integrated Colloidal Spectra. Values determined by integrating the colloidal spectra curves using the trapezoid rule: UVvis C absorbance, Fe concentrations, MALLS angle 50 scattering, and M marine humic-like FDOM. Sta.1 is the Offshore station and Sta.2 is the Estuarine

	UV (absorbance)	Fe (nmol/kg)	MALLS (scattering)	M (emission λ)
Sta.1 5m	0.2622	1656	731	11538
Sta.1 15m	0.1017	692	1526	6180
Sta.1 25m	0.0613	635	734	5149
Sta.2 5m	0.2625	1296	379	8901
Sta.2 15m	0.0732	379	949	3156
Avg Sta.1	**0.14** ± 0.11	**994** ± 574	**997** ± 458	**7622** ± 3430
Avg Sta.2	**0.17** ± 0.13	**837** ± 648	**664** ± 404	**6029** ± 4062

3.4.5 Comparison Between Stations

The FlFFF data were integrated using the trapezoidal rule for carbon absorbance, Fe concentrations, and marine-like FDOM across the colloidal spectrum for each station (Table 3.1). For both sampling stations, the 5 m depth had the greatest integrated UV carbon absorbance, Fe concentrations, and marine humic-like FDOM compared to the other depths (Table 3.1). The 15 m depths at both stations had the highest amount of integrated light scattering (~colloid abundance). Though not significantly different, the Offshore Station 1 overall had a higher integrated Fe, abundance (scattering), and marine humic-like FDOM distribution than at Estuarine Station 2; however, Estuarine Station 2 had a greater overall integrated C distribution, though again not statistically significantly different from Station 1. In addition, all the samples with shape factor data had increasing sphericity with increasing hydrodynamic radius (Figure 3.11). Offshore Station 1 had slightly more spherical colloids with increasing size than Estuarine Station 2, and colloids were most abundant according to overall light scattering in the Offshore Station 1 15 m sample.

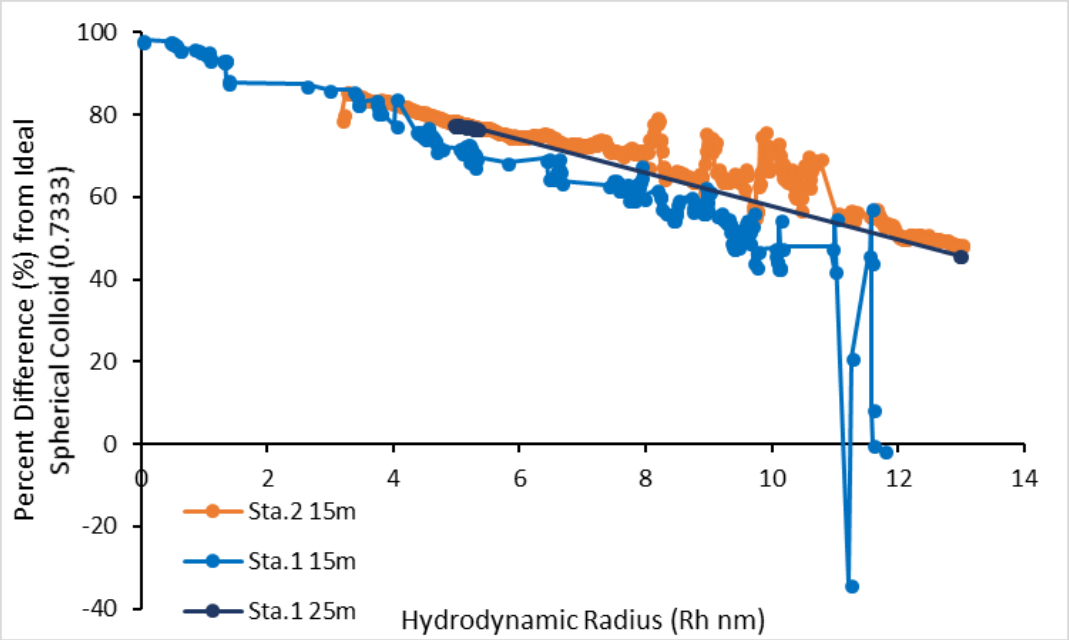

Figure 3.11: Shape Factor (Rg/Rh) Percent Difference. The percent difference from an ideal spherical colloid of 0.7333 Rg/Rh (Kammer et al., 2005) for Offshore Station 1 15 and 25m depths and Estuarine Station 2 15m is displayed.

3.5 Discussion

3.5.1 Major Conclusions

Our primary discovery from the accumulated FlFFF data in Figures 3.9-3.10 was that marine Fe colloids are not uniformly distributed across the colloidal size spectrum, but instead some colloidal sizes have higher Fe concentrations than others. This finding corroborates previous results of a dynamic Fe colloidal distribution in riverine and estuarine environments (Dahlqvist et al., 2004; Hassellöv et al., 1999; Lyvén et al., 2003; Stolpe et al., 2013a; Stolpe et al., 2013b; Stolpe et al., 2010; Stolpe and Hassellöv, 2010). However, in contrast to these earlier freshwater and estuarine studies, we recorded more abundant larger colloids (Rh > 10 nm) than have been observed previously.

Our secondary discovery was that there is a diversity of organic and inorganic Fe colloids across coastal Maine stations. When peaks in Fe and C (UVvis absorption) coincide in the colloidal size spectrum, as a primary interpretation we define this as "organically-bound Fe". However, it is important to note that this interpretation is based on a correlation of organic and Fe species that have concentrations more than three orders of magnitude different, so a correlation does not uniquely identify chemical speciation; to be clear, our method cannot directly measure the presence of "organically-bound" speciation. Ultimately, across the size spectrum, the Fe size distribution was not always correlated with the carbon size distribution (based on UV absorbance), with the distribution of marine-humic like FDOM, or with colloidal abundance (based on scattering intensity). This suggests that colloids in this environment are extremely diverse, even on a single sampling date at only two locations and five total depths.

In order to facilitate interpretation of our results in the context of the prior results in other regions, we used and modified a classification scheme built from a previous study (Stolpe & Hasselov 2010) that recorded four major size populations of colloids: Class I with Rh=0.25-1.5 nm, Class II with Rh=1.5-3.5 nm, Class III with Rh=2.5-5 nm, and Class IV with Rh=3.5-20 nm). While overlapping somewhat in size, in coastal Maine we found more larger colloids that required us to modify the largest Classes III and IV populations by splitting them into Classes III (3.5-5 nm), IV (5-9 nm), V (9-12 nm), VI (12-15 nm), and VII (15-20 nm). We tabulate our results with respect to these colloidal size classes in Table 3.2 (this and prior studies) and Table 3.3 (this study).

Study		Location	Class I (Dh)	Rh		Class II (Dh)	Rh		Class III (Dh)	Rh	
Stolpe et al. 2013a		Alaskan Rivers (REEs)	0.5-3 nm	0.25-1.5	organic, seasonally ubiquitous, fluvic rich	3-8 nm	1.5-4	organic-rich, Fe-rich, spring flood	N/A		
Stolpe et al. 2013b		Alaskan Rivers (TMs)	0.5-3 nm	0.25-1.5	organic, seasonally ubiquitous, fluvic rich	3-8 nm	1.5-4	organic-rich, Fe-rich, spring flood	N/A		
Stolpe et al. 2010		MI and Pear River, MI Bight	0.5-4 nm	0.25-2	CDOM rich, Fe, fluvic rich	3-8 nm	1.5-4	protien like, insitu biological production	N/A		
Stolpe and Hassellov 2010		Gullmarsfjord, Sweden	0.5-3 nm	0.25-1.5	spherical, CDOM rich, Fe, ubquitous	3-7 nm	1.5-3.5	globular	5-10 nm	2.5-5	low iron & organics, polysaccaride rich fibrils
De Salvo et al. 2017		Damariscotta	0.5-3 nm	0.25-1.5	organic rich, ubiquitous, Fe rich	3-7 nm	1.5-3.5	organic-rich	7-10 nm	3.5-5	low iron & organics, polysaccaride rich fibrils
De Salvo et al. 2017		GoMaine Shelf	0.5-3 nm	0.25-1.5	organic rich, ubiquitous, Fe rich	3-7 nm	1.5-3.5	organic-rich	7-10 nm	3.5-5	same as Damariscotta except high Fe at 5m
Class IV (Dh)	Rg		Class V (Dh)	Rg		Class VI (Dh)	Rh		Class VII (Dh)	Rh	
4-40 nm	2-20 nm	Fe rich, summer baseflow									
4-40 nm	2-20 nm	Fe rich, summer baseflow									
5-40 nm	2.5-20 nm	Fe rich, inorganic									
7-40 nm	3.5-20 nm	fibrillar, Fe, upper mixed layer June-July									
10-18 nm	5-9 nm	low Fe, no organic association 15m	18-24 nm	9-12 nm	abundant, organic	24-28 nm	12-15 nm	inorganic at Chlorophyll Max	34-38 nm	15-20 nm	organic rich
N/A			18-24 nm	9-12 nm	abundant, organic	24-28 nm	12-15 nm	inorganic at Chlorophyll Max	34-38 nm	15-20 nm	organic rich

Table 3.2: Intercomparison of this and Previous Studies' Size Classes. Comparing FlFFF-ICPMS size classes and compositional characteristics.

Size		Offshore 5m		Offshore 15m		Offshore 25m		Estuarine 5m		Estuarine 15m	
Small	**C**	organic **rich**	organic	organic **rich**	organic	organic **rich**	organic	organic **rich**	organic	organic **rich**	organic
	Fe		Fe **rich**		low Fe	Fe **rich** (class I)	low Fe	Fe **rich** (class I)	low Fe	Fe (class I)	low Fe
	Abudance			not scattering		not scattering		low abundance			
	M peak			M humic **rich**						M humic **rich** (class I)	
	Shape Factor		non-spherical		non-spherical		non-spherical		non-spherical		non-spherical
	Radius (nm)	class I & 2	class III	class I & 2	class III	class I & 2	class III	class I & 2	class III	class I & 2	class III
Medium	**C**		organic		organic		organic		organic		organic
	Fe		very Fe **rich**				Fe **rich**	low Fe		low Fe	Fe
	Abudance		abundant		abundant		**very** abundant		**very** abundant		abundant
	M peak	M humic	could be bound to m humics		M humic						
	Shape Factor	medium sphericity	medium sphericity	medium sphericity	spherical	medium sphericity	medium sphericity	medium sphericity	medium sphericity	medium sphericity	medium sphericity
	Radius (nm)	class IV	class V	class IV	class V		class V	class IV	class V	class IV	class V
Large	**C**		organic	inorganic	organic		organic		organic		organic
	Fe			Fe	Fe		Fe	Fe **rich**	Fe		Fe
	Abudance		abundant	abundant	abundant		abundant	not abundant	abundant		
	M peak			possible M humic association			possible M humic association	M humic **rich**			M humic
	Shape Factor										
	Radius (nm)		class VII	class VI	class VII		class VII	class VI	class VII		class VII
Hydrography		above chlorophyll max		chlorophyll max		below chlorophyll max		at chlorophyll max		below chlorophyll max	
		particulate rich								particulate rich	
		above pycnocline		slighty above pycnocline		below pycnocline					
		above thermocline		above thermocline		above thermocline					
		Cool ~12.8 C		Coolest 12.17 C		Cool ~12.8 C		Warmer ~13.25		Warm ~13.15	
		Salty ~32.15		Saltier ~32.2		Saltier ~32.55		Fresh ~31.9		Fresh ~31.9	

Table 3.3: Compositional characteristics of Fe colloids per Sample.

All depths at both sites in Maine had three reproducible groups of organic colloids that were identified using UV absorbance: smallest Rh=0-2 nm (Class I and II), medium Rh=10-12 nm (Class V), largest Rh>17 nm (Class VII). The Class I and II colloids had the greatest amount of carbon, while the Class V and VII colloids had approximately equivalent but lower amounts of carbon. The organic-rich Class I and II colloids have also been observed in riverine and lower salinity estuarine environments from the Yukon River, the Mississippi Bight, and the Gullmarsfjord, Sweden (Stolpe et al., 2013a; Stolpe et al., 2013b; Stolpe et al., 2010; Stolpe and Hassellöv, 2010). Together, these previous and our new data confirm that an organic-rich, small colloidal pool may be ubiquitous.

However, prior riverine and estuarine studies did not observe the Class V (Rh=10-12 nm) and Class VII (Rh >17 nm) organic colloid pools that we observed in coastal Maine. The lack of these colloids in previous studies may be related to (1) the fact that these organic colloids did not exist in those sampling regions but do exist in coastal Maine, and/or (2) the fact that the baseline UVvis noise in the larger size fractions may have veiled these smaller carbon abundances. If situation (1), this might indicate that higher salinity waters have larger-sized organic colloids than freshwaters.

In the prior riverine and low-salinity estuarine samples, the smallest Class I colloids (0.25-1.5 nm) were spherical and organic-rich, while in this study these smallest colloids were also organic-rich but were least spherical and also contained Fe. Class II colloids (1.5-3.5 nm) were globular and organic/iron rich in prior studies, while in coastal Maine, we found these colloids to have lower overall abundance that was overshadowed by the high C (UVvis absorbance) and Fe of Class I colloids. Only at the Estuarine Station 2 at 5 m depth was there a clear presence of Class II colloids for Fe. In the Gallmarsfjord study, Class III (2.5-5 nm)

colloids were polysaccharide-rich fibrils (organics signal overshadowed by Class I) that were bound to low concentrations of iron. Similarly, coastal Maine's Class III colloids were very non-spherical, (excluding Estuarine Station 2 at 15m being more spherical), suggesting that they may also be fibrils, with low Fe and organics; however, our rough shape measurements do not preclude other potential shapes and instead only connote "non-spherical." Only at the Offshore Station 1 5m depth were the Class III colloids Fe-rich.

In prior studies, the broadly classified Classes III to IV colloids (3.5-20 nm) were iron-rich and centered near 5-7 nm Rh, with either organic or inorganic composition, depending on location (Stolpe & Hasselov 2010). Under our new Class III and IV classification (5-9 nm Rh), there were only Class IV iron colloids present at the 15 m samples from Estuarine Station 2, and they had low concentrations and no organic association, which is quite different from the literature. At all samples from coastal Maine, however, a group of organic-rich colloids were observed in Class V (9-12 nm Rh), which were never observed in these earlier studies. These Class V colloids were organic-rich and were associated with iron only at depths above and below the chlorophyll maximums at both stations (Offshore Station 1 5m, 25m, and Estuarine Station 2 15m). We hypothesize that this iron association in Class V is not found at the chlorophyll max, possibly due to preferential biological uptake or aggregation of organic Fe.

Class VI colloids (12-15 nm Rh) were present at the chlorophyll maximum at both sampling stations where Offshore Station 1 had a higher abundance compared to Estuarine Station 2. These colloids were uniquely inorganic, as they had iron peaks but no carbon (UVvis absorbance) peaks. This is particularly interesting because the chlorophyll max is also where we see a change in Class V colloids with a loss in Fe association. We hypothesize that the presence of Class VI inorganic colloids at the chlorophyll maximum may be due to preferential uptake of

the more bioavailable organic Fe, leaving behind an increased signature of inorganic Fe colloids. This hypothesis could explain why Offshore Station 1 had a larger Class VI inorganic Fe colloid abundance than Estuarine Station 2 due to the larger concentration of chlorophyll at the max offshore. However, there may also be a unique source of inorganic colloids to the specific depths of these samples, since a phytoplankton preference argument does not explain the lack of inorganic colloids at other depths. It is unique that the inorganic colloids in coastal Maine tend to be characteristically 12-15 nm in hydrodynamic radius. Additional sampling at the chlorophyll max in more coastal Maine during different seasons of freshwater flow and phytoplankton growth are needed to determine the source of these inorganic iron species. Class VII colloids were also never observed in prior literature, though they were consistently observed to be organic-rich in these coastal Maine stations, with varying iron abundance.

With respect to the shape data calculated from the MALLS, colloids in coastal Maine samples varied in shape and became more spherical with increasing size for ~ 0-13 nm radius (notably, we were not able to collect shape factors for Rh=0-4nm, >13-20 nm, or any size for 5 m depths). One previous study imaged the colloidal spectrum in a high salinity estuary using atomic force microscopy and found the opposite trend in the spring flood season with decreasing sphericity in the large-size fraction (Stolpe and Hassellöv, 2010). We may see opposing trends because we sampled in the late fall where there was comparatively low primary production and river runoff. With low primary production, there would be less *in situ* biological production producing nanofibrils, such as EPS, thus resulting in fewer non-spherical colloids at higher size fractions.

Notably, we acknowledge two major caveats that need to be considered when interpreting these FlFFF data. First, because the FlFFF was manufactured to separate engineered spherical

particles that should all behave equally with respect to fluid dynamics, analyzing natural colloids that are not all spherically shaped does affect the elution time and size separation and characterization. For example, fibrillar shaped colloids might elute at varying sizes because they can act like a large colloid or like a small colloid, depending on their orientation in solution. Additionally, aggregation could be accelerated during 0.2 μm filtration or during the FlFFF preconcentration step. Gels for example, which are three dimensional networks of biopolymers imbedded in seawater, quickly aggregate within minutes to hours (Li and Tanaka, 1992; Verdugo and Santschi, 2010), affecting when they would elute as a function of size or whether they aggregate into the larger colloids or even into the particulate size fraction.

Second, the FlFFF does not fractionate colloids from 20 to 200 nm hydrodynamic radius, which leaves us to wonder what happens to these largest colloids and with what they may be comprised. Since the very largest colloids have a very small diffusivity, it is likely they instead are retained at the bottom FlFFF column filter and never elute, only getting removed during the extended acid cleaning step that occurs between samples. Because our method does not analyze colloids >20 nm Rh, we can only speculate what they may be comprised of in coastal Maine. Previous findings in an estuarine environment (Mississippi Bight: Sal 23.5) discovered that this larger size fraction (>20 nm) was dominated by protein-like colloids that were bound to iron (Stolpe et al., 2010). Therefore, we could speculate that the > 20 nm fraction may also be comprised iron-bound proteins.

3.5.2 Regional Conclusions

We had hypothesized that we would see greater overall (integrated) colloidal abundances, C absorbances, and Fe concentrations at the Estuarine Station 2 compared to the Offshore Station 1, due to greater terrestrial input of materials inshore in the estuary. However, the integrated

results from the two stations were not statistically significantly different from each other, which probably results from that fact that Offshore Station 1 still experienced a large estuarine influence from the massive Penobscot watershed, as discussed above. While the Penobscot colloids present at Offshore Station 1 would have to be more aged than the Damariscotta colloids present at Estuarine Station 2, it is impossible to compare the two stations across the small observed salinity gradient as if they were one estuary, since they were undoubtedly sourced differently.

However, there were some reproducible patterns worth highlighting here. Integrated carbon (absorbance), Fe concentrations, and marine humic-like FDOM were consistently higher at the 5 m depth at both stations than the other depths, which may be due to the WMCC and EMCC both bringing in high Fe and C from terrestrial runoff, and the EMCC (which has a marine SSW, LSW, and NASW influence) bringing in more aged marine humic-like FDOM. As seen in Figure 3.5, the Penobscot runoff signature is the freshest and thus diluted with WMCC seawater at the shallowest depth, which may be why we see elevated Fe, C, and marine humic-like FDOM there. In contrast, light scattering was consistently highest at the subsurface 15 m sample at both stations, which may be due to increased scattering signals from the inorganic iron at Offshore Station 1 and due to an increased number of organic (UVvis absorbance) particles at Estuarine Station 2 (Figure 3.7 & 3.10).

Offshore Station 1 reasonably had a higher amount of marine humic-like FDOM, as it receives a more direct marine influence than inside of the Damariscotta River Estuary. However, the two stations had very similar mean integrated C signatures. The similarity may be due to influence from the WMCC bringing in fresh C from Penobscot runoff to Offshore Station 1 while the Damariscotta also introduces a terrestrial runoff signature to Estuarine Station 2. On

the other hand, the estuarine location has a slightly higher mean C signature, which fits with previous finding using the FlFFF-ICPMS method where there is a higher C signature where there is a more direct influence from runoff (Stolpe et al., 2013a; Stolpe et al., 2013b; Stolpe et al., 2010; Stolpe and Hassellöv, 2010). However, because the mean integrated C signature is not significantly different, we cannot confirm this theory without further samples at these two locations in the future.

Although the shape factors for Offshore Station 1 (15 m and 25m) and Estuarine Station 2 (15m) are similar across the colloidal distribution and are not significantly different, there are some key variances to take into consideration. Based on Stolpe and Hassellov's (2010) atomic force microscopy imaging results, less spherical colloids were associated with fibrillar organics that were biogenic in origin, while elongated or globular colloids were associated with metal-rich and organic-poor colloids, and spherical colloids were associated with organic humic acids. Thus, we expected to see more non-spherical colloids where there was more primary production (Sta. 1's chlorophyll max) and more spherical colloids at Estuarine Sta. 2 where there was greater direct runoff influence. However, our results show more comparatively spherical colloids at Offshore Station 1's chlorophyll max, while Estuarine Station 2 had comparatively the least spherical colloids. Because our sampling date occurred when there was little runoff coming from the Penobscott, our observed shape pattern as a function of station location may not persist to seasons with less fluvial input.

The chlorophyll max at Offshore Station 1 is the only sample that has truly spherical colloids (Class V), in direct contrast to our initial hypothesis that this is where we would find the least spherical colloids. However, very spherical colloids are organic in nature, as found in Stolpe and Hassellov's Class I spherical colloids. These spherical colloids were more associated

with humic acids (Stolpe and Hassellöv, 2010; Wilkinson et al., 1999), while more inorganic colloids were less spherical and more globular due to their crystalline and aggregated nature (Buffle et al., 1998; Stolpe and Hassellöv, 2010). So, the very spherical colloids observed at Offshore Station 1 at the 15 m chlorophyll maximum could be a function of increased aged biological constituents from primary production, i.e. marine humics. This hypothesis is supported by the increase in C and in marine humic-like FDOM at the same size fraction (class V) where we see spherical colloids with a shape factor near ideal sphericity of ~0.7333. According to one study, marine humic substances generated from the photooxidation of primary production byproducts (e.g. fatty acids and triglycerides) increased over a 14 day timescale following a bloom (Kieber et al., 1997). Analogously, with the Gulf of Maine Fall bloom starting in September to early October and with our sampling time occurring at the end of October, it is possible that there was an increase in marine humic substances present at the chlorophyll maximum created from the photooxidation of the Fall bloom's primary production byproducts. Furthermore, because our sampling date occurred in the dry season when there was little river runoff, it is less likely that the spherical colloids derive from riverine inputs, i.e. terrestrial humics.

3.6 Conclusion

We present the first results successfully coupling FlFFF to ICPMS for analysis the colloidal carbon and iron size distribution and shape on full salinity samples from coastal Maine. Our primary discovery was that marine iron colloids are not uniformly distributed in size, but instead have unique sizes with higher abundances. We found that the 3-4 colloidal size classes reported in prior studies from low salinity rivers and estuaries need to be expanded to fit the more diverse colloidal classes found in coastal Maine: Class I (0.25-1.5 nm hydrodynamic

radius) is ubiquitously iron and organic-rich; class II (1.5-3.5 nm) is ubiquitously organic rich; class III (2.5-5 nm) is very non-spherical with low concentrations of organic iron; class IV (5-9 nm) found only at Estuarine Station 2 15m is iron-poor; class V (9-12 nm) is organic and comparatively abundant with a decrease in Fe association at the chlorophyll max; class VI (12-15 nm), found at both station's chlorophyll maximum, is iron-rich and inorganic; and class VII (15-20 nm) is ubiquitously organic-rich. Furthermore, we discovered that there are a range of both organically-bound and inorganic Fe colloids at both the estuarine and continental shelf stations, and the shape of these marine colloids increased in sphericity with increasing colloidal size. These conclusions are first steps in breaking open the "black box" that was the iron colloidal size distribution in oceanic waters.

CHAPTER IV

CONCLUSION

Dissolved iron is one of the most important micronutrients for shaping the abundance and community composition of phytoplankton in surface waters. Because colloidal iron composes a significant portion of the dissolved fraction, it is imperative to understand the compositional characteristics of the colloidal size spectrum in oceanic surface waters and how that may change seasonally and spatially in order to understand the role of iron speciation on its bioavailability, transport, and scavenging fate. To characterize colloidal iron in seawater, our new method FlFFF—UV—MALLS—EEMs—ICPMS successfully overcame the major analytical hurdles of measuring the iron colloidal size distribution in seawater and was used to separate marine colloids by size and assess their radius, shape, organic carbon content and character, and iron concentration in coastal Maine waters. The results from this new method answered critical oceanographic questions of colloidal iron's biogeochemical speciation and role in nearshore marine solutions: individual size fractions of colloidal iron are composed of different chemical constituents that, in turn, likely differ in biological and geochemical reactivities, ultimately determining the biological and scavenging fate of the dissolved iron pool. The null hypothesis that all marine iron colloids have the same chemical composition across the size spectrum was disproved, and it was instead shown that there is a dynamic colloidal iron continuum that varies spatially in costal Maine and with depth.

Our next steps are to 1) resolve our issue of procedural blanks by adjusting the FlFFF cleaning steps, and then 2) assess how our observed colloidal size distributions in coastal Maine change as a factor of seasonal variation by analyzing samples from the same stations and depths

during the Spring. During Spring in coastal Maine, our stations receive vast amounts of terrestrial runoff following snow melt and large amounts of primary production in the Spring blooms. Comparing the data collected from October 2017 to future Spring data (anticipated June 2018) will give insight into how terrestrial runoff and phytoplankton blooms may affect the compositional characteristics and physicochemical speciation of the iron colloidal distribution.

Future work beyond the scope of this coastal Maine environment could take this method to analyze the iron colloid spectrum in other oceanic regions to see if the patterns we observed persist in other environments. Ultimately, the findings of this research will have broad implications to various fields (e.g. oceanography, biogeochemistry, land-sea coupling) and, finally, to modeling studies of biogeochemistry and climate change.

REFERENCES

Amon, R.M. and Benner, R. (1996) Bacterial utilization of different size classes of dissolved organic matter. Limnology and Oceanography 41, 41-51.

Azam, F., Fenchel, T., Field, J.G., Gray, J., Meyer-Reil, L. and Thingstad, F. (1983) The ecological role of water-column microbes in the sea. Marine ecology progress series, 257-263.

Baalousha, M., Stolpe, B. and Lead, J. (2011) Flow field-flow fractionation for the analysis and characterization of natural colloids and manufactured nanoparticles in environmental systems: a critical review. Journal of Chromatography A 1218, 4078-4103.

Balch, W.M., Drapeau, D., Bowler, B. and Huntington, T.G. (2012) Step-changes in the physical, chemical and biological characteristics of the Gulf of Maine, as documented by the GNATS time series. Marine Ecology Progress Series 450, 11-35.

Barbeau, K. and Moffett, J. (2000) Laboratory and field studies of colloidal iron oxide dissolution as mediated by phagotrophy and photolysis. Limnology and Oceanography 45, 827-835.

Baskaran, M., Santschi, P.H., Benoit, G. and Honeyman, B. (1992) Scavenging of thorium isotopes by colloids in seawater of the Gulf of Mexico. Geochimica et Cosmochimica Acta 56, 3375-3388.

Batchelli, S., Muller, F.L., Baalousha, M. and Lead, J.R. (2009) Size fractionation and optical properties of colloids in an organic-rich estuary (Thurso, UK). Marine Chemistry 113, 227-237.

Batchelli, S., Muller, F.L., Chang, K.-C. and Lee, C.-L. (2010) Evidence for strong but dynamic iron− humic colloidal associations in humic-rich coastal waters. Environmental science & technology 44, 8485-8490.

Benner, R., Biddanda, B., Black, B. and McCarthy, M. (1997) Abundance, size distribution, and stable carbon and nitrogen isotopic compositions of marine organic matter isolated by tangential-flow ultrafiltration. Marine Chemistry 57, 243-263.

Benoit, G., Oktay-Marshall, S., Cantu, A., Hood, E., Coleman, C., Corapcioglu, M. and Santschi, P. (1994) Partitioning of Cu, Pb, Ag, Zn, Fe, Al, and Mn between filter-retained particles, colloids, and solution in six Texas estuaries. Marine Chemistry 45, 307-336.

Berglund, M. and Wieser, M.E. (2011) Isotopic compositions of the elements 2009 (IUPAC Technical Report). Pure and applied chemistry 83, 397-410.

Bergquist, B., Wu, J. and Boyle, E. (2007) Variability in oceanic dissolved iron is dominated by the colloidal fraction. Geochimica et Cosmochimica Acta 71, 2960-2974.

Boehme, J. and Wells, M. (2006) Fluorescence variability of marine and terrestrial colloids: Examining size fractions of chromophoric dissolved organic matter in the Damariscotta River estuary. Marine Chemistry 101, 95-103.

Boyd, P. and Ellwood, M. (2010) The biogeochemical cycle of iron in the ocean. Nature Geoscience 3, 675-682.

Boyd, P.W., Jickells, T., Law, C., Blain, S., Boyle, E., Buesseler, K., Coale, K., Cullen, J., De Baar, H.J. and Follows, M. (2007) Mesoscale iron enrichment experiments 1993-2005: Synthesis and future directions. science 315, 612-617.

Boyle, E., Edmond, J. and Sholkovitz, E. (1977) The mechanism of iron removal in estuaries. Geochimica et Cosmochimica Acta 41, 1313-1324.

Bruland, K. and Lohan, M. (2006) Controls of trace metals in seawater. The oceans and marine geochemistry 6, 23-47.

Bruland, K.W., Coale, K.H. and Mart, L. (1985) Analysis of seawater for dissolved cadmium, copper and lead: An intercomparison of voltammetric and atomic absorption methods. Marine Chemistry 17, 285-300.

Bruland, K.W., Orians, K.J. and Cowen, J.P. (1994) Reactive trace metals in the stratified central North Pacific. Geochimica et Cosmochimica Acta 58, 3171-3182.

Bruland, K. W., & Rue, E. L. (2001). Iron: Analytical methods for the determination of concentrations and speciation. The Biogeochemistry of Iron in Seawater, 255-289.

Buck, K.N., Lohan, M.C., Berger, C.J. and Bruland, K.W. (2007) Dissolved iron speciation in two distinct river plumes and an estuary: Implications for riverine iron supply. Limnology and Oceanography 52, 843-855.

Buck, K.N., Moffett, J., Barbeau, K.A., Bundy, R.M., Kondo, Y. and Wu, J. (2012) The organic complexation of iron and copper: an intercomparison of competitive ligand exchange-adsorptive cathodic stripping voltammetry (CLE-ACSV) techniques. Limnology and Oceanography: Methods 10, 496-515.

Buffle, J., Wilkinson, K.J., Stoll, S., Filella, M. and Zhang, J. (1998) A generalized description of aquatic colloidal interactions: the three-colloidal component approach. Environmental Science & Technology 32, 2887-2899.

Bundy, R.M., Jiang, M., Carter, M. and Barbeau, K.A. (2016) Iron-binding ligands in the southern California current system: mechanistic studies. Frontiers in Marine Science 3, 27.

Carnegie, R.B. and Barber, B.J. (2001) Growth and mortality of Ostrea edulis at two sites on the Damariscotta River estuary, Maine, USA. Journal of the World Aquaculture Society 32, 221-227.

Chen, M., Dei, R.C., Wang, W.-X. and Guo, L. (2003) Marine diatom uptake of iron bound with natural colloids of different origins. Marine Chemistry 81, 177-189.

Chen, M. and Wang, W.-X. (2001) Bioavailability of natural colloid-bound iron to marine plankton: Influences of colloidal size and aging. Limnology and oceanography 46, 1956-1967.

Coble, P.G. (1996) Characterization of marine and terrestrial DOM in seawater using excitation-emission matrix spectroscopy. Marine chemistry 51, 325-346.

Cronan, C., Piampiano, J. and Patterson, H. (1999) Influence of land use and hydrology on exports of carbon and nitrogen in a Maine river basin. Journal of Environmental Quality 28, 953-961.

Cronan, C.S. (2012) Biogeochemistry of the Penobscot River watershed, Maine, USA: nutrient export patterns for carbon, nitrogen, and phosphorus. Environmental monitoring and assessment 184, 4279-4288.

Cullen, J.T., Bergquist, B.A. and Moffett, J.W. (2006) Thermodynamic characterization of the partitioning of iron between soluble and colloidal species in the Atlantic Ocean. Marine Chemistry 98, 295-303.

Dahlqvist, R., Benedetti, M.F., Andersson, K., Turner, D., Larsson, T., Stolpe, B. and Ingri, J. (2004) Association of calcium with colloidal particles and speciation of calcium in the Kalix and Amazon rivers. Geochimica et Cosmochimica Acta 68, 4059-4075.

De Baar, H.J., Boyd, P.W., Coale, K.H., Landry, M.R., Tsuda, A., Assmy, P., Bakker, D.C., Bozec, Y., Barber, R.T. and Brzezinski, M.A. (2005) Synthesis of iron fertilization experiments: from the iron age in the age of enlightenment. Journal of Geophysical Research: Oceans 110.

Erickson, H.P. (2009) Size and shape of protein molecules at the nanometer level determined by sedimentation, gel filtration, and electron microscopy. Biological procedures online 11, 32.

Fischer, A., Kroon, J., Verburg, T., Teunissen, T. and Wolterbeek, H.T. (2007) On the relevance of iron adsorption to container materials in small-volume experiments on iron marine

chemistry: 55Fe-aided assessment of capacity, affinity and kinetics. Marine Chemistry 107, 533-546.

Fitzsimmons, J.N. and Boyle, E.A. (2012) An intercalibration between the GEOTRACES GO-FLO and the MITESS/Vanes sampling systems for dissolved iron concentration analyses (and a closer look at adsorption effects). Limnology and Oceanography: Methods 10, 437-450.

Fitzsimmons, J.N. and Boyle, E.A. (2014a) Assessment and comparison of Anopore and cross flow filtration methods for the determination of dissolved iron size fractionation into soluble and colloidal phases in seawater. Limnology and Oceanography: Methods 12, 246-263.

Fitzsimmons, J.N. and Boyle, E.A. (2014b) Both soluble and colloidal iron phases control dissolved iron variability in the tropical North Atlantic Ocean. Geochimica et Cosmochimica Acta 125, 539-550.

Fitzsimmons, J.N., Bundy, R.M., Al-Subiai, S.N., Barbeau, K.A. and Boyle, E.A. (2015a) The composition of dissolved iron in the dusty surface ocean: an exploration using size-fractionated iron-binding ligands. Marine Chemistry 173, 125-135.

Fitzsimmons, J.N., Carrasco, G.G., Wu, J., Roshan, S., Hatta, M., Measures, C.I., Conway, T.M., John, S.G. and Boyle, E.A. (2015b) Partitioning of dissolved iron and iron isotopes into soluble and colloidal phases along the GA03 GEOTRACES North Atlantic Transect. Deep Sea Research Part II: Topical Studies in Oceanography 116, 130-151.

Fitzsimmons, J.N., John, S.G., Marsay, C.M., Hoffman, C.L., Nicholas, S.L., Toner, B.M., German, C.R. and Sherrell, R.M. (2017) Iron persistence in a distal hydrothermal plume supported by dissolved–particulate exchange. Nature Geoscience 10, 195.

Floge, S.A. and Wells, M.L. (2007) Variation in colloidal chromophoric dissolved organic matter in the Damariscotta Estuary, Maine. Limnology and oceanography 52, 32-45.

Freimann, P., Schmidt, D. and Schomaker, K. (1983) Mercos—a simple Teflon sampler for ultratrace metal analysis in seawater. Marine Chemistry 14, 43-48.

Geyer, W., Signell, R., Fong, D., Wang, J., Anderson, D. and Keafer, B. (2004) The freshwater transport and dynamics of the western Maine coastal current. Continental Shelf Research 24, 1339-1357.

Giddings, J.C., Yang, F.J. and Myers, M.N. (1976) Theoretical and experimental characterization of flow field-flow fractionation. Analytical Chemistry 48, 1126-1132.

Gledhill, M. and Buck, K.N. (2012) The organic complexation of iron in the marine environment: a review. Frontiers in microbiology 3, 69.

Gledhill, M. and van den Berg, C.M. (1994) Determination of complexation of iron (III) with natural organic complexing ligands in seawater using cathodic stripping voltammetry. Marine Chemistry 47, 41-54.

Grout, H., Sempere, R., Thill, A., Calafat, A., Prieur, L. and Canals, M. (2001) Morphological and chemical variability of colloids in the Almeria-Oran Front in the eastern Alboran Sea (SW Mediterranean Sea). Limnology and oceanography 46, 1347-1357.

Guieu, C., Martin, J.-M., Tankere, S., Mousty, F., Trincherini, P., Bazot, M. and Dai, M. (1998) On trace metal geochemistry in the Danube River and western Black Sea. Estuarine, Coastal and Shelf Science 47, 471-485.

Guo, L. and Santschi, P.H. (1997) Composition and cycling of colloids in marine environments. Reviews of Geophysics 35, 17-40.

Hassellöv, M., Lyvén, B., Haraldsson, C. and Sirinawin, W. (1999) Determination of continuous size and trace element distribution of colloidal material in natural water by on-line coupling of flow field-flow fractionation with ICPMS. Analytical chemistry 71, 3497-3502.

Hassler, C.S., Alasonati, E., Nichols, C.M. and Slaveykova, V. (2011a) Exopolysaccharides produced by bacteria isolated from the pelagic Southern Ocean—role in Fe binding, chemical reactivity, and bioavailability. Marine Chemistry 123, 88-98.

Hassler, C.S., Schoemann, V., Nichols, C.M., Butler, E.C. and Boyd, P.W. (2011b) Saccharides enhance iron bioavailability to Southern Ocean phytoplankton. Proceedings of the National Academy of Sciences 108, 1076-1081.

Heissenberger, A., Herndl, G., Flannigan, D., Lott, J. and Leppard, G. (1994) Ultrastructure of the matrix of marine snow, Abstracts of Papers of the American Chemical Society. Amer Chemical Soc 1155 16th St, NW, Washington, DC 20036, pp. 179-Geoc.

Heissenberger, A. and Herndl, G.J. (1994) Formation of high molecular weight material by free-living marine bacteria. Marine Ecology Progress Series, 129-135.

Hider, R.C. and Kong, X. (2010) Chemistry and biology of siderophores. Natural product reports 27, 637-657.

Hodgkins, G.A. and Dudley, R.W. (2005) Changes in the magnitude of annual and monthly streamflows in New England, 1902-2002, No. 2005-5135.

Honeyman, B. and Santschi, P. (1989) A Brownian-pumping model for oceanic trace metal scavenging: evidence from Th isotopes. Journal of Marine Research 47, 951-992.

Hutchins, D.A., Witter, A.E., Butler, A. and Luther, G.W. (1999) Competition among marine phytoplankton for different chelated iron species. Nature 400, 858-861.

Ji, R., Davis, C.S., Chen, C., Townsend, D.W., Mountain, D.G. and Beardsley, R.C. (2007) Influence of ocean freshening on shelf phytoplankton dynamics. Geophysical Research Letters 34.

Johnson, K.S., Elrod, V., Fitzwater, S., Plant, J., Boyle, E., Bergquist, B., Bruland, K., Aguilar-Islas, A., Buck, K. and Lohan, M. (2007) Developing standards for dissolved iron in seawater. Eos, Transactions American Geophysical Union 88, 131-132.

Johnson, K.S., Gordon, R.M. and Coale, K.H. (1997) What controls dissolved iron concentrations in the world ocean? . Marine chemistry 57, 181-186.

Kammer, F., Baborowski, M. and Friese, K. (2005) Field-flow fractionation coupled to multi-angle laser light scattering detectors: applicability and analytical benefits for the analysis of environmental colloids. Analytica chimica acta 552, 166-174.

Kepkay, P.E. (1994) Particle aggregation and the biological reactivity of colloids. Marine Ecology Progress Series, 293-304.

Kieber, R.J., Hydro, L.H. and Seaton, P.J. (1997) Photooxidation of triglycerides and fatty acids in seawater: Implication toward the formation of marine humic substances. Limnology and Oceanography 42, 1454-1462.

Lagerström, M., Field, M., Séguret, M., Fischer, L., Hann, S. and Sherrell, R. (2013) Automated on-line flow-injection ICP-MS determination of trace metals (Mn, Fe, Co, Ni, Cu and Zn) in open ocean seawater: Application to the GEOTRACES program. Marine Chemistry 155, 71-80.

Laglera, L.M. and van den Berg, C.M. (2009) Evidence for geochemical control of iron by humic substances in seawater. Limnology and Oceanography 54, 610-619.

Lee, J.-M., Boyle, E.A., Echegoyen-Sanz, Y., Fitzsimmons, J.N., Zhang, R. and Kayser, R.A. (2011) Analysis of trace metals (Cu, Cd, Pb, and Fe) in seawater using single batch nitrilotriacetate resin extraction and isotope dilution inductively coupled plasma mass spectrometry. Analytica chimica acta 686, 93-101.

Lee, W.Y. and McAlice, B. (1979) Seasonal succession and breeding cycles of three species of Acartia (Copepoda: Calanoida) in a Maine estuary. Estuaries 2, 228-235.

Leppard, G.G., Heissenberger, A. and Herndl, G.J. (1996) Ultrastructure of marine snow. I. Transmission electron microscopy methodology. Marine Ecology Progress Series, 289-298.

Leppard, G.G., West, M.M., Flannigan, D.T., Carson, J. and Lott, J.N. (1997) A classification scheme for marine organic colloids in the Adriatic Sea: colloid speciation by transmission electron microscopy. Canadian Journal of Fisheries and Aquatic Sciences 54, 2334-2349.

Li, Y. and Tanaka, T. (1992) Phase transitions of gels. Annual Review of Materials Science 22, 243-277.

Lynch, D.R., Holboke, M.J. and Naimie, C.E. (1997) The Maine coastal current: spring climatological circulation. Continental Shelf Research 17, 605-634.

Lyvén, B., Hassellöv, M., Haraldsson, C. and Turner, D. (1997) Optimisation of on-channel preconcentration in flow field-flow fractionation for the determination of size distributions of low molecular weight colloidal material in natural waters. Analytica chimica acta 357, 187-196.

Lyvén, B., Hassellöv, M., Turner, D.R., Haraldsson, C. and Andersson, K. (2003) Competition between iron-and carbon-based colloidal carriers for trace metals in a freshwater assessed using flow field-flow fractionation coupled to ICPMS. Geochimica et Cosmochimica Acta 67, 3791-3802.

Martin, J.H. and Gordon, R.M. (1988) Northeast Pacific iron distributions in relation to phytoplankton productivity. Deep Sea Research Part A. Oceanographic Research Papers 35, 177-196.

Martin, J.M., Dai, M.H. and Cauwet, G. (1995) Significance of colloids in the biogeochemical cycling of organic carbon and trace metals in the Venice Lagoon (Italy). Limnology and Oceanography 40, 119-131.

Mayer, L., Townsend, D., Pettigrew, N., Loder, T., Wong, M., Kistner-Morris, D., Laursen, A., Schoudel, A., Conairis, C. and Brown, J. (1996) The Kennebec, Sheepscot and Damariscotta River estuaries: Seasonal oceanographic data. University of Maine. Department of Oceanography Technical Report.

Mayer, L.M., Schick, L.L. and Loder, T.C. (1999) Dissolved protein fluorescence in two Maine estuaries. Marine Chemistry 64, 171-179.

McAlice, B. (1993) Environmental characteristics of the Damariscotta River estuary, Maine. Darling Marine Center, Special Publication 1, 1-119.

McLaren, J., Mykytiuk, A., Willie, S. and Berman, S. (1985) Determination of trace metals in seawater by inductively coupled plasma mass spectrometry with preconcentration on silica-immobilized 8-hydroxyquinoline. Analytical Chemistry 57, 2907-2911.

Measures, C., Yuan, J. and Resing, J. (1995) Determination of iron in seawater by flow injection analysis using in-line preconcentration and spectrophotometric detection. Marine Chemistry 50, 3-12.

Moore, J. and Braucher, O. (2008) Sedimentary and mineral dust sources of dissolved iron to the world ocean. Biogeosciences 5, 631-656.

Moore, J.K., Doney, S.C., Glover, D.M. and Fung, I.Y. (2001) Iron cycling and nutrient-limitation patterns in surface waters of the World Ocean. Deep Sea Research Part II: Topical Studies in Oceanography 49, 463-507.

Mopper, K., Ramana, K.S. and Drapeau, D.T. (1995) The role of surface-active carbohydrates in the flocculation of a diatom bloom in a mesocosm. Deep Sea Research Part II: Topical Studies in Oceanography 42, 47-73.

Moran, B.S. and Buesseler, K.O. (1993) Size-fractionated 234Th in continental shelf waters off New England: implications for the role of colloids in oceanic trace metal scavenging. Journal of Marine Research 51, 893-922.

Moran, S.B. and Buesseler, K.O. (1992) Short residence time of colloids in the upper ocean estimated from 238U–234Th disequilibria. Nature 359, 221-223.

Morel, F.M., Kustka, A. and Shaked, Y. (2008) The role of unchelated Fe in the iron nutrition of phytoplankton. Limnology and Oceanography 53, 400-404.

Nanolytics. (2018). [Influence of the separation field in F-FFF]. Field-Flow Fractionation. Retrieved from http://www.nanolytics.de/en/other_methods_colloidal_analytics/field-flow_fractionation

National Data Buoy Center. (2017). [Maine Buoys F01 (Central Maine Shelf) and E01 (Penobscot Bay)]. National Oceanic and Atmospheric Administration. Retrieved from https://www.ndbc.noaa.gov/

Nishioka, J., Takeda, S., Wong, C. and Johnson, W. (2001) Size-fractionated iron concentrations in the northeast Pacific Ocean: distribution of soluble and small colloidal iron. Marine Chemistry 74, 157-179.

Niven, S., Kepkay, P. and Boraie, A. (1995) Colloidal organic carbon and colloidal 234 Th dynamics during a coastal phytoplankton bloom. Deep Sea Research Part II: Topical Studies in Oceanography 42, 257-273.

Obata, H., Karatani, H. and Nakayama, E. (1993) Automated determination of iron in seawater by chelating resin concentration and chemiluminescence detection. Analytical Chemistry 65, 1524-1528.

Öztürk, M. and Bizsel, N. (2003) Iron speciation and biogeochemistry in different nearshore waters. Marine chemistry 83, 145-156.

Palma, A.T., Steneck, R.S. and Wilson, C.J. (1999) Settlement-driven, multiscale demographic patterns of large benthic decapods in the Gulf of Maine. Journal of Experimental Marine Biology and Ecology 241, 107-136.

Pershing, A.J., Greene, C.H., Hannah, C., Sameoto, D., Head, E., Mountain, D.G., Jossi, J.W., Benfield, M.C., Reid, P.C. and Durbin, T.G. (2001) Oceanographic responses to climate in the Northwest Atlantic. Oceanography, 76-82.

Pettigrew, N.R., Churchill, J.H., Janzen, C.D., Mangum, L.J., Signell, R.P., Thomas, A.C., Townsend, D.W., Wallinga, J.P. and Xue, H. (2005) The kinematic and hydrographic structure of the Gulf of Maine Coastal Current. Deep Sea Research Part II: Topical Studies in Oceanography 52, 2369-2391.

Powell, R.T., Landing, W.M. and Bauer, J.E. (1996) Colloidal trace metals, organic carbon and nitrogen in a southeastern US estuary. Marine Chemistry 55, 165-176.

Raven, J.A., Evans, M.C. and Korb, R.E. (1999) The role of trace metals in photosynthetic electron transport in O2-evolving organisms. Photosynthesis Research 60, 111-150.

Revelante, N. and Gilmartin, M. (1987) Seasonal cycle of the ciliated protozoan and micrometazoan biomass in a Gulf of Maine estuary. Estuarine, Coastal and Shelf Science 25, 581-598.

Rich, H.W. and Morel, F.M. (1990) Availability of well-defined iron colloids to the marine diatom Thalassiosira weissflogii. Limnology and Oceanography 35, 652-662.

Rue, E.L. and Bruland, K.W. (1995) Complexation of iron (III) by natural organic ligands in the Central North Pacific as determined by a new competitive ligand equilibration/adsorptive cathodic stripping voltammetric method. Marine chemistry 50, 117-138.

Saito, M.A. and Schneider, D.L. (2006) Examination of precipitation chemistry and improvements in precision using the Mg (OH) 2 preconcentration inductively coupled plasma mass spectrometry (ICP-MS) method for high-throughput analysis of open-ocean Fe and Mn in seawater. Analytica Chimica Acta 565, 222-233.

San, S.A., Rivera-Duarte, I. and Flegal, A.R. (1996) Distribution of colloidal trace metals in the San Francisco Bay estuary. Geochimica et Cosmochimica Acta 60, 4933-4944.

Sanders, R.W. (1987) Tintinnids and other microzooplankton—seasonal distributions and relationships to resources and hydrography in a Maine estuary. Journal of Plankton Research 9, 65-77.

Santschi, P.H., Balnois, E., Wilkinson, K.J., Zhang, J., Buffle, J. and Guo, L. (1998) Fibrillar polysaccharides in marine macromolecular organic matter as imaged by atomic force microscopy and transmission electron microscopy. Limnology and Oceanography 43, 896-908.

Santschi, P.H., Guo, L., Baskaran, M., Trumbore, S., Southon, J., Bianchi, T.S., Honeyman, B. and Cifuentes, L. (1995) Isotopic evidence for the contemporary origin of high-molecular weight organic matter in oceanic environments. Geochimica et Cosmochimica Acta 59, 625-631.

Shaked, Y. and Lis, H. (2012) Disassembling iron availability to phytoplankton. Environmental Bioinorganic Chemistry of Aquatic Microbial Organisms, 28.

Sholkovitz, E. (1976) Flocculation of dissolved organic and inorganic matter during the mixing of river water and seawater. Geochimica et Cosmochimica Acta 40, 831-845.

Sholkovitz, E., Boyle, E. and Price, N. (1978) The removal of dissolved humic acids and iron during estuarine mixing. Earth and Planetary Science Letters 40, 130-136.

Sigman, D.M. and Boyle, E.A. (2000) Glacial/interglacial variations in atmospheric carbon dioxide. Nature 407, 859.

Stolpe, B., Guo, L. and Shiller, A.M. (2013a) Binding and transport of rare earth elements by organic and iron-rich nanocolloids in Alaskan rivers, as revealed by field-flow fractionation and ICP-MS. Geochimica et Cosmochimica Acta 106, 446-462.

Stolpe, B., Guo, L., Shiller, A.M. and Aiken, G.R. (2013b) Abundance, size distributions and trace-element binding of organic and iron-rich nanocolloids in Alaskan rivers, as revealed by field-flow fractionation and ICP-MS. Geochimica et Cosmochimica Acta 105, 221-239.

Stolpe, B., Guo, L., Shiller, A.M. and Hassellöv, M. (2010) Size and composition of colloidal organic matter and trace elements in the Mississippi River, Pearl River and the northern Gulf of Mexico, as characterized by flow field-flow fractionation. Marine Chemistry 118, 119-128.

Stolpe, B. and Hassellöv, M. (2007) Changes in size distribution of fresh water nanoscale colloidal matter and associated elements on mixing with seawater. Geochimica et Cosmochimica Acta 71, 3292-3301.

Stolpe, B. and Hassellöv, M. (2010) Nanofibrils and other colloidal biopolymers binding trace elements in coastal seawater: significance for variations in element size distributions. Limnology and Oceanography 55, 187.

Stolpe, B., Hassellöv, M., Andersson, K. and Turner, D.R. (2005) High resolution ICPMS as an on-line detector for flow field-flow fractionation; multi-element determination of colloidal size distributions in a natural water sample. Analytica Chimica Acta 535, 109-121.

Sunda, W.G. (2012) Feedback interactions between trace metal nutrients and phytoplankton in the ocean. Frontiers in Microbiology 3, 204.

Sunda, W.G. and Huntsman, S.A. (1995) Iron uptake and growth limitation in oceanic and coastal phytoplankton. Marine Chemistry 50, 189-206.

Swaby, R. and Ladd, J. (1962) Chemical nature, microbial resistance, and origin of soil humus. Transaction of the joint meeting of commission IV and V. Conference of International Society of Soil Science, New Zealand.

Tagliabue, A., Aumont, O. and Bopp, L. (2014) The impact of different external sources of iron on the global carbon cycle. Geophysical Research Letters 41, 920-926.

Thomas, A.C., Townsend, D.W. and Weatherbee, R. (2003) Satellite-measured phytoplankton variability in the Gulf of Maine. Continental Shelf Research 23, 971-989.

Toner, B.M., Fakra, S.C., Manganini, S.J., Santelli, C.M., Marcus, M.A., Moffett, J.W., Rouxel, O., German, C.R. and Edwards, K.J. (2009) Preservation of iron (II) by carbon-rich matrices in a hydrothermal plume. Nature Geoscience 2, 197.

Toner, B.M., German, C.R., Dick, G.J. and Breier, J.A. (2015) Deciphering the complex chemistry of deep-ocean particles using complementary synchrotron x-ray microscope and microprobe instruments. Accounts of chemical research 49, 128-137.

USGS. (2017). [West, Enfield, Maine Penobscot River Discharge]. National Water Information System. Retrieved from https://waterdata.usgs.gov/me/nwis/current/?type=flow.

Verdugo, P. and Santschi, P.H. (2010) Polymer dynamics of DOC networks and gel formation in seawater. Deep Sea Research Part II: Topical Studies in Oceanography 57, 1486-1493.

Von Der Heyden, B. and Roychoudhury, A. (2015) A review of colloidal iron partitioning and distribution in the open ocean. Marine Chemistry 177, 9-19.

Wang, W.-X. and Dei, R.C. (2003) Bioavailability of iron complexed with organic colloids to the cyanobacteria Synechococcus and Trichodesmium. Aquatic Microbial Ecology 33, 247-259.

Wells, M., Mayer, L. and Guillard, R. (1991) A chemical method for estimating the availability of iron to phytoplankton in seawater. Marine Chemistry 33, 23-40.

Wells, M.L. (1998) Marine colloids: A neglected dimension. Nature 391, 530-531.

Wells, M.L. (2002) Marine colloids and trace metals. Biogeochemistry of marine dissolved organic matter, 367-404.

Wells, M.L. (2004) The colloidal size spectrum of CDOM in the coastal region of the Mississippi Plume using flow field-flow fractionation. Marine chemistry 89, 89-102.

Wells, M.L. and Goldberg, E.D. (1993) Colloid aggregation in seawater. Marine Chemistry 41, 353-358.

Wells, M.L. and Goldberg, E.D. (1994) The distribution of colloids in the North Atlantic and Southern Oceans. Limnology and Oceanography 39, 286-302.

Wells, M.L., Smith, G.J. and Bruland, K. (2000) The distribution of colloidal and particulate bioactive metals in Narragansett Bay, RI. Marine Chemistry 71, 143-163.

Wells, M.L., Zorkin, N.G. and Lewis, A. (1983) The role of colloid chemistry in providing a source of iron to phytoplankton. Journal of Marine Research 41, 731-746.

Wen, L.-S., Santschi, P., Gill, G. and Paternostro, C. (1999) Estuarine trace metal distributions in Galveston Bay: importance of colloidal forms in the speciation of the dissolved phase. Marine Chemistry 63, 185-212.

Wen, L.-S., Stordal, M.C., Tang, D., Gill, G.A. and Santschi, P.H. (1996) An ultraclean cross-flow ultrafiltration technique for the study of trace metal phase speciation in seawater. Marine Chemistry 55, 129-152.

Wilkinson, K.J., Balnois, E., Leppard, G.G. and Buffle, J. (1999) Characteristic features of the major components of freshwater colloidal organic matter revealed by transmission electron and atomic force microscopy. Colloids and Surfaces A: Physicochemical and Engineering Aspects 155, 287-310.

Wong, M.W. and Townsend, D.W. (1999) Phytoplankton and hydrography of the Kennebec estuary, Maine, USA. Marine Ecology Progress Series, 133-144.

Wu, J. (2007) Determination of picomolar iron in seawater by double Mg (OH) 2 precipitation isotope dilution high-resolution ICPMS. Marine Chemistry 103, 370-381.

Wu, J., Boyle, E., Sunda, W. and Wen, L.-S. (2001) Soluble and colloidal iron in the oligotrophic North Atlantic and North Pacific. Science 293, 847-849.

Wu, J. and Boyle, E.A. (1997) Low blank preconcentration technique for the determination of lead, copper, and cadmium in small-volume seawater samples by isotope dilution ICPMS. Analytical Chemistry 69, 2464-2470.

Wu, J. and Luther III, G.W. (1996) Spatial and temporal distribution of iron in the surface water of the northwestern Atlantic Ocean. Geochimica et Cosmochimica Acta 60, 2729-2741.